



SCMS SCHOOL OF ENGINEERING & TECHNOLOGY

BOOK/CONFERENCE DETAILS 2023

SI No:	Name	First Author	Second Author	Third Author	Fourth Author	INDEXING
1	Vinoj P G			CEC2301		conference-book proceedings
2	Anandhi V	CEC2302				conference-book proceedings
3	Dr.Nithya Mohan	BBSH2301				conference-book proceedings
4	Dr.Sanju Sreedharan	CCE2305				conference-book proceedings
6	Dr.Lakshmi Priya	CCE2301				conference-book proceedings
7	Remya Y K	CCE2304				conference-book proceedings
8	Dr.Akhila M	CCE2303				conference-book proceedings
9	Dr. Raghav G R	BME2301 , BME2302				book chapters
10	Anoop M S		BME2301 , BME2302			book chapters
11	Dr.Jayadevan P C			BME2301 , BME2302		book chapters
12	Josna Philip	CCSE2301				conference-book proceedings
13	Dr Manish T I	BCSE2301,CCSE2302, BCSE2304				book chapters
14	Litty Koshy	BCSE2302,BCSE2303				book chapters
15	Dr.Jayanand B	BEE2301				book chapters
16	Beena Puthilath	BEE2302				book chapters
17	Dr.Rag L	CME2301				conference-book proceedings

Total BOOK/CONFERENCE for the calender year 2023	18
---	-----------

TOTAL BOOK/CONFERENCE COUNT FROM 2018-2023	91
---	-----------



PRINCIPAL
SCMS SCHOOL OF ENGINEERING & TECHNOLOGY
VIDYANAGAR, PALLISSERY, KARUKUTTY
ERNAKULAM, KERALA-683 576



International Conference on Transportation Infrastructure Projects : Conception to Execution

↳ TIPCE 2022: **Recent Trends in Transportation Infrastructure, Volume 2** pp 125–141 | [Cite as](#)

Home > Recent Trends in Transportation Infrastructure, Volume 2 > Conference paper

Rollover Stability Analysis of Trucks-Effect of Curve Geometry and Operating Speed

[Y. K. Remya](#) ✉, [Jacob Anitha](#) & [E. A. Subaida](#)

Conference paper | [First Online: 01 July 2023](#)

Part of the [Lecture Notes in Civil Engineering](#) book series (LNCE, volume 347)

Abstract

Road crashes have become a major concern worldwide. Rural highways account for more than 66% of total road fatalities as the speed of vehicles on these highways are very high. Rollover crashes at curved roads in these areas are mostly serious and cause severe damage and injury than other kinds of vehicle crashes. The relatively low rollover stability of heavy commercial

Access via your institution →

Chapter EUR 29.95
Price includes VAT (India)

- Available as PDF
- Read on any device
- Instant download
- Own it forever

Buy Chapter

> eBook EUR 160.49

> Hardcover Book EUR 199.99

Activate Windows
Go to Settings to activate Windows.
Tax calculation will be finalised at checkout



Check for updates

Cite this paper

Remya, Y.K., Anitha, J., Subaida, E.A. (2023). Rollover Stability Analysis of Trucks-Effect of Curve Geometry and Operating Speed. In: Agarwal, A., Velmurugan, S., Maurya, A.K. (eds) Recent Trends in Transportation Infrastructure, Volume 2. TIPCE 2022. Lecture Notes in Civil Engineering, vol 347. Springer, Singapore. https://doi.org/10.1007/978-981-99-2556-8_10

Download citation

[.RIS](#) [.ENW](#) [.BIB](#)

DOI	Published	Publisher Name
https://doi.org/10.1007/978-981-99-2556-8_10	01 July 2023	Springer, Singapore

Print ISBN	Online ISBN	eBook Packages
978-981-99-2555-1	978-981-99-2556-8	Engineering Engineering (RO)

Chapter EUR 29.95
Price includes VAT (India)

- Available as PDF
- Read on any device
- Instant download
- Own it forever

Buy Chapter

> eBook EUR 160.49

> Hardcover Book EUR 199.99

Tax calculation will be finalised at checkout

Purchases are for personal use only

[Learn about institutional subscriptions](#)

Sections

References

[Author information](#)

[Editor information](#)

Author information

Authors and Affiliations

Department of Civil Engineering, Government Engineering College, APJ Abdul Kalam Technological University, Thrissur, 680009, India

Y. K. Remya & E. A. Subaida

Department of Civil Engineering, SCMS School of Engineering and Technology, APJ

Abdul Kalam Technological University, Karukutty, 683576, India

Y. K. Remya

Department of Civil Engineering, Government Polytechnic College, Chelakkara, Thrissur, 680586, India

Jacob Anitha

Corresponding author

Correspondence to [Y. K. Remya](#).

Editor information

Editors and Affiliations

▼ Chapter EUR 29.95
Price includes VAT (India)

- Available as PDF
- Read on any device
- Instant download
- Own it forever

[Buy Chapter](#)

> eBook	EUR 160.49
> Hardcover Book	EUR 199.99

Tax calculation will be finalised at checkout

Purchases are for personal use only

[Learn about institutional subscriptions](#)

Sections

References

[Abstract](#)

[References](#)

[Author information](#)

Activate Windows
Go to Settings to activate Windows.

Home > Environmental Science and Pollution Research > Article

'Remediability Score' as a tool for selecting the most suitable remediation technology for contaminated sites



Research Article | Published: 05 January 2024

Lakshmi Priya ✕

SCMS School of Engineering and Technology, Karukutty, Kerala, India

[View author publications](#)

You can also search for this author in [PubMed](#) | [Google Scholar](#)

Environmental Science and Pollution Research

- [Aims and scope](#) →
- [Submit manuscript](#) →

Lakshmi Priya & George Kuttiparichel Varghese ✉

Access this article

Go to Settings to activate Windows.

About this article



Cite this article

Priya, L., Varghese, G.K. 'Remediability Score' as a tool for selecting the most suitable remediation technology for contaminated sites. *Environ Sci Pollut Res* (2024).

<https://doi.org/10.1007/s11356-023-31687-y>

[Download citation](#) ↓

Received	Accepted	Published
05 March 2023	19 December 2023	05 January 2024

DOI
<https://doi.org/10.1007/s11356-023-31687-y>

Keywords

- [Environmental forensics](#)
- [Fuzzy AHP](#)
- [Remediability](#)
- [Remediation](#)
- [Remediability Score](#)
- [Soil pollution](#)

- [Abstract](#)
- [Data availability](#)
- [References](#)
- [Author information](#)
- [Ethics declarations](#)
- [Additional information](#)
- [Supplementary Information](#)
- [Rights and permissions](#)
- [About this article](#)

Advertisement

Landscape Series

Learn more about this book series.

Activate Windows
Go to Settings to activate Windows.



Advertisement

REMEDIATION

THE JOURNAL OF ENVIRONMENTAL CLEANUP COSTS, TECHNOLOGIES, & TECHNIQUES

RESEARCH ARTICLE

Determination of the remediability score for remediation liability allocation among polluters

Lakshmi Priya, George K. Varghese, Alberto Pivato

First published: 19 April 2023 | <https://doi.org/10.1002/rem.21755>



Volume 33, Issue 3

Summer 2023

Pages 217-226

Advertisement

PDF TOOLS SHARE

PDF TOOLS SHARE

Abstract

When a pollution incident occurs, there can be impact liability and/or remediation liability on the polluter. The impact liability pays for the loss of life and property due to pollution. The remediation liability is to pay for remediating the environment in accordance with applicable laws and regulations. If there is only one polluter in a pollution incident, the entire liability can be placed on the sole polluter. However, liability allocation becomes complex when there are multiple polluters. To allocate the fractional remediation liability among multiple polluters, it is important to identify the factors that determine the cost of remediation so that a just distribution of liability can be made based on the contribution of each polluting party to the factors identified. Along with factors such as "quantity of the chemical released by the polluter," "distribution of the chemical in the environmental medium," "persistence of the chemical in the environmental medium," and so forth, the ease with which the chemical pollutant can be separated from the contaminated medium, which we name as "remediability," is important in deciding the remediation liability. The "remediability" of a chemical is critical in selecting the remediation technologies to be adopted and, consequently, in deciding the cost of remediation. Determination of a remediability score (RS) for each "chemical–environment medium" pair will help in quantifying the ease with which the site can be remediated. The score is envisaged on a 0–100 scale. The higher the score, the more difficult it is to remediate the chemical in the environmental medium under consideration. The score is estimated based on a set of predetermined factors that are characteristic to the

The Law of Compensation: Civil Liability Occupational Health Law, [1]

The Law of Compensation: Civil Liability Occupational Health Law, [1]

Climate-influenced hydrobiogeochemistry and groundwater remedy design: A review

Scott D. Warner, Dawit Bekele, C. Paul Nathanail, Sreeni Chadalavada, Ravi Naidu

Remediation Journal

Advertisement

Activate Window: Go to Settings to activate

Effect of Fines on Static Liquefaction of Sand

Akhila M

Dept. of Civil Engineering
SCMS School of Engineering and
Technology
Ernakulam, India
akhilam@scmsgroup.org

Rangaswamy K

Dept. of Civil Engineering
NIT Calicut
Calicut, India
ranga@nitc.ac.in

Sankar N

Dept. of Civil Engineering
NIT Calicut
Calicut, India
line 5: sankar@nitc.ac.in

Abstract— Several undrained static triaxial tests were performed on soil combinations to study the effect of initial conditions, fines content and plasticity on the undrained response and liquefaction behaviour of sand and soil mixtures. Soils are more liquefiable if they possess less dilation (or contraction) and low levels of stress ratios at failure strain levels. The results are displayed in the form of stress-strain relations, pore pressure developments, stress paths and liquefaction susceptibility of different soil mixtures is evaluated. Findings show that the stress ratios decrease with the decrease of relative densities and increase of consolidation pressures. Non-plastic silty sands behave as less dilative than fine sands due to the rise of pore pressure ratios with fines content. Stress ratios decrease with increase in the plasticity up to 5, and beyond that, increase with plasticity indices up to 15. The decrease or increase of stress ratios is due to the increase or decrease of pore pressures with plasticity indices.

Keywords—low plastic fines, liquefaction, undrained response

I. INTRODUCTION

The term soil liquefaction was initially coined by Terzaghi and Peck (1948). The subject is much older than that; however, Dutch engineers have been engineering against liquefaction for centuries in their efforts to protect their country from the sea. Koppejan et al. (1948) brought the problem of coastal flow slides to the soil mechanics fraternity at the 2nd International Conference in Rotterdam. Soil liquefaction is defined as the transformation of granular material from solid to liquid state as a consequence of increased pore water pressure and reduced effective stress (Marcuson, 1978). In general, the liquefaction susceptibility of soils is determined after conducting laboratory triaxial compression tests under static or cyclic loading conditions. Triaxial compression tests have more advantage in controlling all types of drainage conditions.

Monotonically increasing shear stress has to reach the yield shear strength to trigger static liquefaction and strain softening (Fourie et al., 2001; Kramer and Seed, 1988; Wanatowski and Chu, 2008). Strain-softening subsequently follows the initiation of liquefaction until a reduced post-liquefaction strength is mobilised at large shear strains (Terzaghi et al., 1996). After conducting the laboratory tests, Kramer and Seed (1988) demonstrated that there is a marked increase in static liquefaction susceptibility with an increase in principal effective stress ratios. Lade & Yamamuro (2011) explained the mechanism of instability inside the failure surface and showed that in most cases, static liquefaction occurs in loose silty sands. Sina & Siavash (2014) have conducted triaxial tests in Babolsar sand and experienced the possible states of liquefaction of soil. The investigators (Koppejan et al., 1948; Fourie et al., 2001; Bjerrum, 1971;

Castro, 1969; Hazen, 1918; Muhammad, 2012; Olson, 2001) described several cases of liquefaction flow failures.

However, the accuracy of test results is affected by various factors like specimen preparation, initial conditions, saturation of soil, type of fines, fines content, plasticity, etc. Among those, specimen preparation is one of the critical factors that influence the test property. It is mandatory to choose the method of specimen preparation to represent the actual field deposit. Previous studies have shown that different specimen preparation methods result in different soil fabrics and stress-strain response at small to moderate strain levels. Various methods used to reconstitute the soil specimens in the triaxial testing are moist tamping, slurry deposition, water sedimentation, air pluviation, dry funnel deposition, under compaction, etc.

The present study deals with the effect of fine content and plasticity on the undrained response and liquefaction susceptibility of sand under static loading. Liquefaction susceptibility under static load is expressed in terms of stress ratios and excess pore pressure ratios.

II. MATERIALS USED

To process non-plastic and low plastic soil mixtures for the present study, soil materials of fine sand, crushed stone dust, kaolinite and natural clay were collected from various locations of Kerala state in India. Totally 17 soil combinations were made after blending the non-plastic fines and clay fractions into the fine sand. The silty sands contain up to 40% non-plastic fines and low plastic soil mixtures contains 5 - 40% clay fraction by varying the plasticity indices of 5, 10 and 15. The details regarding materials and their basic properties are explained in Rangaswamy et al. (2020).

III. TRIAXIAL TESTING

The liquefaction susceptibility of soils can be determined after conducting laboratory triaxial compression tests under static or cyclic loading conditions. Triaxial compression tests have more advantage in controlling all types of drainage conditions. The static triaxial tests in undrained conditions were carried out to investigate the liquefaction susceptibility of non-plastic and low plastic soil mixtures. The stages involved in carrying out the triaxial tests, including test equipment, are discussed below.

An automated digital type of static triaxial testing facility (Mfd. by Heico, India) with a computer display of measurements was used to carry out the experiments. It has the features of cell and back pressure control devices, volume

change, LVDT, load cell and pore pressure indicators. All the digital instrumentations of measurement units are connected to data control and acquisition system. Sophisticated software is also provided to monitor the various parameters on the computer screen. Several triaxial tests were performed on cylindrical specimens of sand, non-plastic and low plastic soil combinations. The testing involves the following stages:- specimen preparation, saturation, isotropic consolidation and shearing under undrained conditions. The cylindrical soil specimens were prepared with 50 mm in diameter and 100 mm in height at 50% relative density. The method of moist tamping with the under-compaction procedure suggested by Ladd (1978) has been used for specimen preparation. The saturation of the specimens has accomplished by following the cell and back pressure incremental process until it reaches the pore pressure coefficient B of 0.98 or more. More details on the soil specimen preparation, saturation and consolidation are explained in Akhila et al. (2018).

After consolidating the saturated cylindrical soil specimen with required effective pressure, shearing of the soil specimen is performed according to the standard testing procedure recommended by Bishop and Henkal (1969). The strain rate of 0.625 mm/min was maintained throughout the test. During shearing of the specimen, continuous records of the excess pore water pressure and axial strains were obtained. Each experiment was continued until it reaches the residual strain level.

IV. RESULTS AND DISCUSSION

A. Undrained response of fine sand

This section begins with a study of the effects of initial conditions, i.e., density and consolidation pressure, on the undrained static triaxial response of fine sand. Further, it discusses the effects of fines content and plasticities on the undrained behaviour of fine sand. Liquefaction susceptibility of soil combinations has to be addressed qualitatively based on the behaviour of soil as either contractive or dilative under undrained static triaxial loading.

In general, liquefaction susceptibility of soil specimens is evaluated in terms of static stress ratios and pore pressure ratios causing failure strain of 20%. Hence the effect of both the relative densities and consolidation pressures on liquefaction susceptibility of sand is explored in terms of stress and pore pressure ratios at 20% strain, as shown in Fig. 1. Herein, deviator stresses and excess pore pressures at 20% axial failure strain are normalised with the corresponding consolidation pressures to obtain the static stress ratios and pore pressure ratios respectively.

The results show that the stress ratios decrease with a decrease in relative densities and increase in consolidation pressures. At low levels of relative densities, Fig. 1(a) indicates that the reduction in stress ratios with consolidation pressures is less significant; however, it is more predominant at higher relative densities. The decrease in stress ratios is due to the increase in pore pressures with consolidation pressures as shown in Fig. 1(b). At low consolidation pressures, the reduction of stress ratios is very high due to the increase of pore pressure ratios with a decrease of relative densities. The results illustrate that the soils consolidated at low pressures

have high static stress ratios and more resistance to liquefaction. The dense soil specimens are more resistant to liquefaction due to high-stress ratios. Table 1 shows the quantitative increase in stress ratios causing liquefaction with the decrease of consolidation pressures. The increase in stress ratios with the decrease in the pressures from 150 to 50 kPa was found to about 37 - 95%. The quantitative increase in stress ratios causing liquefaction with relative densities are reported in Table 2. The increase in stress ratios with increase in the relative densities from 25 to 75% was found to about 562 - 719%.

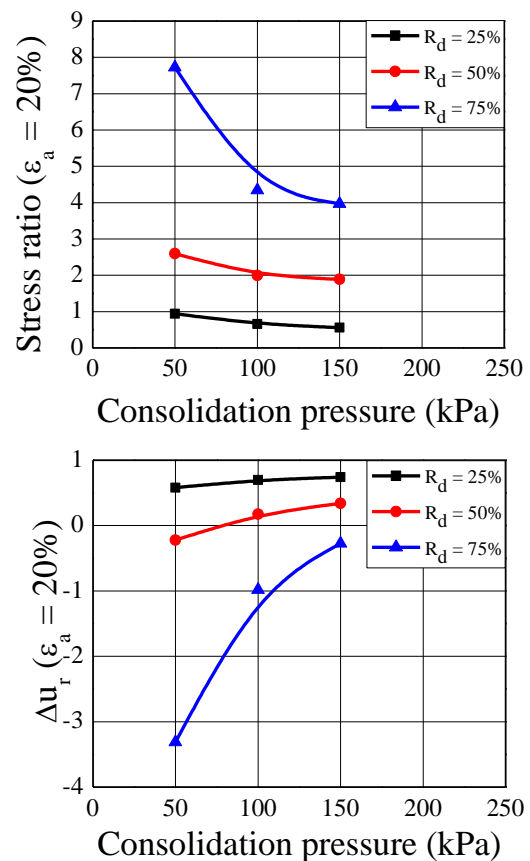


Fig. 1: Effect of consolidation with the denseness of sand

Table 1: Percentage increase in stress ratios with pressures

Consolidation pressures, kPa,	Percentage increase (at difference D_r)		
	25%	50%	75%
150	--	--	--
100	16.72	5.71	9.34
50	67.79	37.5	94.6

Table 2: Percentage increase in stress ratios with densities

Relative densities, %	Percentage increase (at different pressures)		
	150	100	50
25	--	--	--
50	236	204	175
75	606	562	719

B. Effect of fines

Several undrained static triaxial tests were performed on sand-silt mixtures (with the fines content of 10, 20, 30 and 40% constituted at different relative densities) to study the effect of fines content on the undrained response of fine sand. Effect of fines content on liquefaction susceptibility of sand is mentioned in terms of stress ratios and pore pressure ratios causing 20% strain. The results illustrate that the silty sands with high fines content have low static stress ratios and are more susceptible to liquefaction. It is observed from Fig. 3(a) that, at higher relative densities, decrease in stress ratios with fines content is clearly visible; however, the stress ratios of silty sands are almost identical at a low relative density of 25%. It indicates that the effect of fines on liquefaction strength of sand at loose condition is virtually insignificant. It is evident that the trend of the pore pressure build-up during shearing is same in all the silty sands as shown in Fig. 3(b).

The quantitative decrease in stress ratios causing liquefaction with the increase in the fines content is shown in table 3. The reduction in stress ratios with increase in the fines content from 0 to 40% was found to about 34.5 - 50.4% depending upon the applied consolidation pressures. At a relative density of 75%, the maximum reduction of stress ratio with fines content was found to be 55%. However, loose silty sands with 25% relative density have almost similar stress ratios within a maximum of 5% variation.

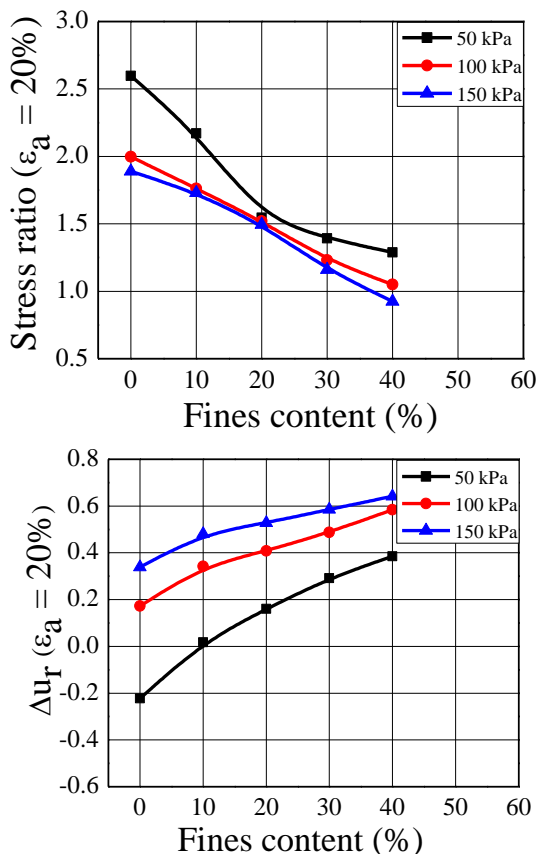


Fig. 2: Effect of non-plastic fines with consolidation pressures on (a) stress ratios and (b) pore pressure ratios at 20% strain level

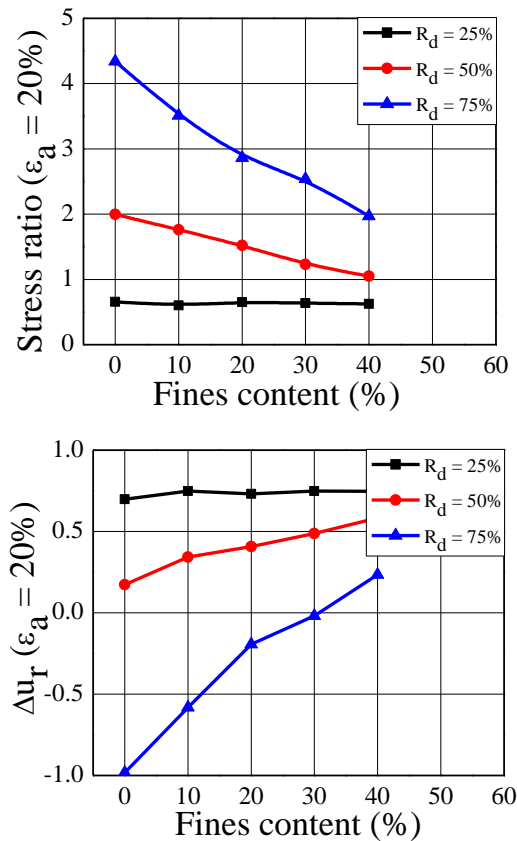


Fig. 3: Effect of non-plastic fines with the denseness of soils on (a) stress ratios and (b) pore pressure ratios at 20% strain level

Table 3: Percentage decrease in stress ratios at 20% strain level with fines content

Fines content (%)	Percentage decrease in stress ratios at a particular density of				
	R _d =50%			R _d =25%	R _d =75%
	$\sigma_3=150$ kPa	$\sigma_3=100$ kPa	$\sigma_3=50$ kPa	$\sigma_3=100$ kPa	$\sigma_3=100$ kPa
0	--	--	--	--	--
10	8.3	11.8	16.4	4	19
20	20.8	23.9	40.5	1	34
30	28	38.3	46.4	3	42
40	34.5	47.4	50.4	5	55

C. Effect of plasticity

Undrained static triaxial tests were performed on soil mixtures possessing plasticity indices of 0, 5, 10 and 15 to study the effect of plasticity on the undrained response of fine sand.

Effect of plasticity on liquefaction susceptibility of soil mixtures with fines content is explored in terms of stress ratios and pore pressure ratios causing 20% strain as shown in Fig. 4(a) and Fig. 4(b) respectively. Results show that the stress ratios decrease with the increase of plasticity index up to 5 and beyond that, it increases with plasticity index up to 15. The decrease or increase of stress ratios is due to the

increase or decrease of pore pressures with plasticity indices, as shown in Fig. 4(b).

Table 4 shows the quantitative decrease or increase in stress ratios at 20% axial strain with the increase of plasticity indices. The reduction in stress ratios with an increase in the plasticity from 0 to 5 was found to be about 11 - 31% depending upon the fines content. Further, the increase in stress ratios with an increase in plasticity from 5 to 15 was found to be about 3.7 - 50.1 %.

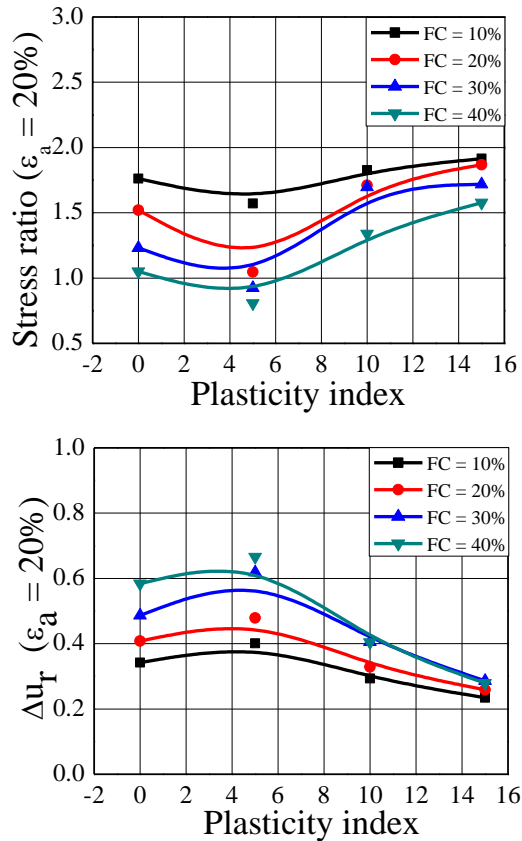


Fig. 4: Effect of plasticity on (a) stress ratios and (b) pore pressure ratios at 20% strain level

Table 4: Percentage decrease or increase in stress ratios at 20% strain level with plasticity indices

PI	Percentage decrease or increase in stress ratios of soil mixtures with			
	FC=10%	FC=20%	FC=30%	FC=40%
0	--	--	--	--
5	-11	-31	-24	-23.1
10	+3.7	+12.6	+37.8	+27.5
15	+8.7	+22.8	+39.5	+50.1

V. CONCLUSIONS

- i. Stress ratios decrease with the decrease in the relative densities and an increase in the consolidation pressures. However, the reduction in stress ratios with the increase of consolidation pressures or decrease of relative densities is less significant at low relative densities and high pressures respectively. The decline in stress ratios is due to the increase of pore pressures. Soils confined

at low normal pressures exhibit as more dilative and highly resistant to liquefaction.

- ii. The reduction in stress ratios with an increase in the fines content from 0 to 40% has found to be about 34.5 - 50.4% by decreasing the application of consolidation pressures from 150 to 50 kPa. At a relative density of 75%, the maximum reduction of stress ratio with fines content has found to 55%. However, loose silty sands with 25% relative density have stress ratios within a maximum of 5% variation.
- iii. Stress ratios decrease with increase in the plasticity up to 5 and beyond that, it increases with plasticity indices up to 15. The decrease or increase of stress ratios is due to the increase or decrease of pore pressures with plasticity indices. The reduction in stress ratios with increase in the plasticity from 0 to 5 has found to be about 11 - 31% depending upon the fines content. Further, the increase in stress ratios with increase in the plasticity from 5 to 15 has found to be about 8.7 - 50.1 %.

REFERENCES

- [1] Akhila M, Rangaswamy K and Sankar N: Undrained response and liquefaction resistance of sand-silt mixtures, *Geotechnical and Geological Engineering*, doi: <https://doi.org/10.1007/s10706-018-00790-0>, 2018.
- [2] Bishop A W and Henkel D J: *The Measurement of Soil Properties in the Triaxial Test*, William Clowes AND Sons Ltd., London, 1969.
- [3] Bjerrum L: *Sub-aqueous slope failures in Norwegian fjords*, Norwegian Geotechnical Institute, Oslo, Norway, 1971.
- [4] Castro G: *Liquefaction of sands*, PhD Thesis, Harvard Soil Mechanics Series, Harvard University, Cambridge, MA, 1969
- [5] Degregorio B V: Loading systems, sample preparation and liquefaction, *Journal of Geotechnical Engineering (ASCE)*, No.116, 1990, pp 805-821.
- [6] Fourie A B, Blight G E and Papageorgiou G: Static liquefaction as a possible explanation for the Merriespruit tailings dam failure. *Canadian Geotechnical Journal*, Vol.38, No.4, 2001, pp 707-719.
- [7] Hazen A: A study of the slip in the Calaveras Dam, *Engineering News-Record*, Vol.81, No.26, 1918, pp 1158-1164.
- [8] Koppejan A W, van Wamelen B M and Weinberg L J H: Coastal landslides in the Dutch province of Zeeland, *Second International Conference on Soil Mechanics and Foundation Engineering*, Rotterdam, Holland, 1948, pp 89-96.
- [9] Kramer S L and Seed H B: Initiation of soil liquefaction under static loading conditions, *Journal of Geotechnical Engineering*, (ASCE), Vol.114, No.2, 1988, pp 412-430.
- [10] Ladd R S: Preparing test specimens using undercompaction, *Geotech. Testing J.*, ASTM, 1(1), 1978, pp 16-23.
- [11] Lade P V and Yamamuro J A: Evaluation of static liquefaction potential of silty sand slopes, *Canadian Geotechnical Journal*, Vol.48, 2011, pp 247-264.

- [12] Li and Dafalias: Anisotropic critical state theory: Role of fabric, *Journal of Engineering Mechanics*, Vol.138, No.3, 2012, pp 263-275.
- [13] Marcuson W F III: Definition of terms related to liquefaction, *J. Geotech. Engrg. Div., ASCE*, Vol.104, No.9, 1978, pp 1197–1200.
- [14] Muhammad K: Case history-based analysis of liquefaction in sloping ground, Department of Civil and Environmental Engineering, University of Illinois, Urbana, 489, 2012.
- [15] Mulilis J P, Seed H B, Chan J K, Mitchell J K and Arulanandan K: Effects of sample preparation on sand liquefaction, *Journal of the Geotechnical Eng. Div., ASCE*, Vol.13 (GT2), 1977, pp 91-108.
- [16] Olson S M: Liquefaction analysis of level and sloping ground using field case histories and penetration resistance, Department of Civil and Environmental Engineering, University of Illinois, Urbana, Illinois, 2001.
- [17] Rahman Lo and Dafalias: constitutive modelling of static liquefaction of sand with fines, *Proceedings of 6th International Conference on Earthquake Geotechnical Engineering*, Christchurch, New Zealand, 2015.
- [18] Rangaswamy K, Akhila M and Sankar N: Effects of fines content and plasticity on liquefaction of sands, *Proceedings of the Institution of Civil Engineers – Geotechnical Engineering*, <https://doi.org/10.1680/jgeen.19.00270>.
- [19] Sina and Siavash: Evaluation of Babolsar sand behaviour by using static triaxial tests and comparison with case history, *Open Journal of Civil Engineering*, Vol.4, 2014, pp 181-197.
- [20] Tatsuoka F, Ochi K, Fujii S and Okamoto M: Cyclic undrained triaxial and torsional shear strength of sands for different preparation methods. *Soils and Foundations*, Vol.26, No.3, 1986, pp 23-41.
- [21] Terzaghi K and Peck R B: *Soil mechanics in engineering practice*: New York, John Wiley and Sons, 1948.
- [22] Terzaghi K, Peck R B and Mesri G: *Soil Mechanics in Engineering Practice*, Third Edition Wiley, New York, 1996.
- [23] Thevanayagam S and Martin G R: Liquefaction in silty soils—screening and remediation issues,” *Soil Dynamics and Earthquake Engineering*, Vol.22(9), 2002, pp 1035- 1042.
- [24] Vaid Y P, Sivathayalan S and Stedman D: Influence of specimen- reconstituting method on the undrained response of sand, *Geotech. Testing J., ASTM*, Vol.22, No.3, 1999, pp 187–195.
- [25] Wanatowski D and Chu J: Effect of specimen preparation method on the stress-strain behaviour of sand in plane-strain compression tests. *Geotechnical Testing Journal*, Vol.31, No.4, 2008.
- [26] Zlatovic S and Ishihara K: Normalized behaviour of very loose nonplastic soil: Effects of fabric, *Soils and Foundations*, Tokyo, Vol.37, No.4, 1997, pp 47–56.

Chapter 9

Corrosion behaviour of additive manufactured materials and composites

Raghav Gurumoorthy Raaja

SCMS School of Engineering and Technology

Nagarajan K. Jawaharlal

KLN College of Engineering

~~Ashok Kumar Rajendran, Gibin George,
and Jenson Joseph Earnest Raghav~~

~~SCMS School of Engineering and Technology~~

CONTENTS

9.1	Introduction	121
9.2	Effect of Different Process Parameters on the Refinement of Microstructures and Corrosion-Resistant Properties	124
9.2.1	Porosity of AM Manufactured alloys	125
9.2.2	Surface roughness of AM processed alloys	126
9.3	Corrosion Behaviour of Additive Manufactured Alloys	128
9.3.1	Titanium-based additive manufactured alloys	128
9.3.2	Aluminium-based AM alloys	129
9.3.3	Iron-based AM alloys	130
9.4	Scope for Future Works	131
9.5	Conclusion	132
	References	134

9.1 INTRODUCTION

Additive manufacturing (AM) or 3D printing has become one of the emerging fields for the manufacture of 3D and complex components [1]. The additive manufacturing (AM) process involves the deposition of powder metals or liquid polymers in layer-by-layer method to obtain the finished object [2,3]. This method is most widely used for the production of complex shapes which is very difficult to manufacture using conventional manufacturing process.

In additive manufacturing the powder materials or polymer wires are melted using laser or electron beam sources and deposited layer by layer as

per the 3D design which is fed into the system [4,5]. Hence the main advantage of AM when compared with other traditional manufacturing processes are obvious; the foremost advantage is the ability to produce most complex components along with very minimal material wastage. The other major advantage is less production time for complex shapes compared to conventional process. Because of the abovementioned advantages the AM process is widely used for the production of complex aerospace components [6]. In the recent past, additive manufacturing (AM) process has improved a lot and a variety of alloys can be developed using AM process. However, it is necessary to explore the different properties of AM manufactured alloys such as mechanical, tribological and corrosion-resistant properties [7,8]. Even though there are more studies which help us understand the mechanical properties of AM manufactured metals and alloys, there are very few studies which let us know about the corrosion behaviour of alloys developed using additive manufacturing process.

The additive manufacturing of metals and its alloys is classified into two main categories, namely powder bed fusion systems and powder-fed systems. The powder-fed systems are also known as direct laser deposition (DLD) technique. In the DLD method metal powders and heating will be supplied to the substrate simultaneously [9–13]. The powder bed fusion systems are further classified into selective laser melting (SLM), selective laser sintering (SLS) and electron beam melting (EBM) [14,15].

Selective laser melting works in a bed in which metal powders are fed through the powder dispenser. The high-energy laser is rastered on to the powder bed as per the computer-aided design (CAD) so as to produce the components layer by layer. Figure 9.1 shows the schematic representation of SLM machine setup. Here the powders are fed into the building platform using recoater arm and then high-energy laser is used to raster the layer for consolidation. After successful consolidation of one layer, this process is repeated to form another layer. The approximate thickness of layers is 80 μm [16]. The entire process was carried out inside the vacuum chamber under argon or nitrogen atmosphere so as to avoid oxidation [17]. The alloys obtained through SLM techniques exhibit fine and smooth microstructure as the result of high cooling rates, which are greater than $6 \times 10^6 \text{ }^\circ\text{C/s}$. The cooling rates also play a vital role in achieving good surface roughness (Ra) which is in the range of 9–16 μm in SLM produced alloys [18,19].

The electron beam machining (EBM) process is similar to LM process but utilizes electron beam as the source of heating as shown in Figure 9.2. The production of electron beams requires very high vacuum up to 10^{-6} torr. The vacuum chamber also helps in reduction of oxidation of metals and alloys [21]. It is to be noted that in all types of additive manufacturing process, the microstructures of the alloys obtained depend upon the different production parameters. Thereby the microstructure of the alloys controls the important properties such as mechanical, tribological and corrosion-resistant properties [22,23].

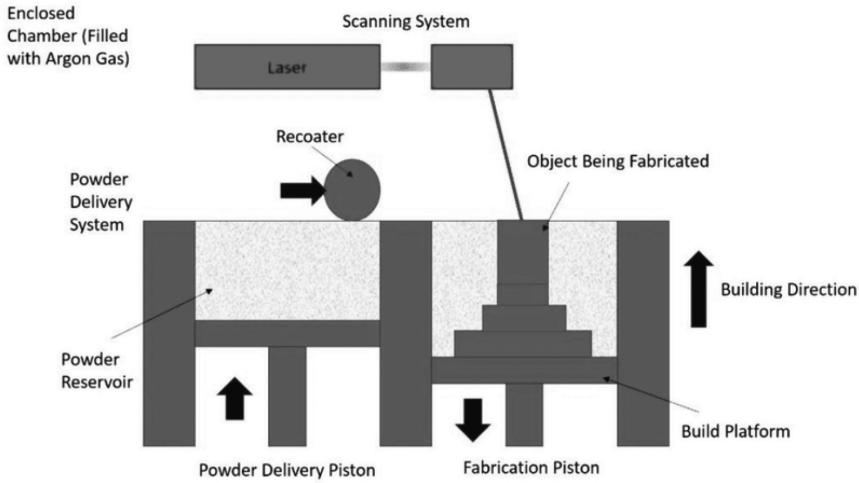


Figure 9.1 Pictorial representation of selective laser melting (SLM) process [20].

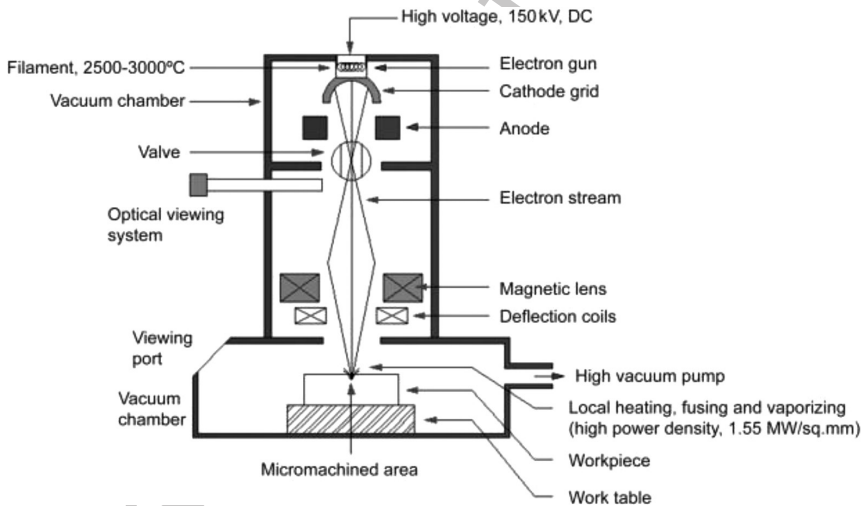


Figure 9.2 Schematic representation of electron beam machining (EBM) process [24].

In powder bed fusion such as SLM, EBM, and SLS the major parameters are the intensity of laser or electron beams, laser/electron spot size and speed of transverse motion. Other important factors which affect the alloy thermal properties are pattern of scanning, thickness of different layers and the temperature of the powder bed. On the other hand, in direct laser deposition powders of size 50–150 μm are fed into the built substrate along with heating through laser source. Also argon gas is passed into the vacuum

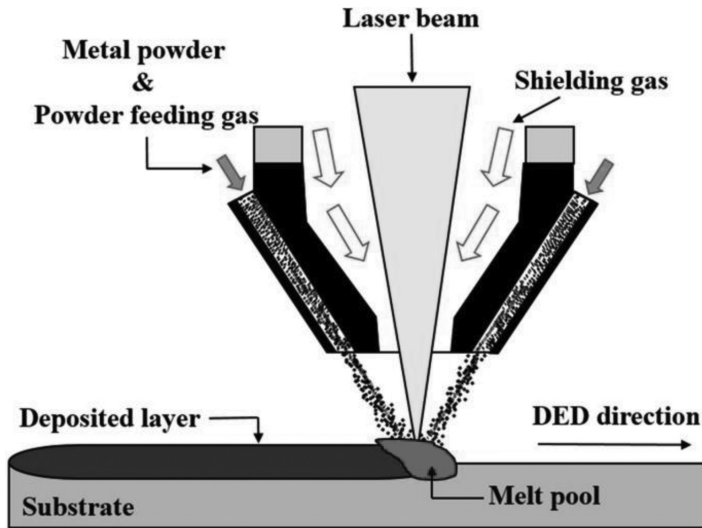


Figure 9.3 Pictorial representation of direct laser deposition (DLD) process [33].

chamber so as to maintain inert atmosphere [25,26]. The important parameters which control the microstructure of the DLD alloys are laser energy, powder size and the amount of powder injected through the nozzle. The raster speed of laser scan and laser spot size also play a vital role in refining the microstructure of the DLD alloys [27,28]. Figure 9.3 shows the pictorial representation of DLD process. It is also to be noted that SLM technique is used to machine stainless steels, titanium-based alloys, aluminium-based alloys, whereas the DLD and EBM methods are widely used to machine titanium-based alloys and stainless steels [29–32].

9.2 EFFECT OF DIFFERENT PROCESS PARAMETERS ON THE REFINEMENT OF MICROSTRUCTURES AND CORROSION-RESISTANT PROPERTIES

As discussed earlier the AM processed alloys possess a different and refined microstructure compared to other conventional manufacturing process because of the influence of different parameters involved in the AM process. In the case of SLM method, the metal powders fed into the powder bed undergo intensive heating normally greater than 2,000°C which is then followed by very fast-paced solidification process [34]. Due to this heating many thermal cycles are involved as the result of heat transfer between powder particles as well as with the surrounding. Due to the high-temperature exposure and very fast cooling rate along with the heat transfer, thermal cycles result in improved and refined microstructures. But as the result of

this rapid heating and cooling there may be formation of few defects such as cracks, surface roughness and porosity [35,36]. Hence these defects might play a vital role in determining mechanical, tribological and corrosion resistance properties of AM manufactured alloys.

9.2.1 Porosity of AM Manufactured alloys

There are few studies which explain the effect of laser energy and scanning rate on the porosity of alloys developed through AM process. Selective laser melting (SLM) method was employed by Shang et al. [37] to study the effect of laser scanning rate on the porosity of 316L stainless steel specimens. In this study the laser energy was kept constant at 195 W, whereas the scanning rate of laser beam is varied in the order between 700 and 1,082 mm/s. The results show that porosity is directly proportional to the scanning rate. The increase in scanning rate results in improper melting which in turn affects the porosity of the alloys. The porosity which occurs in AM manufactured alloys may influence the corrosion-resistant properties of the metals and alloys [38]. The porosity of the additive manufactured alloys, especially Selective Laser Melting method, is classified into two types. One type of porosity can be found at the surrounding of improperly melted powders and another type of porosity is due to the presence of gases in between powder particles during atomization (gas) process, therefore by controlling the machining parameters we can reduce the porosity of additive manufactured alloys which in turn can reduce the corrosion behaviours of the additive manufactured alloys [39–41]. Another more accurate way to study the influence of machining parameters on porosity of additive manufactured of powders, also known as volumetric energy density (E_v) which is calculated by equation (9.1).

$$E_v = \frac{e}{rdt} \quad (9.1)$$

where e is the energy of laser,
 r is scanning rate,
 d is hatch diameter,
 t is thickness of powder layer.

The energy density of laser plays a vital role in controlling the porosity of additive manufactured alloys [42,43]. The Ti6Al4V alloys were produced with porosity less than 0.1% by Hang et al. at an energy density of 120 J/mm³. The laser density of 105 J/mm³ was enough to produce 316L stainless steels with porosity of approximately 0.3% using Selective Laser Melting (SLM) process [36]. It is also to be noted that laser energy density is not the only factor reducing the porosity of additive manufactured alloys. Other parameters such as diameter of laser, scanning rate and hatch style are also very important in controlling the porosity of the additive manufactured (AM)

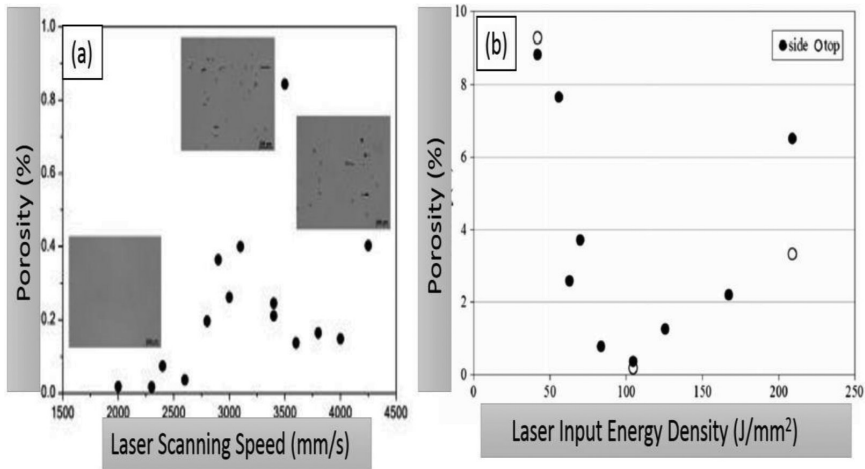


Figure 9.4 Graphical representation (a) porosity vs laser scanning speed [44] (b) porosity vs laser energy density of various SLM manufactured 316L stainless steel [45].

alloys as shown in Figure 9.4. Hence more studies should be carried out to find out the exact relationship between process parameters and porosity.

Porosity is one of the major causes for pitting corrosion in additive manufactured components, especially in selective laser melting (SLM) of 316L stainless steel in acidic media. The corrosion normally initiates at the location of pores [38]. Schaller et al. [46] employed electrochemical corrosion analysis to study the corrosion behaviour of 17-4 PH stainless steel manufactured using SLM process. The results showed that the porosity larger than 50 μm results in pitting corrosion, whereas when the porosity was around 10 μm there is no pitting corrosion. But when the normality of acids was increased and also when highly acidic acids such as sulphuric acid was utilized there is evidence of pitting corrosion in 316L stainless steels [45]. The size and shape of the pores also have a significant effect on the pitting corrosion performance; moreover, the pores which are irregular in shape will corrode easily due to the accumulation of ions at the edges and the corners. However, there are very few studies based on size distribution of pores, and hence more studies are required to be carried out to understand the effect of porosity, which includes size of the pores and l/d (aspect ratio) of the pores, on the corrosion behaviour of additive manufactured components.

9.2.2 Surface roughness of AM processed alloys

The selective laser melting (SLM) manufactured components have very high surface roughness (R_a). Wang et al. [47] reported that surface roughness (R_a) of the metals and its alloys are in the range of 10–30 μm , which is

very much higher than that of surface roughness produced by conventional process such as milling. He also found that the energy density of laser (ω) plays a very important role in deciding the surface roughness of SLM manufactured components. He reported that when the ω value is around $100\text{--}160\text{ J/mm}^3$, the surface roughness is low around $10\text{ }\mu\text{m}$, but when the ω values is reduced to 70 J/mm^3 , the surface roughness increases up to $15\text{ }\mu\text{m}$.

The main reasons for high surface roughness in SLM process are the evaporation and Marangoni force that exists because of melting of powders. The expansion of entrapped gases stops the flow of melt and thereby increases the melt pool which is highly unstable. This melt pool increases the surface roughness (Ra). When the layers of powders are thick, more gas expansion takes place. Hence the surface roughness can be reduced by decreasing the powder layer thickness [45,48]. However, by decreasing the layer thickness, the overall time for completing the machining increases rapidly. The improper melting of powders and formation of metal droplets also known as balling effect are the major reason for increase in surface roughness [49]. When the power of laser is very low the metallic powders are not completely melted and few solid particles stick on to the surface of the solidified components. Hence the increase in laser power can increase the melt rate and thereby increase wettability which in turn reduces the balling phenomenon [50]. Thus surface roughness can be reduced when the energy density of laser is high enough to melt the powder particles as shown in Figure 9.5. It is also to be noted that if the laser intensity is very high it can also reduce the surface finish of the components.

Normally the morphology of the surface is very important for the corrosion resistance properties. The corrosion rate increases with increase in surface roughness of the additive manufactured alloys such as copper, Mg and Al-based alloys [51,52]. Therefore, improving the surface finish by overcoming all defects was the major challenge for 3D printed or additive manufactured components. Thus many research works should be carried out to study the effects of post-processing surface treatments on additive manufactured components.

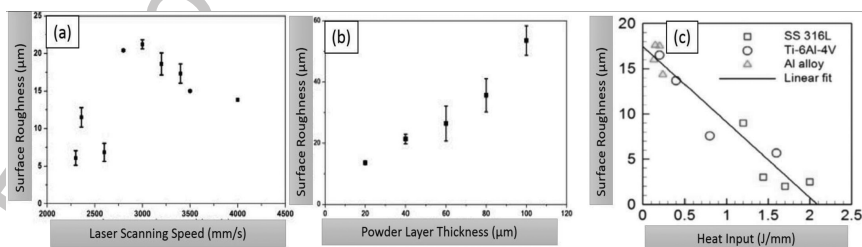


Figure 9.5 The relationship between surface roughness and (a) laser scanning speed, (b) powder layer thickness [44] and (c) heat input [45].

9.3 CORROSION BEHAVIOUR OF ADDITIVE MANUFACTURED ALLOYS

In this section various types of alloys manufactured through additive manufacturing technique are summarized and their corrosion behaviour is explored so as to provide an insight for young researchers who are trying to study the corrosion behaviour of additive manufactured alloys. Recent developments in additive manufacturing (AM) processes have made it versatile and a wide variety of metal alloys can be now prepared using additive manufacturing methods. The common types of alloys are titanium-based alloys, iron-based alloys and aluminium-based alloys.

9.3.1 Titanium-based additive manufactured alloys

Titanium-based alloys have very large industrial applications because of their properties. But a major disadvantage is their machining cost and a very large machining time when machined using conventional manufacturing processes. Hence titanium and its alloys are widely considered for manufacturing through additive manufacturing (AM) process [53–56]. Dehoff et al. [57] reported nearly 50% reduction in production cost for the titanium alloy-based engine bracket manufactured using AM process. Ti6Al4V alloy was one of the titanium alloys which was widely utilized for the production of biomedical, dental and automobile applications. It is also reported that Ti6Al4V alloys fabricated using Selective Laser Melting (SLM) have very minimal pitting corrosion, approximately around 150 mV, in sodium chloride solution. It also exhibits passivation curves which is the measure of corrosion resistance [58]. This improvement in corrosion resistance is due to the presence of α' -martensite as shown in Figure 9.6. The rapid cooling process was the reason for the formation of α' -martensite and it also possesses β -grains. Normally in SLM manufactured Ti6Al4V alloys

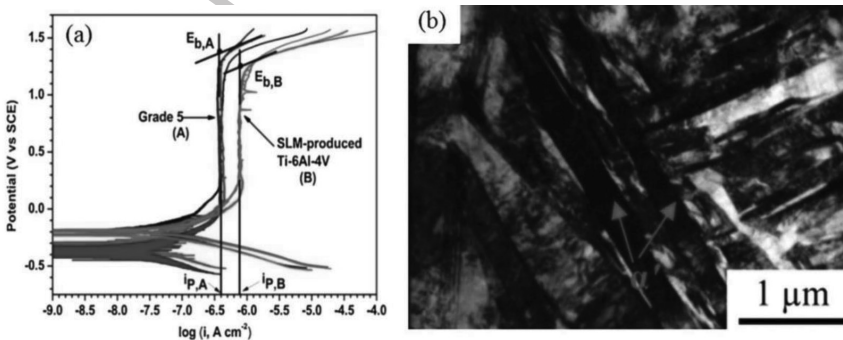


Figure 9.6 (a) Potentiodynamic polarization curves (tafel curves) of SLM manufactured Ti6Al4V alloy and Grade 5 alloy in NaCl solution (3.5 wt.%) [58]. (b) TEM image of SLM manufactured Ti6Al4V alloy [61].

the β -phase contains more vanadium presence along with oxides; hence, the β -phase is more stable compared to the α -phase. The stable β -phase plays a vital role in increasing the corrosion resistance of Ti6Al4V alloys [59]. But the percentage of β -phase present in additive manufactured Ti6Al4V alloys is very less compared to conventional manufacturing process. So it can be concluded that the SLM manufactured titanium alloys show very poor corrosion resistance [60].

9.3.2 Aluminium-based AM alloys

The selective laser melting (SLM) technique was broadly utilized for the manufacture of various aluminium-based alloys such as Al-Zn, Al-12Si, Al-50Si, Al-Cu and Al-10Si-M alloys [62–64]. Among these alloys Al-10Si-Mg alloys were widely studied by the researchers [65,66]. It is also noted as shown in Figure 9.7a and b. The corrosion potential of Al and Si particles differs, that is, Si has higher corrosion potential compared to that of Al which has low corrosion potential. This difference in corrosion potential leads to galvanic corrosion as shown in Figure 9.7c. Hence to overcome

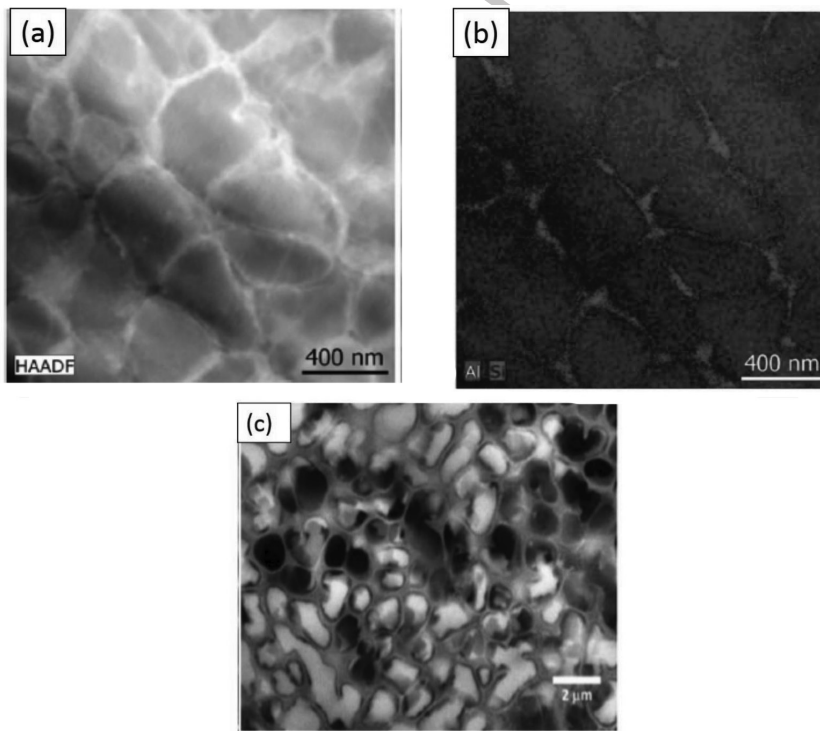


Figure 9.7 (a)STEM image of SLM manufactured Al-10Si-Mg alloy, (b) EDS mapping of Al and Si [68], (c) SEM image of corroded surface [45].

this galvanic corrosion the SLM manufactured Al-10Si-Mg alloys are subjected to heat treatment so as to improve the bonding of alloys and also to enable the formation of intermetallics, which thereby improve corrosion resistance [67].

9.3.3 Iron-based AM alloys

Stainless steels (austenitic) such as 316L and 304L will have austenitic phase when machined using SLM process, whereas only α -phase is formed if it is machined using Direct Laser Deposition (DLD) process [69–71]. The dislocation in grains also plays an important role in improvement of hardness of the alloy steel. It is also to be noted that nanoscale oxide formation has influence in deciding the mechanical and corrosion resistance of iron-based alloys [72]. Some studies also show that there is not much impact of porosity in corrosion behaviour of 316L stainless steel manufactured using SLM process as shown in Figure 9.8. Sander et al. [39] reported the corrosion behaviour of SLM-fabricated 316L stainless steel. They fabricated the 316L specimens at different scan rates and laser energies. The results exhibit that the scan rate and laser energy do not have any effect on corrosion resistance of 316L stainless steel, whereas the increase in porosity due to the faster scan rate and improper melting resulted in reduction in passivation potential, and hence increase in corrosion rate of 316L stainless steel samples as shown in Figure 9.9. The corrosion analysis of normal 316L SS samples and

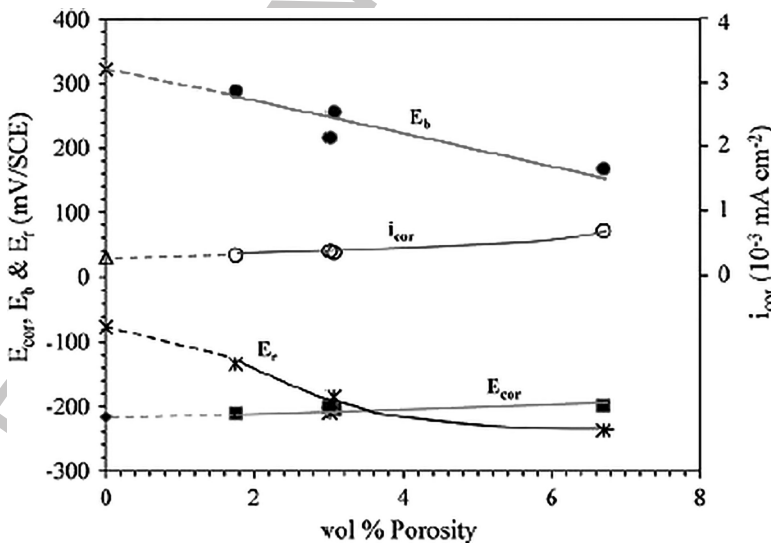


Figure 9.8 Relationship between Vol % of porosity and corrosion potential (E_{cor}), repassivation potential (E_r), breakdown potential (E_b) and corrosion current density (i_{cor}) of SLM manufactured alloys [74].

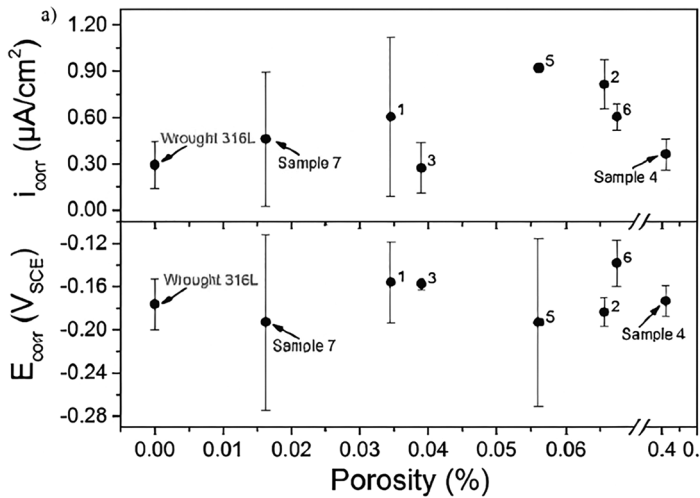


Figure 9.9 Porosity vs corrosion potential (E_{corr}) and corrosion current density (i_{corr}) [39].

heat-treated SLM manufactured 316L SS was carried out by Hemmasian Etefagh et al. [73] who reported that the heat treatment process has eliminated the residual stress, thereby increasing the corrosion potential. The corrosion behaviour of Laser Powder Bed Fusion (LPBF) manufactured 316L samples in 0.1 M HCl solution was studied by Trelewicz et al. [4]. Corrosion current density of LPBF manufactured 316L SS samples was much higher compared to wrought samples, when studied using potentiodynamic polarization test. The main reason for the decrease in corrosion resistance was the microstructure of LPBF manufactured 316L SS.

9.4 SCOPE FOR FUTURE WORKS

- The review gives an insight into the corrosion behaviour of AM alloys, many research articles are explored and their findings are reported. Most of the studies are not systematic and concentrate on one specific area and lack in-depth analysis of corrosion phenomena. Hence based on the studies, the following gaps have been identified:
- Corrosion analysis of additive manufactured alloys was carried out in different acidic and brine media and also with various concentration and pH levels, and hence it is very difficult to compare studies on one alloy with other.
- In the same way, corrosion analysis of additive manufactured alloys was carried out using different corrosion studies such as weight loss method, potentiodynamic polarization method, electrochemical

impedance analysis etc.; hence, it is very difficult to compare studies on one alloy with other.

- The lack of standards for carrying out corrosion test was also one of the important factors to be addressed. Many studies compared wrought or cast irons with AM counterparts but few studies show the difference in properties between cast and AM alloys. Similarly, few studies compared only the different types of alloys produced by AM process but not discussed the alloys prepared by other methods. Hence the conclusions derived from the study may not be conclusive.
- There are very few studies on the exposure of AM alloys to nuclear radiation and also there are very minimal studies on the effect of gases especially hydrogen in AM manufactured alloys.
- Similarly, the corrosion analysis of AM manufactured alloys is limited to materials such as titanium alloys, aluminium alloys and iron-based alloys. But AM process can be utilized to even wide range of metals and their alloys.
- The work has a deficiency in parting the variables, i.e., it is very tedious to show trends from changes in porosity and also chemical factors simultaneously.

9.5 CONCLUSION

An outline of the recent status of some metal matrix alloys manufactured employing additive manufacturing was presented with a focus on correlating the relationship between the defects caused due to the microstructure and their effects on corrosion resistance properties. We can conclude that the high temperature evolved during manufacturing using SLM results in high dislocation densities and refinement of grain size, which in turn improves the tensile strength. Corrosion properties depend on the formation of alpha and beta phases and their structure compared to that of alloys fabricated using conventional methods. In the coming days, many materials can be manufactured using AM process, and hence the optimization of various parameters involved such as laser density, raster velocity and size of powder particles is very important in reducing the surface roughness, porosity and also to increase the strength of the alloys. However, the intrinsic relationship between the microstructural characteristics and the corrosion behaviour of the AM-fabricated components should be actively focused as well. The qualities of the input powder material and their effects on the fabrication process should be the first focus of research. It is critical to include the following three major components when describing a powder: particle microstructure, particle morphology and particle chemistry [75]. The focus of the current research is on the morphological characterization of powders and their impact on the characteristics of manufactured parts.

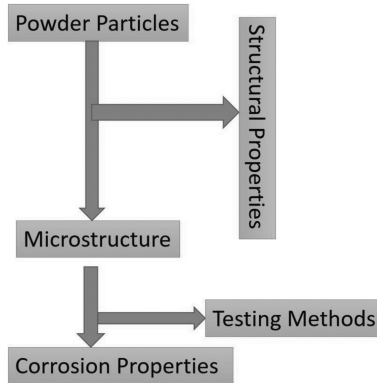


Figure 9.10 Pictorial representation of relationship between powder, microstructure and corrosion properties of AM manufactured alloys.

The mechanical and anti-corrosive qualities of the final consolidated components may be impacted by whether the feedstock powders are argon or nitrogen atomized, and whether the construction chambers are in argon or nitrogen atmosphere [76]. Figure 9.10 is a pictorial representation of AM-produced component powder, microstructure and related corrosion behaviour. The relationship between important structural properties and corrosion resistance must be established. For instance, typical MnS additions formed in wrought 316L SS were exchanged by Mn-Si oxides of nano regime in the SLM manufactured components, which reduces the vulnerability to pitting [77] and also the microstructural irregularities in the SLM manufactured components which otherwise lead to diverse growth rates (SCC) [78]. For the corrosion testing methodologies, there's an egregious lack of norms for which standardized experimentations are enforced, and presently, a wide range of distinct corrosion experimentation techniques (weight loss method, impedance analysis, potentiodynamic polarization) are indeed very difficult to compare. The standardization of testing methods and procedures as formulated by some professional bodies will be a solution for standardization problems. In general, the defects in the SLMed parts (such as pores and MPBs) usually comprise the corrosion resistance; therefore, a heat treatment process combining the hot isostatic pressing should be carried out to homogenize the composition and refine the microstructure, thereby reducing the porosity of the alloys. Thus, further exploration in this area is also warranted. Another post-processing method involves surface treatment, but surface treatment has lot of challenges which have to be addressed with the SLM manufactured metals. The various other techniques such as alkali-acid heat treatment, sandblasting, electrochemical etching and electrochemical deposition can be considered according to the properties of the raw material used. Conversely, the porous

materials manufactured using AM process cannot be easily surface modified compared to solid materials. Therefore, we have very little choice for selecting the methods of manufacture. Therefore, additional exploitation in this area is also required.

REFERENCES

- [1] D. R. Eyers and A. T. Potter, "Industrial additive manufacturing: A manufacturing systems perspective," *Computers in Industry*, vol. 92–93, pp. 208–218, 2017, doi: 10.1016/j.compind.2017.08.002.
- [2] D. L. Bourell, "Perspectives on additive manufacturing," *Annual Review of Materials Research*, vol. 46, no. 1, pp. 1–18, 2016, doi: 10.1146/annurev-matsci-070115-031606.
- [3] D. W. Rosen, "A review of synthesis methods for additive manufacturing," *Visual and Physical Prototyping*, vol. 11, no. 4, pp. 305–317, 2016, doi: 10.1080/17452759.2016.1240208.
- [4] J. R. Trelewicz, G. P. Halada, O. K. Donaldson, and G. Manogharan, "Microstructure and corrosion resistance of laser additively manufactured 316L stainless steel," *JOM*, vol. 68, no. 3, pp. 850–859, 2016, doi: 10.1007/s11837-016-1822-4.
- [5] M. Attaran, "The rise of 3-D printing: The advantages of additive manufacturing over traditional manufacturing," *Business Horizons*, vol. 60, no. 5, pp. 677–688, 2017, doi: 10.1016/j.bushor.2017.05.011.
- [6] P. Han, "Additive design and manufacturing of jet engine parts," *Engineering*, vol. 3, no. 5, pp. 648–652, 2017, doi: 10.1016/J.ENG.2017.05.017.
- [7] J. K. Telford, "A brief introduction to design of experiments," *Johns Hopkins APL Technical Digest*, vol. 27, no. 3, p. 9, 2007.
- [8] J. Gong, Y. Li, Z. Hu, Z. Zhou, and Y. Deng, "Ultrasensitive NH₃ gas sensor from polyaniline nanograin enched TiO₂ fibers," *The Journal of Physical Chemistry C*, vol. 114, no. 21, pp. 9970–9974, 2010, doi: 10.1021/jp100685r.
- [9] Y. Hu and W. Cong, "A review on laser deposition-additive manufacturing of ceramics and ceramic reinforced metal matrix composites," *Ceramics International*, vol. 44, no. 17, pp. 20599–20612, 2018, doi: 10.1016/j.ceramint.2018.08.083.
- [10] M. K. Mallik, C. S. Rao, and V. V. S. K. Rao, "Effect of heat treatment on hardness and wear behavior of weld deposited Co-Cr-Mo alloy," *Matéria (Rio de Janeiro)*, vol. 20, no. 2, pp. 544–549, 2015, doi: 10.1590/S1517-707620150002.0054.
- [11] Y. Shi, Z. Lu, Y. Ren, and G. Yang, "Microstructure and tensile properties of laser engineered net shaped reduced activation ferritic/martensitic steel," *Materials Characterization*, vol. 144, pp. 554–562, 2018, doi: 10.1016/j.matchar.2018.08.010.
- [12] Y. Li, Y. Hu, W. Cong, L. Zhi, and Z. Guo, "Additive manufacturing of alumina using laser engineered net shaping: Effects of deposition variables," *Ceramics International*, vol. 43, no. 10, pp. 7768–7775, 2017, doi: 10.1016/j.ceramint.2017.03.085.

- [13] M. Ziętala et al., "The microstructure, mechanical properties and corrosion resistance of 316L stainless steel fabricated using laser engineered net shaping," *Materials Science and Engineering: A*, vol. 677, pp. 1–10, 2016, doi: 10.1016/j.msea.2016.09.028.
- [14] L. E. Murr et al., "Metal fabrication by additive manufacturing using laser and electron beam melting technologies," *Journal of Materials Science & Technology*, vol. 28, no. 1, pp. 1–14, 2012, doi: 10.1016/S1005-0302(12)60016-4.
- [15] S. Singh, V. S. Sharma, and A. Sachdeva, "Progress in selective laser sintering using metallic powders: A review," *Materials Science and Technology*, vol. 32, no. 8, pp. 760–772, May 2016, doi: 10.1179/1743284715Y.0000000136.
- [16] R. S. Keefe, and P. D. Harvey. Cognitive impairment in schizophrenia. *Handbook of Experimental Pharmacology*, 213, pp. 11–37, 2012. doi: 10.1007/978-3-642-25758-2_2.
- [17] P. K. Gokuldoss, S. Kolla, and J. Eckert, "Additive manufacturing processes: Selective laser melting, electron beam melting and binder jetting—Selection guidelines," *Materials*, vol. 10, no. 6, 2017, doi: 10.3390/ma10060672.
- [18] J. Suryawanshi, K. G. Prashanth, S. Scudino, J. Eckert, O. Prakash, and U. Ramamurty, "Simultaneous enhancements of strength and toughness in an Al-12Si alloy synthesized using selective laser melting," *Acta Materialia*, vol. 115, pp. 285–294, 2016, doi: 10.1016/j.actamat.2016.06.009.
- [19] T. DebRoy et al., "Additive manufacturing of metallic components – Process, structure and properties," *Progress in Materials Science*, vol. 92, pp. 112–224, 2018, doi: 10.1016/j.pmatsci.2017.10.001.
- [20] L. Jiao, Z. Chua, S. Moon, J. Song, G. Bi, and H. Zheng, "Femtosecond laser produced hydrophobic hierarchical structures on additive manufacturing parts," *Nanomaterials*, vol. 8, no. 8, p. 601, 2018, doi: 10.3390/nano8080601.
- [21] B. Vayre, F. Vignat, and F. Villeneuve, "Metallic additive manufacturing: state-of-the-art review and prospects," *Mechanics & Industry*, vol. 13, no. 2, pp. 89–96, 2012, doi: 10.1051/meca/2012003.
- [22] H. Gu, H. Gong, D. Pal, K. Rafi, T. L. Starr, and B. E. Stucker, "Influences of energy density on porosity and microstructure of selective laser melted 17-4PH stainless steel," 2013. <http://dx.doi.org/10.26153/tsw/15572>
- [23] G. Sander et al., "Corrosion of additively manufactured alloys: A review," *Corrosion*, vol. 74, no. 12, pp. 1318–1350, 2018, doi: 10.5006/2926.
- [24] B. Bhattacharyya, "Chapter 1 - Introduction," in *Electrochemical Micromachining for Nanofabrication, MEMS and Nanotechnology*, B. Bhattacharyya, Ed. William Andrew Publishing, 2015, pp. 1–23. doi: 10.1016/B978-0-323-32737-4.00001-3.
- [25] R. Koike et al., "Evaluation for mechanical characteristics of Inconel625–SUS316L joint produced with direct energy deposition," *Procedia Manufacturing*, vol. 14, pp. 105–110, 2017, doi: 10.1016/j.promfg.2017.11.012.
- [26] Q. Chao, T. Guo, T. Jarvis, X. Wu, P. Hodgson, and D. Fabijanic, "Direct laser deposition cladding of AlxCoCrFeNi high entropy alloys on a high-temperature stainless steel," *Surface and Coatings Technology*, vol. 332, pp. 440–451, 2017, doi: 10.1016/j.surfcoat.2017.09.072.
- [27] L. Song, V. Bagavath-Singh, B. Dutta, and J. Mazumder, "Control of melt pool temperature and deposition height during direct metal deposition process,"

- The International Journal of Advanced Manufacturing Technology*, vol. 58, no. 1, pp. 247–256, 2012, doi: 10.1007/s00170-011-3395-2.
- [28] N. Shamsaei, A. Yadollahi, L. Bian, and S. M. Thompson, “An overview of Direct Laser Deposition for additive manufacturing; Part II: Mechanical behavior, process parameter optimization and control,” *Additive Manufacturing*, vol. 8, pp. 12–35, 2015, doi: 10.1016/j.addma.2015.07.002.
- [29] K. Guan, Z. Wang, M. Gao, X. Li, and X. Zeng, “Effects of processing parameters on tensile properties of selective laser melted 304 stainless steel,” *Materials & Design*, vol. 50, pp. 581–586, 2013, doi: 10.1016/j.matdes.2013.03.056.
- [30] W. Xu, E. W. Lui, A. Pateras, M. Qian, and M. Brandt, “In situ tailoring microstructure in additively manufactured Ti-6Al-4V for superior mechanical performance,” *Acta Materialia*, vol. 125, pp. 390–400, 2017, doi: 10.1016/j.actamat.2016.12.027.
- [31] W. H. Kan et al., “A critical review on the effects of process-induced porosity on the mechanical properties of alloys fabricated by laser powder bed fusion,” *Journal of Materials Science*, vol. 57, pp. 9819–9865, 2022, doi: 10.1007/s10853-022-06990-7.
- [32] P. Wang, H. C. Li, K. G. Prashanth, J. Eckert, and S. Scudino, “Selective laser melting of Al-Zn-Mg-Cu: Heat treatment, microstructure and mechanical properties,” *Journal of Alloys and Compounds*, vol. 707, pp. 287–290, 2017, doi: 10.1016/j.jallcom.2016.11.210.
- [33] J.-S. Lim, W.-J. Oh, C.-M. Lee, and D.-H. Kim, “Selection of effective manufacturing conditions for directed energy deposition process using machine learning methods,” *Scientific Reports*, vol. 11, no. 1, p. 24169, 2021, doi: 10.1038/s41598-021-03622-z.
- [34] E. Liverani, S. Toschi, L. Ceschini, and A. Fortunato, “Effect of selective laser melting (SLM) process parameters on microstructure and mechanical properties of 316L austenitic stainless steel,” *Journal of Materials Processing Technology*, vol. 249, pp. 255–263, 2017, doi: 10.1016/j.jmatprotec.2017.05.042.
- [35] J. H. Martin, B. D. Yahata, J. M. Hundley, J. A. Mayer, T. A. Schaedler, and T. M. Pollock, “3D printing of high-strength aluminium alloys,” *Nature*, vol. 549, no. 7672, pp. 365–369, 2017, doi: 10.1038/nature23894.
- [36] J. A. Cherry, H. M. Davies, S. Mehmood, N. P. Lavery, S. G. R. Brown, and J. Sienz, “Investigation into the effect of process parameters on microstructural and physical properties of 316L stainless steel parts by selective laser melting,” *The International Journal of Advanced Manufacturing Technology*, vol. 76, no. 5–8, pp. 869–879, 2015, doi: 10.1007/s00170-014-6297-2.
- [37] Y. Shang, Y. Yuan, D. Li, Y. Li, and J. Chen, “Effects of scanning speed on in vitro biocompatibility of 316L stainless steel parts elaborated by selective laser melting,” *The International Journal of Advanced Manufacturing Technology*, vol. 92, no. 9, pp. 4379–4385, 2017, doi: 10.1007/s00170-017-0525-5.
- [38] E. Otero, A. Pardo, M. V. Utrilla, E. Sáenz, and F. J. Perez, “Influence of microstructure on the corrosion resistance of AISI type 304L and type 316L sintered stainless steels exposed to ferric chloride solution,” *Materials Characterization*, vol. 35, no. 3, pp. 145–151, 1995, doi: 10.1016/1044-5803(95)00099-2.

- [39] G. Sander et al., "On the corrosion and metastable pitting characteristics of 316L stainless steel produced by selective laser melting," *Journal of the Electrochemical Society*, vol. 164, no. 6, pp. C250–C257, 2017, doi: 10.1149/2.0551706jes.
- [40] A. L. Maximenko and E. A. Olevsky, "Pore filling during selective laser melting - assisted additive manufacturing of composites," *Scripta Materialia*, vol. 149, pp. 75–78, 2018, doi: 10.1016/j.scriptamat.2018.02.015.
- [41] R. Laquai, B. R. Müller, G. Kasperovich, J. Haubrich, G. Requena, and G. Bruno, "X-ray refraction distinguishes unprocessed powder from empty pores in selective laser melting Ti-6Al-4V," *Materials Research Letters*, vol. 6, no. 2, pp. 130–135, 2018, doi: 10.1080/21663831.2017.1409288.
- [42] S. M. Yusuf and N. Gao, "Influence of energy density on metallurgy and properties in metal additive manufacturing," *Materials Science and Technology*, vol. 33, no. 11, pp. 1269–1289, 2017, doi: 10.1080/02670836.2017.1289444.
- [43] J. Kluczyński, L. Śniezek, K. Grzelak, and J. Mierzyński, "The influence of exposure energy density on porosity and microhardness of the SLM additive manufactured elements," *Materials*, vol. 11, no. 11, p. 2304, 2018, doi: 10.3390/ma11112304.
- [44] C. Qiu, C. Panwisawas, M. Ward, H. C. Basoalto, J. W. Brooks, and M. M. Attallah, "On the role of melt flow into the surface structure and porosity development during selective laser melting," *Acta Materialia*, vol. 96, pp. 72–79, 2015, doi: 10.1016/j.actamat.2015.06.004.
- [45] D. Kong, C. Dong, X. Ni, and X. Li, "Corrosion of metallic materials fabricated by selective laser melting," *npj Materials Degradation*, vol. 3, no. 1, p. 24, 2019, doi: 10.1038/s41529-019-0086-1.
- [46] R. F. Schaller, J. M. Taylor, J. Rodelas, and E. J. Schindelholz, "Corrosion properties of powder bed fusion additively manufactured 17-4 PH stainless steel," *Corrosion*, vol. 73, no. 7, pp. 796–807, 2017, doi: 10.5006/2365.
- [47] D. Wang, Y. Liu, Y. Yang, and D. Xiao, "Theoretical and experimental study on surface roughness of 316L stainless steel metal parts obtained through selective laser melting," *Rapid Prototyping Journal*, vol. 22, no. 4, pp. 706–716, 2016, doi: 10.1108/RPJ-06-2015-0078.
- [48] Y. Tian, D. Tomus, P. Rometsch, and X. Wu, "Influences of processing parameters on surface roughness of Hastelloy X produced by selective laser melting," *Additive Manufacturing*, vol. 13, pp. 103–112, 2017, doi: 10.1016/j.addma.2016.10.010.
- [49] N. T. Aboulkhair, I. Maskery, C. Tuck, I. Ashcroft, and N. M. Everitt, "On the formation of AlSi10Mg single tracks and layers in selective laser melting: Microstructure and nano-mechanical properties," *Journal of Materials Processing Technology*, vol. 230, pp. 88–98, 2016, doi: 10.1016/j.jmatprotec.2015.11.016.
- [50] J. P. Kruth, L. Froyen, J. Van Vaerenbergh, P. Mercelis, M. Rombouts, and B. Lauwers, "Selective laser melting of iron-based powder," *Journal of Materials Processing Technology*, vol. 149, no. 1, pp. 616–622, 2004, doi: 10.1016/j.jmatprotec.2003.11.051.
- [51] R. Walter and M. B. Kannan, "Influence of surface roughness on the corrosion behaviour of magnesium alloy," *Materials & Design*, vol. 32, no. 4, pp. 2350–2354, 2011, doi: 10.1016/j.matdes.2010.12.016.

- [52] D. Kong et al., "Surface monitoring for pitting evolution into uniform corrosion on Cu-Ni-Zn ternary alloy in alkaline chloride solution: Ex-situ LCM and in-situ SECM," *Applied Surface Science*, vol. 440, pp. 245–257, 2018, doi: 10.1016/j.apsusc.2018.01.116.
- [53] S. Pal, M. Finšgar, T. Bončina, G. Lojen, T. Brajljeh, and I. Drstvenšek, "Effect of surface powder particles and morphologies on corrosion of Ti-6Al-4V fabricated with different energy densities in selective laser melting," *Materials & Design*, vol. 211, p. 110184, 2021, doi: 10.1016/j.matdes.2021.110184.
- [54] T. Majumdar, N. Eisenstein, J. E. Frith, S. C. Cox, and N. Birbilis, "Additive manufacturing of titanium alloys for orthopedic applications: A materials science viewpoint," *Advanced Engineering Materials*, vol. 20, no. 9, p. 1800172, 2018, doi: 10.1002/adem.201800172.
- [55] C. Phutela, N. T. Aboulkhair, C. J. Tuck, and I. Ashcroft, "The effects of feature sizes in selectively laser melted Ti-6Al-4V parts on the validity of optimised process parameters," *Materials*, vol. 13, no. 1, p. 117, 2020, <https://doi.org/10.3390/ma13010117>.
- [56] L.-C. Zhang, H. Attar, M. Calin, and J. Eckert, "Review on manufacture by selective laser melting and properties of titanium based materials for biomedical applications," *Materials Technology*, vol. 31, no. 2, pp. 66–76, 2016, doi: 10.1179/1753555715Y.0000000076.
- [57] R. Dehoff et al., "Case study: Additive manufacturing of aerospace brackets," *Advanced Materials and Processes*, vol. 171, no. 3, pp. 19–22.
- [58] N. Dai, L.-C. Zhang, J. Zhang, Q. Chen, and M. Wu, "Corrosion behavior of selective laser melted Ti-6Al-4V alloy in NaCl solution," *Corrosion Science*, vol. 102, pp. 484–489, 2016, doi: 10.1016/j.corsci.2015.10.041.
- [59] J.-R. Chen and W.-T. Tsai, "In situ corrosion monitoring of Ti-6Al-4V alloy in H₂SO₄/HCl mixed solution using electrochemical AFM," *Electrochimica Acta*, vol. 56, no. 4, pp. 1746–1751, 2011, doi: 10.1016/j.electacta.2010.10.024.
- [60] F. Toptan et al., "Corrosion and tribocorrosion behaviour of Ti6Al4V produced by selective laser melting and hot pressing in comparison with the commercial alloy," *Journal of Materials Processing Technology*, vol. 266, pp. 239–245, 2019, doi: 10.1016/j.jmatprotec.2018.11.008.
- [61] X. Zhao et al., "Comparison of the microstructures and mechanical properties of Ti-6Al-4V fabricated by selective laser melting and electron beam melting," *Materials & Design*, vol. 95, pp. 21–31, 2016, doi: 10.1016/j.matdes.2015.12.135.
- [62] T. Gu, B. Chen, C. Tan, and J. Feng, "Microstructure evolution and mechanical properties of laser additive manufacturing of high strength Al-Cu-Mg alloy," *Optics & Laser Technology*, vol. 112, pp. 140–150, 2019, doi: 10.1016/j.optlastec.2018.11.008.
- [63] M. L. Montero-Sistiaga et al., "Changing the alloy composition of Al7075 for better processability by selective laser melting," *Journal of Materials Processing Technology*, vol. 238, pp. 437–445, 2016, doi: 10.1016/j.jmatprotec.2016.08.003.
- [64] X. Ai et al., "A high Fe-containing AlSi12 alloy fabricated by laser powder bed fusion," *Journal of Materials Research and Technology*, vol. 18, pp. 4513–4521, 2022, doi: 10.1016/j.jmrt.2022.04.008.

- [65] A. Zakay and E. Aghion, "Effect of post-heat treatment on the corrosion behavior of AlSi10Mg alloy produced by additive manufacturing," *JOM*, vol. 71, no. 3, pp. 1150–1157, 2019, doi: 10.1007/s11837-018-3298-x.
- [66] J. de Damborenea, A. Conde, M. Gardon, G. A. Ravi, and M. A. Arenas, "Effect of growth orientation and heat treatment on the corrosion properties of AlSi10Mg alloy produced by additive manufacturing," *Journal of Materials Research and Technology*, vol. 18, pp. 5325–5336, 2022, doi: 10.1016/j.jmrt.2022.05.021.
- [67] R. I. Revilla and I. De Graeve, "Influence of Si content on the microstructure and corrosion behavior of additive manufactured Al-Si Alloys," *Journal of the Electrochemical Society*, vol. 165, no. 13, pp. C926–C932, 2018, doi: 10.1149/2.0101814jes.
- [68] J. Wu, X. Q. Wang, W. Wang, M. M. Attallah, and M. H. Loretto, "Microstructure and strength of selectively laser melted AlSi10Mg," *Acta Materialia*, vol. 117, pp. 311–320, 2016, doi: 10.1016/j.actamat.2016.07.012.
- [69] J. Lei, J. Xie, S. Zhou, H. Song, X. Song, and X. Zhou, "Comparative study on microstructure and corrosion performance of 316 stainless steel prepared by laser melting deposition with ring-shaped beam and Gaussian beam," *Optics & Laser Technology*, vol. 111, pp. 271–283, 2019, doi: 10.1016/j.optlastec.2018.09.057.
- [70] O. O. Salman, C. Gammer, A. K. Chaubey, J. Eckert, and S. Scudino, "Effect of heat treatment on microstructure and mechanical properties of 316L steel synthesized by selective laser melting," *Materials Science and Engineering: A*, vol. 748, pp. 205–212, 2019, doi: 10.1016/j.msea.2019.01.110.
- [71] K. Abd-Elghany and D. L. Bourell, "Property evaluation of 304L stainless steel fabricated by selective laser melting," *Rapid Prototyping Journal*, vol. 18, no. 5, pp. 420–428, 2012, doi: 10.1108/13552541211250418.
- [72] R. F. Schaller, A. Mishra, J. M. Rodelas, J. M. Taylor, and E. J. Schindelholz, "The role of microstructure and surface finish on the corrosion of selective laser melted 304L," *Journal of the Electrochemical Society*, vol. 165, no. 5, pp. C234–C242, 2018, doi: 10.1149/2.0431805jes.
- [73] A. Hemmasian Ertefagh and S. Guo, "Electrochemical behavior of AISI316L stainless steel parts produced by laser-based powder bed fusion process and the effect of post annealing process," *Additive Manufacturing*, vol. 22, pp. 153–156, 2018, doi: 10.1016/j.addma.2018.05.014.
- [74] Y. Sun, A. Moroz, and K. Alrbaey, "Sliding wear characteristics and corrosion behaviour of selective laser melted 316L stainless steel," *Journal of Materials Engineering and Performance*, vol. 23, no. 2, pp. 518–526, 2014, doi: 10.1007/s11665-013-0784-8.
- [75] G. Chen, S. Y. Zhao, P. Tan, J. Wang, C. S. Xiang, and H. P. Tang, "A comparative study of Ti-6Al-4V powders for additive manufacturing by gas atomization, plasma rotating electrode process and plasma atomization," *Powder Technology*, vol. 333, pp. 38–46, 2018, doi: 10.1016/j.powtec.2018.04.013.
- [76] A. Aksoy and R. Ünal, "Effects of gas pressure and protrusion length of melt delivery tube on powder size and powder morphology of nitrogen gas atomised tin powders," *Powder Metallurgy*, vol. 49, no. 4, pp. 349–354, 2006, doi: 10.1179/174329006X89425.

- [77] T. Kurzynowski, K. Gruber, W. Stopyra, B. Kuźnicka, and E. Chlebus, “Correlation between process parameters, microstructure and properties of 316 L stainless steel processed by selective laser melting,” *Materials Science and Engineering: A*, vol. 718, pp. 64–73, 2018, doi: 10.1016/j.msea.2018.01.103.
- [78] A. Strondl, O. Lyckfeldt, H. Brodin, and U. Ackelid, “Characterization and control of powder properties for additive manufacturing,” *JOM*, vol. 67, no. 3, pp. 549–554, 2015, doi: 10.1007/s11837-015-1304-0.

T&F Proofs – Not for Distribution

Part II

Fabrication—the art of realization

Chapter 5

Fabrication techniques for printed and wearable electronics

G R Raghav, M S Anoop, P C Jayadevan, R Ashok Kumar,
K J Nagarajan and D Muthukrishnan

In the modern era, smart devices play an important role in day-to-day life, and their widespread applications are getting huge demand globally. Innovation in the field of the Internet of Things paves new possibilities for future endeavors of mankind. Printed electronics is a sustainable way for achieving the widespread popularity of smart devices around the world and this technology is in its nascent stage. In the current scenario, massive amounts of e-waste generated due to the digital revolution and its disposal become a greater challenge for sustainability. Printed electronics are composed in a process of registering thin functional material (ink) layer combinations on a low-cost substrate that will degrade naturally. This article discusses the possibilities of printed electronics and its ability to hurdle the limitations of traditional high-cost electronics, based on rigid silicon, and the production of different devices on flexible substrates. Efficient use of materials, optimized energy consumption both in production and utilization, reduction in hazardous substances, and enhanced recyclability are the several benefits associated with printed electronics technology. The additive manufacturing method is used in printed electronics technology and the rate of production is much improved as compared with other processes. The materials used for printed electronics like ink and substrates are derived from synthetic or natural polymers. The above-stated reasons make printed electronics a technology for the future digital revolution. This article discusses various fabrication techniques like lithographic process for the production of printed electronics and its application in a sustainable manner.



5.1 Introduction

Printed or wearable electronics have good potential to be utilized as eco-friendly and biodegradable electronics so as to reduce electronic wastes, which is also known as

e-waste. Electronic wastes are due to the large number of electronic devices, which are disposed of every day [1, 2]. Another advantage of printed or wearable electronics is that it can be used in complex surfaces. Wearable devices thus help in improving the country's economic growth because of the sudden surge in printed or stretchable electronic devices. Now due to the advancement of artificial intelligence, electronic devices with artificial intelligence assistance have a great impact on the electronics industry. There are many conventional manufacturing processes to manufacture printed or wearable electronic devices. But due to the wastage of materials, and in order to avoid secondary operations such as etching and masking, the additive manufacturing process is most preferred in recent times. The printing process is also known as the additive method of manufacturing electronic applications by depositing electronic materials using functional inks along with the normal printing process [3]. As discussed earlier, this process thus eliminates the need for etching and masking and thereby involves environmentally friendly cleaner production compared to that of other traditional methods [4].

Nowadays a lot of sports and fitness equipment utilizes these wearable technologies in monitoring exercise and detecting the glucose level of diabetics [5]. Also, recently many printed and wearable devices have been made up of flexible or stretchable materials, which are used as sensors, that have close contact with human skin [6, 7].

The printing of electronic devices is classified into two types, one is contact type and the other is non-contact type. In the contact printing method, the die or pattern is immersed in a functional ink, and it is transferred onto the substrate by means of physical transfer. Screen printing, offset printing, flexography, and pad printing are the few types of contact printing [8].

On the other hand, in the non-contact printing process, the functional ink is sprayed via a nozzle onto the target substrate. There are two common types of non-contact printing processes, (i) inkjet printing and (ii) aerosol printing [9]. Normally the printing process is characterized by three steps or stages:

- (i) Selection of materials
- (ii) Printing process
- (iii) Sintering/drying process

After transferring ink onto the substrate either by contact or non-contact mode, it is very important to sinter the printed surface so as to achieve the desired properties of ink and the substrate. Figure 5.1 shows the steps involved in printed electronics manufacturing. Even though producing flexible electronic devices with required properties and specification is difficult for mass production, current technology and materials development has shown a positive trend in both performance and biodegradable properties. Because of this development, printed or wearable devices are developed for varying applications such as Radio Frequency Identification devices (RFID), organic light emitting diodes, thin-film transistors (TFT), photo-voltaic cells, energy devices such as batteries, and different types of sensor devices [10–12].

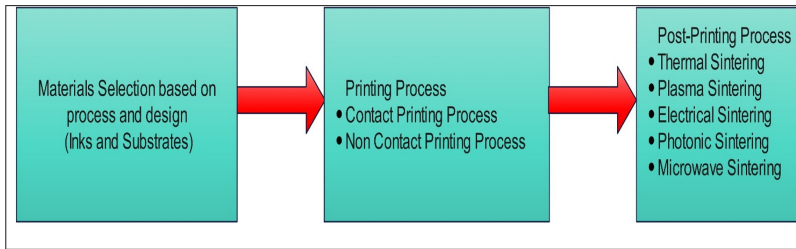


Figure 5.1. The steps involved in printed electronics manufacturing.

In this chapter, we provide the basic principle of various printing or fabrication techniques used for the development of wearable electronics. Further, this chapter will give clear insight into different materials and substrates employed.

5.2 Different types of flexible and printed electronic materials

In this part, we will explore the different types of materials used in flexible or printed electronics.

5.2.1 Inks used in printed electronics

In the production of wearable/printed electronics, inks play a vital role in creating structures or skeleton, which has a particular function. For printing of very complex electronic parts, different types of inks are used such as insulator/dielectric inks, semiconductor inks, and conducting inks. An important property of functional inks is the compatibility with other inks for simultaneous application, and it should be able to form uniform homogenous layers over the substrate. The inks used for wearable devices contain solvents, polymers, or resins. The inks can be made up of either organic or inorganic materials. Sometimes some additives will be added to improve the properties of the inks and avoid clogging of inks [13, 14].

5.2.1.1 Conducting ink materials

There are different types of conductive inks that are synthesized as nanoparticles. The nanoparticle inks are then dissolved onto the conductive polymer matrix [15]. Mostly metal nanoparticles are used as conductive ink material. Even though metal nanoparticle-dispersed inks have better properties, the synthesis of metal nanoparticles is very difficult and requires more time and labor. Moreover, stabilizers are necessary to prevent agglomeration in functional inks. The sintering process, which is the post-printing process, requires heating above 100 °C so as to cure macro particle-dispersed inks, whereas, for nanoparticle-dispersed inks, the sintering temperature can be less than 100 °C [16]. Silver nanoparticle inks are one type of conducting inks. The silver nanoparticle-dispersed inks are toxic due to the evolution of silver ions; hence, the application of nanosilver inks is limited [17]. On the other hand, metal-organic decomposition inks use metal particles as precursors and evaporable alcohols as solvents. Thus, the agglomeration of nanoparticles is prevented. But due to the evaporation of the solvents, there may be non-

uniformity in the deposited patterns. This non-uniformity will result in a decrease in conductivity [18]. Nonetheless, this drawback can be overcome by applying or printing successive layers one over another using the same ink [19].

The most widely used conductive inks are aluminum, copper, gold, and silver metal-dispersed inks. When talking about properties, silver-based conductive inks have better conductivity compared to that of copper-based inks. The silver-based inks have a good ability to resist oxidation. However, with the increase in oxidation, the conductivity decreases. The oxidation of metal nanoparticle-dispersed inks can be prevented by coating antioxidants over the nanoparticles or *in situ* synthesis in an organic solvent with a protective layer. Whereas the above-said methods are temporary solutions to control oxidation, new methods such as forming a bio-metallic core-shell or formation of a thick shell are made up of non-oxidizing conductive materials [15]. Gold is also one of the important conductive ink materials, which is eco-friendly and can be cured at very low temperatures. Whereas gold conductive inks are costly compared to other conductive inks. Another ink is aluminum-based ink, which can be synthesized using organic solvents, but aluminum inks are reactive in nature and tend to oxidize very quickly.

Apart from metal-dispersed inks, carbon-based inks such as carbon nanotubes (CNTs), graphene, and C60 can be altered and modified for applications such as conductive inks. The CNT's reinforced metallic conductive inks exhibit better stability, conductivity, and flexibility. The conductivity of CNT's reinforced metallic inks increases with the increase in thickness. The graphene and C60 also exhibit good light transmittance, flexibility, and conductivity. The light transmittance decreases when the number of graphene layers increases, whereas the conductivity increases with an increase in graphene layers [16, 20].

The recent development in conductive inks is the conducting polymers-based inks. They are very cheap, very light in weight, flexible in nature, and can be used in aqueous solvents as well as organic solvents. The main disadvantage of conductive polymer inks is their poor conductivity compared to metal inks, and production of conductive polymer inks is very difficult due to their processing difficulties, stability, and lesser solubility compared to metals. The polymer-based conductive inks are classified into the following types:

- (i) Organic metal chelates
- (ii) Conjugated polymers
- (iii) Polymer electrolytes

The poly(3,4-ethylenedioxythiophene) polystyrene sulfonate is one type of conductive polymer that has good conductivity and decent temperature stability. There are a few other conductive polymers for the application of functional inks such as polypyrrole, polyacetylene, and polyacene [21]. Apart from the above materials, there are conducting ceramics, which are doped to improve conducting properties of ceramics. For example, aluminum-coated zinc oxide, indium-coated tin oxide (ITO), and gallium-coated zinc oxide. Among these, the ITO is most widely used for electronics applications, owing to its enhanced conductivity. But it should be noted that indium is a rare earth material, and hence, it is very costly [22]. Normally there

are two types of ITO conductive inks. One type of ink is *in situ* sol–gel-based inks, and another type is nanoparticle-dispersed conductive ink. The sol–gel-derived ITO conductive inks have better conductivity compared to nanoparticle-dispersed ITO inks.

5.2.1.2 Dielectric ink materials

In printed or wearable electronics, the capacitor and insulator layers are made up of dielectric materials. In order to be a good insulator, the layers of dielectric materials should be thick and uniform. However, it is difficult to print dielectric materials as compared to conductive materials. There are some substrate materials that are dielectric in nature such as silk, gelatine, cellulose, etc [2]. There are many dielectric materials based on polymers, with less density, less toughness, and less curing temperature. The most widely used dielectric polymers are polydimethylsiloxane (PDMS), polylactic acid (PLA), polymethyl methacrylate (PMMA), and polyvinyl alcohol [22].

5.2.1.3 Semiconducting ink materials

The semiconducting material is most commonly used as an active layer. There are many semiconducting materials such as silicon, CNTs, and different derivatives of graphene owing to their mechanical and semiconducting properties. The multiple layers of graphene can improve the semiconducting properties of wearable devices. There are few ceramic materials that can be used as semiconductors. But semiconducting ceramic materials are very rare and expensive. They also require high sintering temperatures for curing the printed layers [23, 24].

In flexible and printed electronic applications, the semiconducting functional inks can also be prepared by dissolving polymers in specific solvents. Hence, these types of polymer-based semiconducting inks can be used either as p-type or n-type materials. Polymers like polyfluorenes are most widely used as semiconducting polymers. Poly(3-alkyl thiophene) is an example of a p-type semiconducting material that uses holes for charge transfer, whereas n-type conducting polymers such as poly(9,9-dioctyl-fluorene-co-bithiophene) (F8T2) uses electrons for charge transfer [2].

5.2.2 Substrate materials for printed electronics

The substrate forms the base for any printed electronic devices. This substrate can also act as an insulator. The conventional substrate materials are strong and can remain rigid for quite a long period. Even though these materials possess good rigidity, conventional substrates are more brittle; hence, it is very difficult to machine conventional substrates for flexible or wearable devices. However, the development of flexible, biodegradable, and light polymer substrates has resulted in the rapid improvement of wearable devices with a long service life [25]. The substrate can be made up of natural or synthetic materials. These substrates are highly flexible, heat resistant, thin, low weight, and low cost [21]. Another important step in printed electronics is post-treatment, also known as the sintering process.

This sintering process might damage the surface of the substrate. So, materials with good thermal resistance should be considered for substrates.

5.2.2.1 *Biodegradable polymeric substrates*

Nowadays paper-based substrates are replacing conventional printed electronics because of their flexibility, biodegradability, and low cost [26]. However, the paper substrates have disadvantages such as porosity, surface roughness, and poor resistance to moisture. But the properties of paper-based substrates can be improved by metallic or ceramic coating as per the application [27]. Nano cellulose is another important contender for substrates because of its heat resistance, better surface smoothness, transparent nature, and good mechanical properties [21, 28]. Similarly, starch, silk, and shellac were also considered for the fabrication of substrates. Silk is a biodegradable material with better properties. Shellac is also a naturally available resin that can be used for preparing substrates in printed electronics. These materials have good surface smoothness, and further, these materials are relatively cheaper [28].

5.2.2.2 *Synthetic polymer substrates*

Polymer-based substrates are most widely used for printed electronic substrates. Polyethylene terephthalate (PET), polycarbonate, polyethylene naphthalate (PEN), and polyimide are the most commonly used synthetic polymers in flexible electronic applications [2]. Because of its high flexibility, transparency, and resistance to solvent, PET is the most preferable and commonly used substrate material in flexible electronic devices. Polycarbonate substrates have high rigidity, are light in weight, and possess good mechanical properties. Although PEN has good transparency, it is very costly [29].

There are a few synthetic biodegradable polymers such as PLA, polyvinyl alcohol, PDMS, and polyethylene glycol, which can be utilized for the fabrication of substrates. The PLA is stiff in nature but possesses very poor heat resistance. Whereas PDMS can be used as substrates in flexible or stretchable electronic applications owing to their elastic nature. The need for producing flexible devices increases day by day. The research based on the direct printing of flexible or wearable electronics on polymer and fabric substrates is getting widespread acceptance.

5.3 Fabrication methods for printed electronics

Figure 5.2 shows the different types of fabrication methods in developing printed or wearable electronic devices. It includes inkjet printing, offset printing, gravure printing, screen printing, and flexography. These methods are also classified into two types: contact and non-contact printing processes [8]. The inkjet printing and aerosol printing are contactless printing processes. There are some methods that involve both printing and deposition or coating techniques. The basic purpose of this printing or deposition is to develop multiple layers of structures that can be a conductive layer, semiconducting structure, or insulating structure for printed

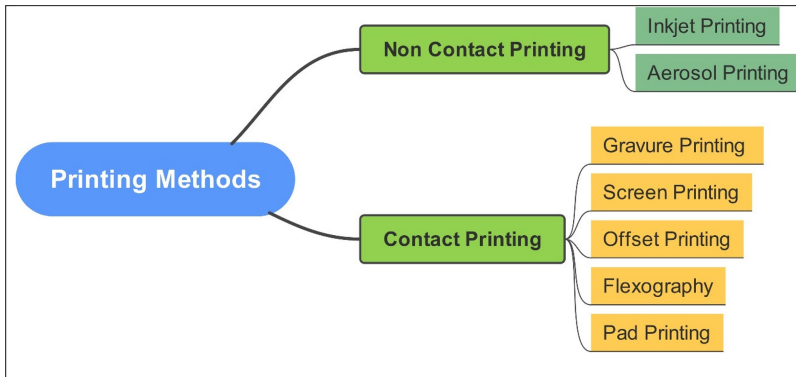


Figure 5.2. The different types of fabrication methods in developing printed or wearable electronic devices.

electronic devices. After the coating or deposition process, the functional inks will change their phase and orientation. This change in phase and flow rate on the coated substrate are mainly due to the viscosity of the ink material. It is also to be noted that the higher the viscosity, the higher the efficiency. The density of the ink is also important property for developing effective wearable devices. The surface tension is the property by which the ink can stick to the surface of the substrate. The evaporation rate and sintering temperature of the ink also play a vital role in the quality of flexible electronic devices [30]. The most commonly available printed electronic device is RFID stickers or flexible antennae, where antennas can be printed. The printing of RFID on flexible or printed substrates is a very efficient method, since it is a lighter, smaller, and cheaper device compared to conventional RFID antennas. The high-volume production techniques for printed electronics are offset printing, gravure method, and flexographic method. These techniques are utilized for the mass production of solar cells, sensors, etc. The organic or inorganic conducting materials can be printed using flexography and offset methods. The organic semiconductors and insulators are coated using the gravure printing method.

Recently, many new novel printing methods are identified and employed in the manufacturing of flexible or wearable devices. Devaraj *et al* developed a method known as the form-fuse method. In this method, silver nanoparticles are coated on polymer films by using an aerosol jet with mask and without mask. The entire process is carried out in a vacuum to develop desired shape and pattern. The sintering process is carried out to reduce the resistivity of printed materials [31]. Constante *et al* [32] also developed a new 4D coating method employing a 3D extrusion process along with melt-electro writing, which proves to be a good potential method for the development of flexible devices. Table 5.1 shows the important parameters of different printing methods. The inkjet method is more suited for high-quality research applications. The screen printing method is most useful for printing multiple layers, whereas the flexographic and gravure methods

Table 5.1. Parameters of different printing methods.

S. No.	Printing methods	Throughputs m ² s ⁻¹	Resolution lines cm ⁻¹	Operating speed m min ⁻¹
1	Gravure printing process	3–60	20–400	100–1000
2	Screen printing process	2–3	50	10–15
3	Offset printing process	3–30	100–200	100–900
4	Flexography printing process	3–30	60	100–700
5	Inkjet printing process	0.01–0.5	60–250	15–500

are useful for mass production. The output rate of the inkjet printing method is 0.5 m² s⁻¹, which is much less compared to other methods.

5.3.1 Contact printing of flexible electronics

In contact printing, the functional ink is transferred onto the substrate directly. This method is also known as roll-to-roll printing or transfer printing. The roll is used to transfer the ink to the substrate. The major disadvantage of this method is the large time consumption and high initial cost of the equipment. But the production cost is low and has good reproducibility, which makes them favorites for mass production [33, 34].

5.3.1.1 Gravure printing method

Gravure printing is the process in which the design to be printed on the substrate is first engraved on the printing cylinder, also known as the gravure cylinder. The doctor blade, which is made of steel, is used to remove the excess ink present in the printing cylinder before the ink is transferred to the impression cylinder from where the design is transferred onto the surface of the substrate as shown in figure 5.3. The printing cylinder is made up of rubber. The printing or gravure cylinder is made up of steel coated with copper. This process utilizes inks with low viscosity and possesses good efficiency. This method of printing proved to be more economical with good-quality printing. The quality of printing can be improved by using electrostatic forces for transferring ink onto the substrate [9].

It is to be noted that many devices such as antennas, TFTs, pressure sensors, surface-enhanced Raman scattering (SERS), and electrochemical sensors are developed using the gravure printing method [35]. Recently a wrinkle-structured solvent-excluded surface substrate developed for the detection of drugs like cocaine was fabricated by Maddipatla *et al* as shown in figure 5.4(A). In this study, the wrinkle-shaped structures were developed on the thermoplastic polyurethane (TPU) substrates by varying the proportions and printing silver ink of 150 nm particle size onto the TPU substrate using the gravure process [36]. Another recent study also utilizes the gravure printing process for fabricating a novel RFID antenna made up of paper substrate as shown in figure 5.4(B). In this work, Zhu *et al* manufactured a

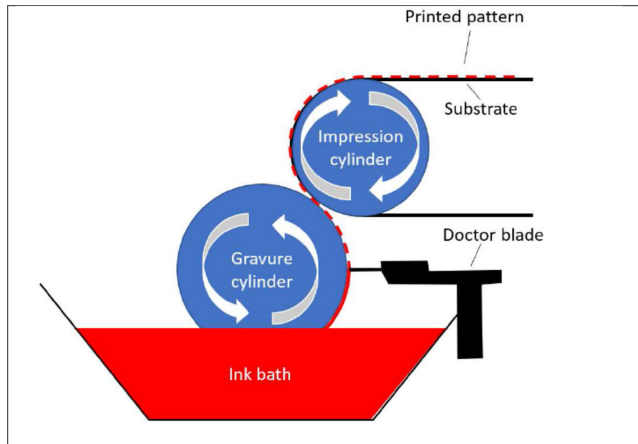


Figure 5.3. The Schematic representation of the Gravure printing process, reprinted from [13] with permission from MDPI, Copyright (2021).

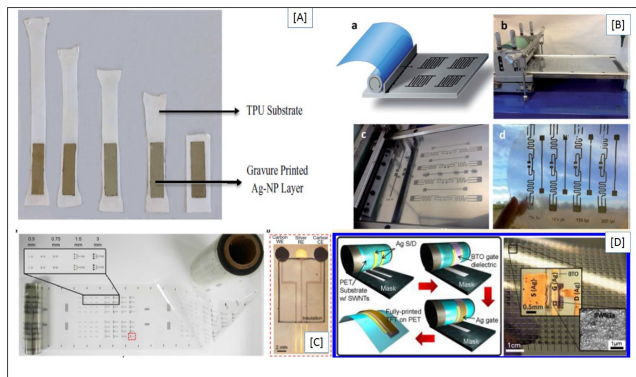


Figure 5.4. (A) Wrinkle SERS substrate, reprinted from [36] with permission from Elsevier, Copyright (2019). (B) RFID antenna made up of nano-paper, reprinted from [37] with permission from RSC, Copyright (2014). (C) PET-based electrochemical sensors for the detection of heavy metals, ions, and metabolites, reprinted from [38] with permission from ACS, Copyright (2018). (D) High-performance TFT made up of CNTs, reprinted from [39] with permission from ACS, Copyright (2013).

nano-structured paper by employing cellulose nanofibers and UHIF RFID tag, also known as squiggle, fabricated by depositing silver ink onto the paper substrate [37]. Bariya *et al* developed electrochemical sensors using PET for the detection of heavy metals, ions, and metabolites as shown in figure 5.4(C). Here the working and counter electrode is the carbon electrode, and silver is used as the reference electrode [38]. Lau *et al* fabricated CNT-based TFTs through the gravure printing process as shown in figure 5.4(D). In this work, silver ink is deposited as drain, gate, and source electrodes on WCNT-coated PET substrates. The nano barium titanate is printed as insulator layers. This gated TFT exhibits better performance, high flexibility, and minimal hysteresis [39]. In the process of gravure printing, the gravure cylinder, also

known as the printing cylinder, contains patterns that are very expensive, and further during the process of printing, a small percentage of the inks gets clogged due to evaporation and dries out in the printing cylinder, thereby reducing the quality of succeeding printings. The availability of functional ink is very low in the case of both gravure and flexography printing processes. These two processes are widely adopted in all graphics and packaging applications because of their ability for mass production. The major disadvantage or task involved in these two printing processes is that the development of functional ink, which requires hours of research and development, incurs more cost. Owing to the above details, the research undertaken based on the gravure and flexography printing process is very minimal when compared to that of the inkjet and screen printing process.

5.3.1.2 Screen printing

The screen printing process is also known as push-through method, which uses an ink of sticky nature. The ink is transferred onto the substrate through a screen, which may be made up of wire, plastic, and metals. This method can be done using bare hands or by using fully or semi-automatic systems. The coating machine consists of the following parts: (i) stencil, (ii) squeegee, and (iii) screen as shown in figure 5.5. The squeegee is the material that is made up of rubber. The design to be printed on the substrate is engraved on the screen, and the ink is allowed to pass through the screen either by means of pushing or squeezing the screen. Thus, the ink is transferred onto the substrate [40].

In this process, the quality of printing depends on wire diameter, the thickness of the emulsion, the mesh count of the screen, offset height, and screen deflection angle. This process has a good output rate at a low cost, and there is very minimal wastage of materials. The screen printing is very famous for its flexibility. There are many flexible or wearable electronics such as wearable sensors fabricated using a screen printing process and exhibiting similar properties to that of conventionally manufactured electronic devices. A piezoelectric touch sensor was fabricated using screen printing by Emamian *et al* [41]. They fabricated the sensor using polyvinylidene fluoride-based piezoelectric layer covered at the top and bottom by silver layers.

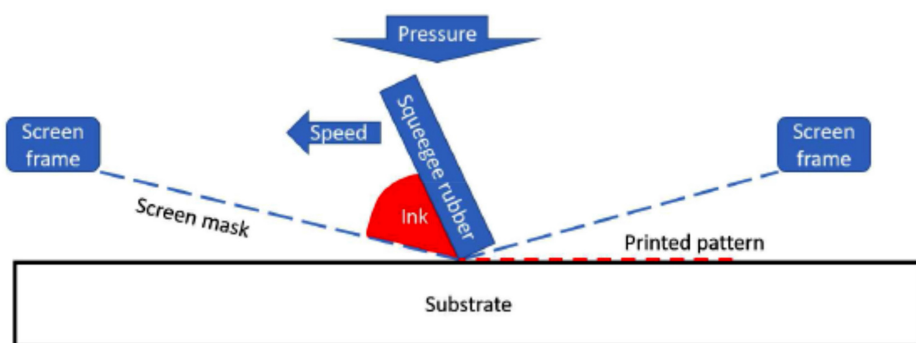


Figure 5.5. Schematic representation of screen printing, reprinted from [13] with permission from MDPI, Copyright (2021).

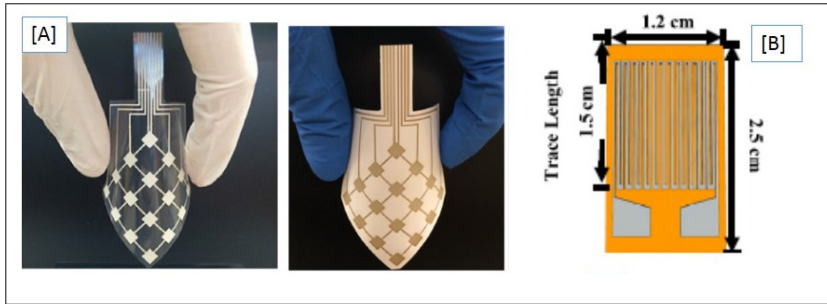


Figure 5.6. (A) Touch sensor based on polyvinylidene fluoride on PED and paper substrates, reprinted from [41] with permission from Elsevier, Copyright (2017). (B) Schematic representation of the RTD sensor, reprinted from [42] with permission from IEEE, Copyright (2019).

These layers are coated using a screen printing process on PET and paper substrate as shown in figure 5.6(A). This PET substrate sensor has an observed sensitivity of 1.2 V N^{-1} , and the paper substrate sensors exhibit 0.3 V N^{-1} sensitivity. Hence, these sensors have good potential in applications such as robotics and sensors in automobiles. A sensor for temperature detection was developed by Turkani *et al.* They fabricated Ni-coated polyimide substrate sensors for detecting a wide range of resistance temperatures starting from $-60 \text{ }^\circ\text{C}$ to $180 \text{ }^\circ\text{C}$. This flexible resistance temperature detector (RTD) exhibits good repeatability and stability at all temperatures [42]. Figure 5.6(B) represents the RTD sensors. A flexible and stretchable sensor was fabricated by Bose *et al* using the screen printing process. The ink used for printing is silver ink, and the substrate is made up of TPU. The outcomes of the above work are that 20% of strain was detected by the wavy configured sensor, and they also exhibited excellent flexibility compared to conventional sensors. There are many studies that show that the screen printing process is the most viable and cost efficient [43–46]. This process can be utilized for the fabrication of flexible, wearable, and stretchable electronics [47, 48].

5.3.1.3 Offset printing process

This method is also known as the indirect printing method, because the ink is transferred from the initial or printing cylinder to the intermediate or blanket cylinder. From the blanket cylinder, the ink is transferred onto the substrate as shown in figure 5.7. The water roller will apply a small amount of water to the undesired part of the pattern so as to remove the ink. Surface engineering is an important aspect of offset printing. The image or desired areas accept the presence of ink but reject water, whereas undesired or non-image areas repel ink and accept water. The spreading of ink can be controlled by the surface energy. The ink is transferred to the paper substrate at pressure. In this process, the multiple layers of inks are coated simultaneously without an intermediate drying process; hence, this process is also called a wet-on-wet printing process. The coated inks are dried due to evaporation, absorption, and polymerization [49, 50].

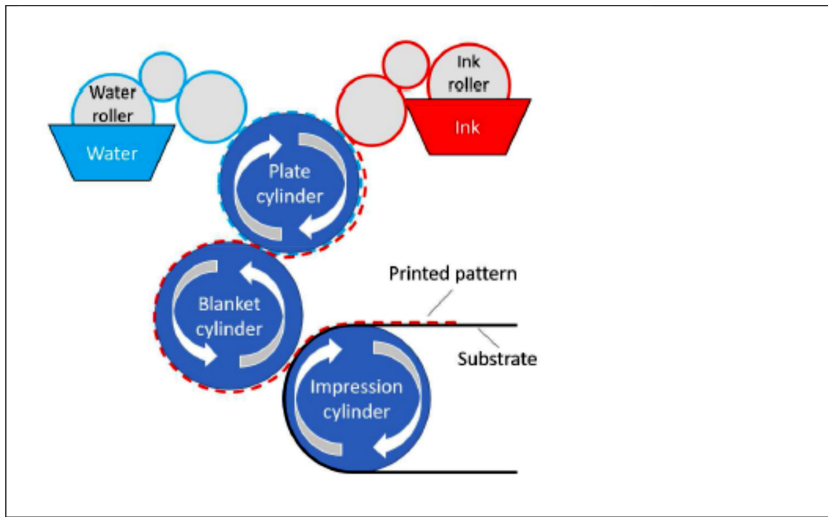


Figure 5.7. Schematic representation of the offset printing process, reprinted from [13] with permission from MDPI, Copyright (2021).

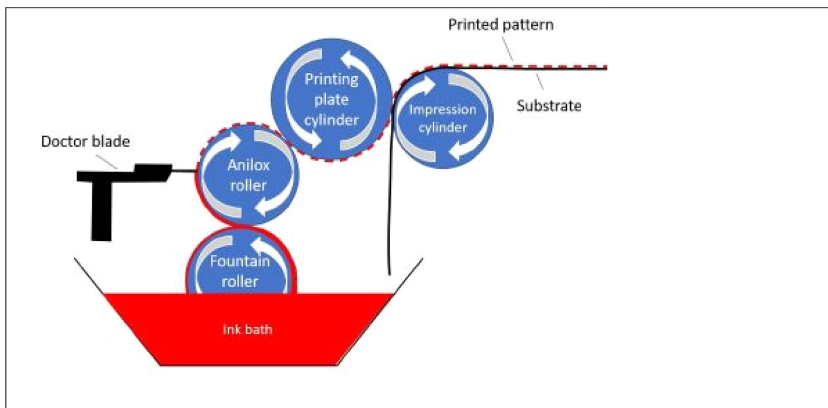


Figure 5.8. Schematic representation of the flexography printing process, reprinted from [13] with permission from MDPI, Copyright (2021).

5.3.1.4 Flexography printing process

The flexographic printing process is a kind of roll-to-roll printing process that has high throughput. Flexographic printing is also known as the rotational printing process. This method is an indirect contact-based printing method that has the ability to print ink of varying thicknesses with good resolution. As shown in figure 5.8, the flexography printing machine consists of the following parts [40]:

- (i) Printing cylinder
- (ii) Anilox cylinder

- (iii) Impression cylinder
- (iv) Ink reservoir
- (v) Doctor blade

A cylinder made of steel, which is otherwise called an anilox cylinder is used to transfer ink from the reservoir. The cylinder is engraved with a design on its surface, normally the anilox cylinder is made up of ceramics or chromium. Then the ink is transferred onto the printing cylinder, which is also known as a printing plate. Then from the printing plate, the ink is transferred to the target substrate. When compared to screen printing and inkjet printing, the flexographic process has high processing speed. This method is most widely used in printing graphics and in printing operations in packaging industries. There are only very few studies in flexible electronics manufacturing through the flexographic printing process [51, 52]. CNT-based flexible TFTs were developed by Higuchi *et al* as shown in figures 5.9(A) and (B). They deposited nano silver ink, resist ink, and polyimide ink as source, gate and drain gates electrodes, CNT patterner, and insulator over a thin film made up of PEN fabricated through a flexographic printing process. The CNTs synthesized using chemical vapor deposition were coated out of the TFT electrodes. The TFT developed using flexographic printing has exhibited good stability and mobility. A paper-based sensor (strain) was developed by Maddipatla *et al*. They developed silver ink-coated strain gauges through a flexographic printing process. The strain gauges are of different lengths. This sensor has the ability to detect even small displacements of the order of 1 mm with good repeatability [53].

5.3.1.5 Pad printing process

Pad printing is a method in which a 2D pattern or cliché is printed on a 3D substrate or object, as shown in figure 5.10. This process utilizes an indirect offset printing method, in which the ink is transferred from the cliché or a stereotype using a silicon pad. This process is widely used as a replacement for the screen printing process. The products such as transistor electrodes are manufactured using this printing process [55].

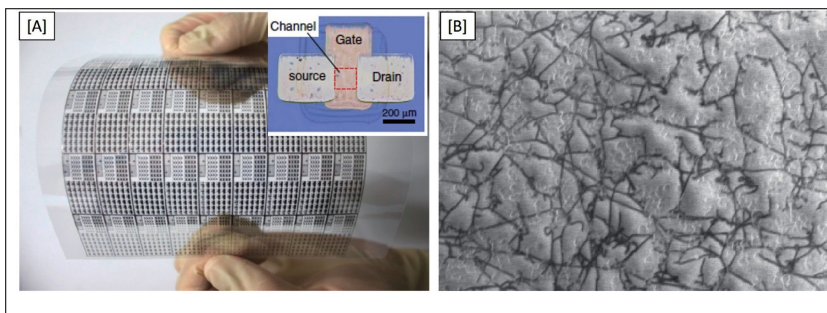


Figure 5.9. (A) TFT sensor based on CNTs fabricated on PEN substrate using flexography process. (B) Scanning electron microscopy image of CNT film [54], reprinted from [54] with permission from IOP Publishing, Copyright (2013).

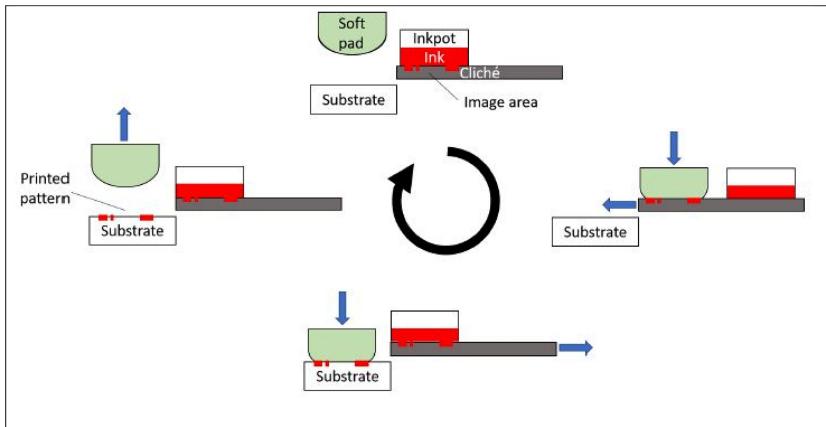


Figure 5.10. Schematic representation of the pad printing process, reprinted from [13] with permission from MDPI, Copyright (2021).

5.3.2 Non-contact printing methods

The non-contact printing process is one in which the nozzles are utilized to spray the ink onto the substrate without any contact with the substrate. The advantage of non-contact printing is that the life of the nozzle is longer because of less contamination, although the non-contact printing process is slow compared to the roll-to-roll manufacturing process. However, the efficiency of the non-contact mode is higher compared to the contact printing process, and it is possible to print computer-aided design (CAD) models, which is not feasible in the contact printing process. Hence, contact printing can be used to manufacture prototypes or used for highly demanded products [56].

5.3.2.1 Inkjet printing process

The inkjet printing process is a type of additive manufacturing process, which transfers ink onto the substrate based on digital CADs and does not utilize any physical patterns. Normally, the inkjet printing process uses inks with low viscosities so that deposition on ink will be easily compared to highly viscous ink. The inkjet printing process is of two types: (i) drop-on-demand and (ii) continuous printing. A voltage source is used to maintain a continuous flow of ink on the substrate. The inkjet printers, which use a thermal source, are very widely used in the packaging and graphic designing industries. In drop-on-demand inject printing, the inks are forced toward the substrate based on the digital signal received from the computers [40, 57]. The droplets can be generated either by means of piezoelectric or thermal methods, which is shown in figures 5.11(A) and (B). In thermal energy-based inkjet printers, the inks are enforced out of the printer nozzle by means of vaporization of ink. The volume of the printer nozzle is compressed or decompressed based on the digital input from the computers and the inks are dispersed out of the nozzle in piezoelectric printers. However, the drop-on-demand-based inkjet printing process was most widely used in flexible or wearable electronic fabrication processes owing

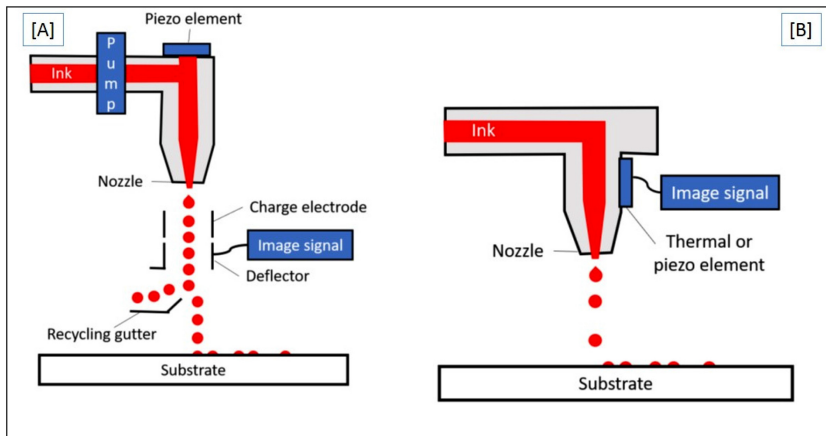


Figure 5.11. Schematic representation of (A) continuous printing and (B) drop-on-demand printing, reprinted from [13] with permission from MDPI, Copyright (2021).

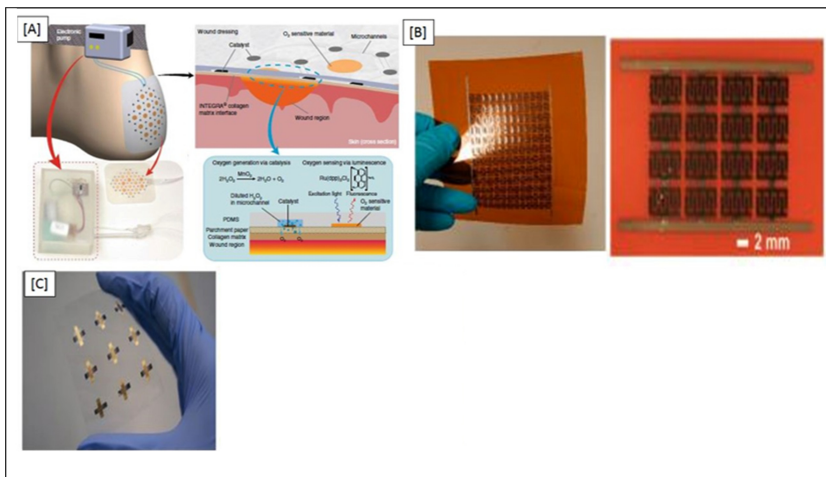


Figure 5.12. (A) Represents the bandage made up of flexible paper for sensing and delivery of oxygen in the treatment of chronic wounds, reprinted from [59] with permission from SPIE, Copyright (2018). (B) Supercapacitors based on graphene used as electrodes, reprinted from [65] with permission from ACS, Copyright (2017). (C) Metal–insulator–metal capacitor fabricated using inkjet printing, reprinted from [61] with permission from Nature, Copyright (2019).

to its advantages such as cost efficiency, high resolution, and easy fabrication without masks [58].

There are various types of flexible or wearable devices that are manufactured through inkjet printing methods. A paper-based oxygen-sensing and delivery sensor in bandage form was fabricated using an inkjet printing process by Ochea *et al.* This bandage was intended to treat chronic wounds as shown in figure 5.12(A). In this work, parchment paper was employed as the substrate over which manganese oxide

and ruthenium inks are deposited, which has the ability to generate and measure oxygen in the wounded area. It is also reported that by varying the thickness of the manganese oxide layer, the oxygen concentration was controlled. The ruthenium coated on the substrate facilitates contactless measuring of oxygen at the wounded region owing to the fluorescence nature of ruthenium ink. These smart bandages also possess good mechanical properties and flexibility compared to that of conventional bandages but also possess additional properties such as oxygen generation, delivery, and therapeutics [59].

The wounds are not the same in nature; it varies according to the type of injuries, location of injuries, and the depth of injuries. Hence, the different concentration of oxygen generation and different therapeutics is necessary. The fabrication of smart bandages that should be done using the inkjet printing process is very important to carry out further research and to customize bandages for mass production. Hence, the importance of this work is in the treatment of wounds [60].

A graphene based super micro capacitors manufactured using exfoliation of graphene using electrochemical process for the application of electrodes and collectors of current and poly(4-styrenesulfonic acid) as ink. The image of the supercapacitors is shown in figure 5.12(B). A metal–insulator–metal capacitor fabricated by Mikolajek *et al* using inkjet printers as shown in figure 5.12(C). The silver ink is coated as metal electrodes and the PMMA/BST₁ is coated as an insulator on PET substrate using inkjet printing process. By using this process, thin, homogeneous, and smooth layers along with better resolution and fewer defects. This PMMA/BST composite insulator layer shows a better dielectric constant when compared to that of pure PMMA [61]. A flexible microfluidic sensor was designed and fabricated by Narakathu *et al* using inkjet printing. This silver-coated sensor has the capacity to detect different hazardous chemicals such as cadmium sulfide, molybdenum disulphate, and mercury sulfide by electrochemical impedance spectroscopy [62]. Because of the attractive characteristics of the inkjet printing process, which includes high resolution and ease of fabrication, a lot of researchers are attracted to develop devices such as SERS substrate sensors for detecting gases, antennas, and bandages [63]. In the inkjet printing process, the clogging of nozzles happens due to the faster rate of evaporation and agglomeration of ink particles, which in turn reduces the efficiency of inkjet printing. Hence, frequent cleaning of the nozzle is a big challenge. Also, the nozzle cartridges for one-time use are usually expensive, owing to the inkjet printing process speed, which is very slow, and the use of the nozzle increases the production time compared to other contact printing processes [64].

Q5

5.3.2.2 Aerosol printing process

In the aerosol printing process, the ink is atomized so as to reduce the size of the ink droplets in the range of 1–5 μm in diameter as shown in figure 5.13. The ultrasonic technique or pneumatic method can be utilized to atomize the ink droplets. This system is entirely maintained in vacuum condition, and the ink is directed toward the ceramic nozzle by means of nitrogen gas and transferred onto the substrate under high pressure. It is possible to print on conformal as well as plane surfaces. However,

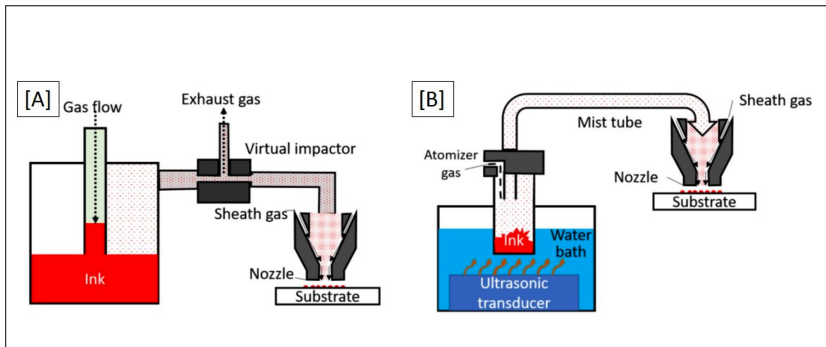


Figure 5.13. Schematic representation of (A) pneumatic aerosol printing and (B) ultrasonic aerosol printing, reprinted from [13] with permission from MDPI, Copyright (2021).

in order to print complex designs, it is necessary to control the beam. Thus, by varying the size of the nozzle, it is possible to control the beam. It is also to be noted that the distance between the nozzle and the substrate should be less than 10 mm or above 1 mm so as to achieve good accuracy because if these boundary conditions are crossed, then there is a possibility of overspray defects in the pattern printed on the substrate. The aerosol printing process also does not need any physical pattern, digital models can be printed using this technique. The following are the advantages of the aerosol printing process: (i) there is no contamination or clogging of the nozzle, and (ii) even small sizes such as 10 μm can be fabricated with high resolution using this process. Conversely, the main shortcoming of the aerosol printing process is the speed. The machining rate is 12 m min^{-1} , which is slow compared to other processes. Hence, this process is not considered for mass production [56, 66, 67].

5.4 Conclusions

The advancement of flexible or wearable electronic devices via different additive manufacturing or printing processes is rising exponentially owing to apparent reasons such as low cost, fast fabrication, light weight, and need for thin devices. In this chapter, the importance of flexible or wearable electronics and the processes to be carried out before and after printing, along with many recently developed flexible electronic devices utilizing different processes, is explored. It is to be noted that there are many scientific difficulties that still exist in manufacturing flexible or wearable electronic devices, which needs to be focused to perform research in a better way, and in adopting suitable advanced printing methods for the fabrication of flexible or wearable devices. One such challenge is the wet film thickness from the screen printing process, which results in more spreading of ink, and the resolution of the printing will be less if the wet ink is not sintered immediately.

Additionally, the evaporation of solvent present in the ink leads to a reduction in the quality of the mesh. This is due to the exposure of the printed surface to the atmosphere for a longer duration during the printing process [68].

In addition, the drawbacks like drying of inks, the viscosity of inks, the quantity of inks, an incorrect volume of anilox roller, and the working speed of the printers result in a squashed ink look at the exterior edges of the patterns printed using the flexographic printing process.

Because of many different issues in fabrication processes, there are enormous inconsistencies in the development of flexible or wearable devices, which leads to unreliability and unsteady performance. To overcome the above-said drawbacks in flexible or wearable devices, the improvisation and standardization of various printing parameters are necessary to develop devices with better reliability, stability, and repeatability. So as to maintain standards and to improve flexible and wearable electronics research to the next level, standardization of all parameters that have a great impact on flexible electronics fabrication is necessary. The parameters include CAD designs, characterization, printing parameters such as deposition time, humidity, and temperatures, post-printing processes such as sintering, mechanical testing, etc. Researchers around the world are working to develop advanced manufacturing systems to develop the research area of flexible or wearable devices to the next level. Hence, implementing these new additive printing methods for flexible or wearable electronic applications would possibly lead to cost-efficient and reliable production. Thus, it is possible to revolutionize the application of flexible or wearable devices in many areas such as agriculture, health, automobile, defense, and food industries.

References

- [1] Zeng X, Yang C, Chiang J F and Li J 2017 Innovating e-waste management: from macroscopic to microscopic scales *Sci. Total Environ.* **575** 1–5
- [2] Tan M J, Owth C, Chee P L, Kyaw A K K, Kai D and Loh X J 2016 Biodegradable electronics: cornerstone for sustainable electronics and transient applications *J. Mater. Chem. C* **4** 5531–58
- [3] Maddipatla D, Narakathu B B and Atashbar M 2020 Recent progress in manufacturing techniques of printed and flexible sensors: a review *Biosensors* **10** 199
- [4] Dizon J R C, Espera A H, Chen Q and Advincula R C 2018 Mechanical characterization of 3D-printed polymers *Addit. Manuf.* **20** 44–67
- [5] Liu Y, Wang H, Zhao W, Zhang M, Qin H and Xie Y 2018 Flexible, stretchable sensors for wearable health monitoring: sensing mechanisms, materials, fabrication strategies and features *Sensors* **18** 645
- [6] Yao S, Swetha P and Zhu Y 2018 Nanomaterial-enabled wearable sensors for healthcare *Adv. Healthcare Mater.* **7** 1700889
- [7] Nakata S, Arie T, Akita S and Takei K 2017 Wearable, flexible, and multifunctional healthcare device with an ISFET chemical sensor for simultaneous sweat pH and skin temperature monitoring *ACS Sens.* **2** 443–8
- [8] Kipphan H 2001 Printing technologies with permanent printing master *Handbook of Print Media: Technologies and Production Methods* ed H Kipphan (Berlin: Springer) pp 203–448
- [9] Kipphan H 2001 Printing technologies without a printing plate (NIP technologies) *Handbook of Print Media: Technologies and Production Methods* ed H Kipphan (Berlin: Springer) pp 675–758

- [10] Chang J S, Facchetti A F and Reuss R 2017 A circuits and systems perspective of organic/printed electronics: review, challenges, and contemporary and emerging design approaches *IEEE J. Emerg. Sel. Top. Circuits Syst.* **7** 7–26
- [11] Hashmi S G, Özkan M, Halme J, Zakeeruddin S M, Paltakari J and Grätzel M *et al* 2016 Dye-sensitized solar cells with inkjet-printed dyes *Energy Environ. Sci.* **9** 2453–62
- [12] Kjar A and Huang Y 2019 Application of micro-scale 3D printing in pharmaceuticals *Pharmaceutics* **11** 390
- [13] Wiklund J, Karakoç A, Palko T, Yiğitler H, Ruttik K and Jäntti R *et al* 2021 A review on printed electronics: fabrication methods, inks, substrates, applications and environmental impacts *J. Manuf. Mater. Process.* **5** 89
- [14] Magdassi S 2009 *The Chemistry of Inkjet Inks* (Singapore: World Scientific)
- [15] Kamyshny A and Magdassi S 2014 Conductive nanomaterials for printed electronics *Small* **10** 3515–35
- [16] Izdebska J 2016 Aging and degradation of printed materials *Printing on Polymers: Fundamentals and Applications* (Oxford, UK: Elsevier) PDL Handbook Series 353–70
- [17] Martin D P, Melby N L, Jordan S M, Bednar A J, Kennedy A J and Negrete M E *et al* 2016 Nanosilver conductive ink: a case study for evaluating the potential risk of nanotechnology under hypothetical use scenarios *Chemosphere* **162** 222–7
- [18] Valentine A D, Busbee T A, Boley J W, Raney J R, Chortos A and Kotikian A *et al* 2017 Hybrid 3D printing of soft electronics *Adv. Mater.* **29** 1703817
- [19] Choi Y, dong S K and Piao Y 2019 Metal–organic decomposition ink for printed electronics *Adv. Mater. Interfaces* **6** 1901002
- [20] Janczak D, Słoma M, Wróblewski G, Młóżniak A and Jakubowska M 2014 Screen-printed resistive pressure sensors containing graphene nanoplatelets and carbon nanotubes *Sensors* **14** 17304–12
- [21] Suganuma K 2014 Introduction *Introduction to Printed Electronics* (New York: Springer) pp 1–22
- [22] Cui Z 2016 Introduction *Printed Electronics* (New York: Wiley) pp 1–20
- [23] Ji T, Sun M and Han P 2014 A review of the preparation and applications of graphene/semiconductor composites *Carbon* **70** 319
- [24] Kim M, Safron N S, Han E, Arnold M S and Gopalan P 2010 Fabrication and characterization of large-area, semiconducting nanoporated graphene materials *Nano Lett.* **10** 1125–31
- [25] Hwang S W, Tao H, Kim D H, Cheng H, Song J K and Rill E *et al* 2012 A physically transient form of silicon electronics *Science* **337** 1640–4
- [26] Kim S 2020 Inkjet-printed electronics on paper for RF identification (RFID) and sensing *Electronics* **9** 1636
- [27] Agate S, Joyce M, Lucia L and Pal L 2018 Cellulose and nanocellulose-based flexible-hybrid printed electronics and conductive composites—a review *Carbohydrate Polym.* **198** 249–60
- [28] Välimäki M K, Sokka L I, Peltola H B, Ihme S S, Rokkonen T M J and Kurkela T J *et al* 2020 Printed and hybrid integrated electronics using bio-based and recycled materials—increasing sustainability with greener materials and technologies *Int. J. Adv. Manuf. Technol.* **111** 325–39
- [29] Fischer T, Rühling J, Wetzold N, Zillger T, Weissbach T and Göschel T *et al* 2018 Roll-to-roll printed carbon nanotubes on textile substrates as a heating layer in fiber-reinforced epoxy composites *J. Appl. Polym. Sci.* **135** 45950

Q6



- [30] Torrisi F, Hasan T, Wu W, Sun Z, Lombardo A and Kulmala T S *et al* 2012 Inkjet-printed graphene electronics *ACS Nano* **6** 2992–3006
- [31] Devaraj H and Malhotra R 2019 Scalable forming and flash light sintering of polymer-supported interconnects for surface-conformal electronics *J. Manuf. Sci. Eng.* **141** 041014
- [32] Constante G, Apsite I, Alkhamis H, Dulle M, Schwarzer M and Caspari A *et al* 2021 4D biofabrication using a combination of 3d printing and melt-electrowriting of shape-morphing polymers *ACS Appl. Mater. Interfaces* **13** 12767–76
- [33] Khan S, Lorenzelli L and Dahiya R S 2015 Technologies for printing sensors and electronics over large flexible substrates: a review *IEEE Sens. J.* **15** 3164–85
- [34] Saengchairat N, Tran T and Chua C K 2017 A review: additive manufacturing for active electronic components *Virtual Phys. Prototyp.* **12** 31–46
- [35] Reddy A S G, Narakathu B B, Atashbar M Z, Rebros M, Rebrosova E and Joyce M K 2011 Fully printed flexible humidity sensor *Procedia Eng.* **25** 120–3
- [36] Maddipatla D, Janabi F, Narakathu B B, Ali S, Turkani V S and Bazuin B J *et al* 2019 Development of a novel wrinkle-structure based SERS substrate for drug detection applications *Sens. Bio-Sens. Res.* **24** 100281
- [37] Zhu H, Narakathu B B, Fang Z, Tausif Aijazi A, Joyce M and Atashbar M *et al* 2014 A gravure printed antenna on shape-stable transparent nanopaper *Nanoscale* **6** 9110–5
- [38] Bariya M, Shahpar Z, Park H, Sun J, Jung Y and Gao W *et al* 2018 Roll-to-roll gravure printed electrochemical sensors for wearable and medical devices *ACS Nano* **12** 6978–87
- [39] Lau P H, Takei K, Wang C, Ju Y, Kim J and Yu Z *et al* 2013 Fully printed, high performance carbon nanotube thin-film transistors on flexible substrates *Nano Lett.* **13** 3864–9
- [40] Kipphan H (ed) 2001 *Handbook of Print Media: Technologies and Production Methods* (Berlin: Springer) p 1207
- [41] Emamian S, Narakathu B B, Chlahawi A A, Bazuin B J and Atashbar M Z 2017 Screen printing of flexible piezoelectric based device on polyethylene terephthalate (PET) and paper for touch and force sensing applications *Sensors Actuators A* **263** 639–47
- [42] Turkani V S, Maddipatla D, Narakathu B B, Altay B N, Fleming P D and Bazuin B J *et al* 2019 Nickel based RTD fabricated via additive screen printing process for flexible electronics *IEEE Access* **7** 37518–27
- [43] Dhanabalan S S, Arun T, Periyasamy G, N D, N C and Avaniathan S R *et al* 2022 Surface engineering of high-temperature PDMS substrate for flexible optoelectronic applications *Chem. Phys. Lett.* **800** 139692
- [44] Sundar D S, Raja A S, Sanjeeviraja C and Jeyakumar D 2017 High temperature processable flexible polymer films *Int. J. Nanosci.* **16** 1650038
- [45] Sundar D S, Sivanantharaja A, Sanjeeviraja C and Jeyakumar D 2016 Synthesis and characterization of transparent and flexible polymer clay substrate for OLEDs *Mater. Today: Proc.* **3** 2409–12
- [46] Shanmuga sundar D, Sivanantha Raja A, Sanjeeviraja C and Jeyakumar D 2016 Highly transparent flexible polydimethylsiloxane films—a promising candidate for optoelectronic devices *Polym. Int.* **65** 535–43
- [47] Cinti S and Arduini F 2017 Graphene-based screen-printed electrochemical (bio)sensors and their applications: efforts and criticisms *Biosens. Bioelectron.* **89** 107–22
- [48] Cao R, Pu X, Du X, Yang W, Wang J and Guo H *et al* 2018 Screen-printed washable electronic textiles as self-powered touch/gesture tribo-sensors for intelligent human-machine interaction *ACS Nano* **12** 5190–6

- [49] Hakola E 2009 Principles of conventional printing ed P Oittinen and H Saarelna *Papermaking Science and Technology* (Finland: Finnish Paper Engineers' Association) pp 40–87
- [50] Dhanabalan S S, R S, Madurakavi K, Thirumurugan A, M R and Avaniathan S R *et al* 2022 Flexible compact system for wearable health monitoring applications *Comput. Electr. Eng.* **102** 108130
- [51] Shrestha S, Yerramilli R and Karmakar N C 2019 Microwave performance of flexo-printed chipless RFID tags *Flex. Print. Electron.* **4** 045003
- [52] Fung C M, Lloyd J S, Samavat S, Deganello D and Teng K S 2017 Facile fabrication of electrochemical ZnO nanowire glucose biosensor using roll to roll printing technique *Sensors Actuators B* **247** 807–13
- [53] Maddipatla D, Narakathu B B, Avuthu S G R, Emamian S, Eshkeiti A and Chlaihawi A A *et al* 2015 A novel flexographic printed strain gauge on paper platform *IEEE Sensors* **2015** 1–4
- [54] Higuchi K, Kishimoto S, Nakajima Y, Tomura T, Takesue M and Hata K *et al* 2013 High-mobility, flexible carbon nanotube thin-film transistors fabricated by transfer and high-speed flexographic printing techniques *Appl. Phys. Express* **6** 085101
- [55] Knobloch A, Bernds A and Clemens W 2001 Printed polymer transistors *1st Int. IEEE Conf. on Polymers and Adhesives in Microelectronics and Photonics Incorporating POLY, PEP & Adhesives in Electronics Proc. (Cat No01TH8592)* pp 84–90
- [56] Saengchairat N, Tran T and Chua C K 2017 A review: additive manufacturing for active electronic components *Virtual Phys. Prototyp.* **12** 31–46
- [57] Izdebska-Podsiadly J and Thomas S 2015 *Printing on Polymers: Fundamentals and Applications* (Amsterdam: Elsevier)
- [58] Corzo D, Almasabi K, Bihar E, Macphee S, Rosas-Villalva D and Gasparini N *et al* 2019 Digital inkjet printing of high-efficiency large-area nonfullerene organic solar cells *Adv. Mater. Technol.* **4** 1900040
- [59] Ochoa M, Rahimi R, Zhou J, Jiang H, Yoon C K and Osci M *et al* 2018 A manufacturable smart dressing with oxygen delivery and sensing capability for chronic wound management *Micro- and Nanotechnology Sensors, Systems, and Applications X* 10639; T George, A K Dutta and M S Islam (Bellingham, WA: SPIE) p 106391C
- [60] Maddipatla D, Narakathu B B, Ochoa M, Rahimi R, Zhou J and Yoon C K *et al* 2019 Rapid prototyping of a novel and flexible paper based oxygen sensing patch via additive inkjet printing process *RSC Adv.* **9** 22695–704
- [61] Mikolajek M, Reinheimer T, Bohn N, Kohler C, Hoffmann M J and Binder J r 2019 Fabrication and characterization of fully inkjet printed capacitors based on ceramic/polymer composite dielectrics on flexible substrates *Sci. Rep.* **9** 13324
- [62] Narakathu B B, Avuthu S G R, Eshkeiti A, Emamian S and Atashbar M Z 2015 Development of a microfluidic sensing platform by integrating PCB technology and inkjet printing process *IEEE Sens. J.* **15** 6374–80
- [63] Abutarboush H F and Shamim A 2018 A reconfigurable inkjet-printed antenna on paper substrate for wireless applications *IEEE Antennas Wirel. Propag. Lett.* **17** 1648–51
- [64] Martin G D, Hoath S D and Hutchings I M 2008 Inkjet printing—the physics of manipulating liquid jets and drops *J. Phys. Conf. Ser.* **105** 012001
- [65] Li J, Sollami Delekta S, Zhang P, Yang S, Lohe M R and Zhuang X *et al* 2017 Scalable fabrication and integration of graphene microsupercapacitors through full inkjet printing *ACS Nano* **11** 8249–56

- [66] Dimitriou E and Michailidis N 2021 Printable conductive inks used for the fabrication of electronics: an overview *Nanotechnology* **32** 502009
- [67] Chen Y D, Nagarajan V, Rosen D W, Yu W and Huang S Y 2020 Aerosol jet printing on paper substrate with conductive silver nano material *J. Manuf. Processes* **58** 55–66
- [68] Joannou G 1988 Screen inks ed R H Leach, C Armstrong, J F Brown, M J Mackenzie, L Randall and H G Smith *The Printing Ink Manual* (Boston, MA: Springer) pp 481–514

QUERY FORM

BOOK TITLE: Advances in Flexible and Printed Electronics

AUTHOR: Shanmuga Sundar Dhanabalan and Arun Thirumurugan

CHAPTER TITLE: Fabrication techniques for printed and wearable electronics

Page 3

Q1

Please expand the following acronyms in the text as appropriate: "UHIF," "WCNT," and "BST."

Page 3

Q2

The following acronyms have been expanded in the text: "PEDOT: PSS" as "poly (3,4-ethylenedioxythiophene) polystyrene sulfonate," "PI" as "polyimide," "SES" as "solvent-excluded surface," and "EIS" as "electrochemical impedance spectroscopy." Please confirm or make any necessary changes.

Page 3

Q3

The following acronyms have been defined in the text: "SERS" as "surface-enhanced Raman scattering," "TPU" has been defined "thermoplastic polyurethane," and "CAD" as "computer-aided design." Please confirm or make any necessary changes.

Page 12

Q4

Figures 5.5, 5.7, 5.8, and 5.12 are of low resolution. Please provide better resolution figures (at least 300 ppi at 80 mm).

Page 18

Q5

Please complete the sentence "By using this process, thin, homogeneous, and smooth...".

Q6

Reference [26] in the original source file was a duplicate of Reference [21], and hence, the repeated version has been deleted from the reference list and subsequent references have been reordered. Please check.

Comparative Performance Evaluation of Wire-bonded Micro Heat Pipes with Acetone and Water as Working fluid

Rag R L

Mechanical Engineering

SCMS School of Engineering and Technology

Cochin, India

ragrajanl@gmail.com

Rupesh S

Mechanical Engineering

PES College of Engineering, Mandya

Karnataka, India

mailtorupeshs@gmail.com

Abstract— Thermal management of high-heat-flux dissipation-rate micro-electro-mechanical systems (MEMS) using micro heat pipes is an exciting new field. Desktop computers are cooled using heavy metal sinks and fans. Wire sandwiched micro heat pipes are analysed computationally; they are a novel type of micro heat pipe that uses an array of wires sandwiched between two metallic plates to create the flow channels. Work fluid is carried through the system by the sharp corners between the wires and plates, which serve as liquid arteries. The temperature distribution in the micro heat pipes is obtained by solving the numerical model with a finite difference approach. By calculating effective thermal conductivity values from the temperature profiles, we can compare the heat pipe's performance using acetone and water as the working fluid. With an effective thermal conductivity of 168.83 kW/m²K, acetone shows substantial improvement over water in heat pipes.

Keywords- acetone, effective thermal conductivity, micro heat pipe, water

Nomenclature

A	=	area of cross-section in m ²
k	=	thermal conductivity in W/m K
L	=	length of the heat pipe in m
Q	=	heat in W
q	=	heat flow rate in W/m ²
T	=	temperature in K
ΔT	=	temperature difference, $T-T_{amb}$ in K

Subscripts

c	=	cross-section
eff	=	effective

I. INTRODUCTION

Progress in modern technology is often driven by innovations in microelectronics, aims at progress in the ability of computing with improvement in speed of processing, and reduction in the size of components and devices. The challenges in the miniaturization of silicon components and the enhancement of their performance have led to the development of high-power electronic devices and CPUs with high packing densities. This has opened the way for the advancement of

electronic devices with very high levels of heat generation rates, for a variety of industrial applications. As modern electronics demands very rigid specifications regarding miniaturization, reliability and power-component density, optimal thermal management of microelectronics has become a key issue for the designer and the engineer in recent times.

In general, for cooling electronic devices, there are many existing conventional methods. Passive air cooling is one basic way of cooling electronic devices, where the convective currents occur without the support of external power. The difference in temperature and subsequent changes in the density of the medium causes the flow. Forced air cooling systems are used as a common method for cooling in CPUs, where a fan will enhance the flow over the heat sinks for effective cooling. Liquids like water are used in forced liquid systems which are another set of cooling techniques used in electronic cooling. Of all the three methods, the second one has a prominent usage in electronic cooling due to its simplicity in design and manufacturing and cost-effective nature. Though the method is common and simple, bulky heat sinks utilize more material for manufacturing. The fan also increases the dust deposit over the components which in turn forms to be an insulator as the thickness of the deposit increases.

To remove heat from the source with smaller dimensions to a remote location, micro heat pipes are the best options. The micro heat pipe, as defined by Cotter (1984) has 'channels which are so small, that the mean curvature of the vapour-liquid interface is comparable in magnitude to the reciprocal of the hydraulic radius of the flow channel' [1]. Even though micro heat pipes poses evaporator, adiabatic and condenser sections and rely on the thermal phenomenon similar to that in conventional heat pipe [2], [3], they are physically distinct and compact from the former due to the absence of wick. In micro heat pipes, liquid arteries formed by the non-circular cross sections enables the transfer of working fluid from the condenser to evaporator sections. [7]. Micro heat pipes and heat spreaders continue to be the optimal solution for heat sinks and miniature equipments and devices respectively,

owing to their effective heat transport capability with trivial temperature gradient in the flow direction (high thermal conductance).

The wire-sandwiched micro heat pipe essentially consists of an array of channels, developed from sandwiching an array of wires within the metal plates. The ease in its construction, simple structure and adaptability to many heat-generating surfaces, made the micro heat pipes with wire bonds, a favorable option for cooling electronic devices. Each channel in the array acts as an individual micro heat pipe as depicted in Fig. 1. It comprises of an evaporator which is externally heated, an adiabatic segment devoid of any heat transfer and a condenser experiencing convective cooling. The area of cross-section of the liquid and the vapour change longitudinally from the evaporator end to the condenser end is displayed in Fig 1(c).

The conceptual wire-bonded micro heat pipes were initially presented by Wang and Peterson [4] as a one-dimensional analytical-steady-state model. The liquid-vapour phase interactions were analysed in the model and found the highest heat transfer performance. The fabrication easiness, better integration capability with electronic devices, and suitability for spacecraft applications were major attractions of the new model. The experimental validation in the studies proved the feasibility of the design and determined the optimum values for the design. The combination of aluminium - fluid acetone was used in the proposed design.

The performance investigation of a wire-bonded micro heat pipe array was done by Launay et al. [5]. A copper-water system was used to determine the capillary limitations in the temperature field and experimentally compare the charged micro heat pipes with empty channels. A numerical model was also used for predicting the effects of angle of contact, quantity of charge and fluid distribution.

To evaluate the efficiency of wire-bonded micro heat pipes, Rag and Sobhan [6] created a transient one-dimensional model. In order to derive the velocity, pressure, and temperature distributions, a fully implicit finite difference approach was used to solve the mass, momentum, and energy conservation equations. The efficiency of the wire-bonded micro heat pipe was determined by computing its effective thermal conductivity. Using the working fluid's constant thermo-physical properties, the equations accounted for longitudinal area fluctuations, phase shift, and frictional effects. Rag and Sobhan [7] used the same one-dimensional transient model to analyse the effects of operational and geometrical variables on effective thermal conductivity. Maximum values of effective thermal conductivity were achieved by optimising these parameters within the usable range. The transient variation of thermo-physical parameters was incorporated into a numerical model and quantitative measures of thermal conductivity were obtained by varying the input heat flux at the evaporator and condenser heat transfer coefficient by Rag et al. [8]. More realistic operational and performance characteristics were obtained when it comes to a wide variety of operational parameters.

In the present analysis, the temperature profiles are predicted computationally using an in-house code and evaluated the efficacy of a wire-bonded micro heat pipe which can be used for replacing the existing heat sink in a desktop computer. The already developed transient one-dimensional model is modified to accommodate two different working fluids, water and acetone, compatible with copper as the material of the micro heat pipes [2]. An experiment using acetone-aluminum system was used in a previous study [4] for validation of results in another study [6], acetone is considered as the second fluid for the present analysis. The dimension details of the micro heat pipes were listed in Table 1.

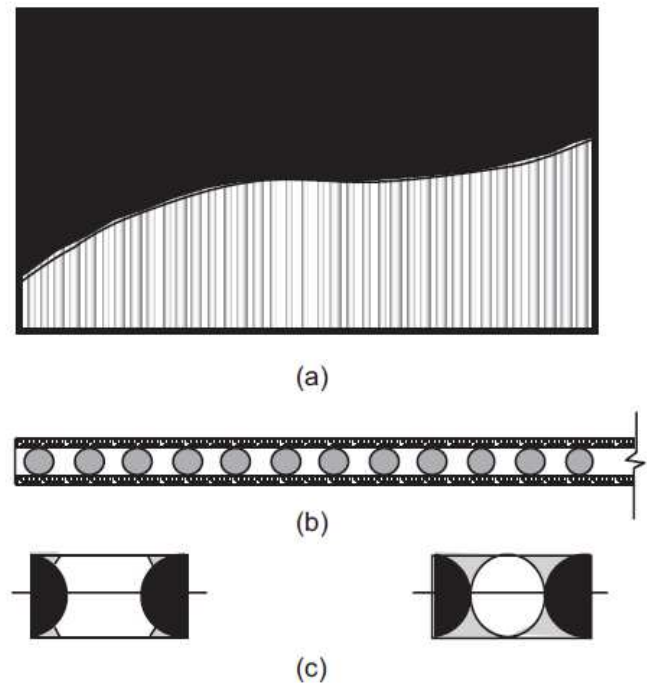


Fig. 1. Schematic of a wire sandwiched micro heat pipe

TABLE I. PHYSICAL PROBLEM DETAILS

Parameter	Value
Solid Material	Copper
Working Fluids	Acetone/ Water
Heat Pipe length	125 mm
Wire radius	0.8 mm
Wire-pitch	2 mm
Evaporator length	20 mm
Adiabatic section length	85 mm

II. FORMULATION

Line connections are only present at either end of the wires wedged between the parallel plates. Any two such wires

form a miniature heat pipe, with vapour flowing along the middle and liquid moving around the edges of the plate and wires. The wire-bonded micro heat pipe can be broken down into an evaporator section that takes in heat and releases it to the surroundings, an adiabatic section that does not exchange heat with anything else, and a condenser section that releases heat to the surroundings or the cooling media that is circulating around it. The analysis takes into account the fact that the vapour and liquid cross-sectional areas will change along the length. A one-dimensional numerical model is employed for transient analysis since the most significant changes in flow characteristics occur along the flow's longitudinal axis. These presumptions constitute the basis for the formulation of the governing equations:

1. Vapor and liquid laminar flow.
2. No-slip liquid and vapour boundary conditions.
3. Vapor saturation.
4. Meniscus radius of curvature consistency.

For a quasi-steady state, the Laplace Young equation can be used to connect the pressure differential between the liquid and vapour phases to the meniscus radius at a given axial point. Pressure, velocity, and temperature profiles are analysed to determine the micro heat pipes' efficiency by solving the equations for mass, momentum, and energy in differential form for the liquid and vapour phases. As a function of the radius of the meniscus, the longitudinal area of the liquid and vapour phases are accounted for in their respective governing equations. The equation of state establishes a connection between the vapour pressure and temperature, which is then restated in terms of vapour momentum to ensure convergence. The liquid pressure is approximated using the Hagan-Poiseuille equation, but for more converged results, the numbers are re-entered into the liquid momentum equation. Although triangle-shaped micro heat pipes [5, 9] use the same approach and mathematical formulation, the calculations must account for unique area characteristics. Previous papers contain the area parameters and the governing equations.

III. SOLUTION PROCEDURE

A custom FORTRAN programme is used to implement a Finite Difference technique to solve the governing equations. The first and second-order derivatives in the finite difference formulation were calculated using central differences. The thermo-physical qualities that vary with temperature are accounted for in the programme. In addition to the conventional solution procedure's [6]-[8] phases, a new function is introduced to define the working fluid's characteristics. Choosing the working fluid allowed the code to make use of the fluid's temperature-dependent thermophysical features and produce more accurate predictions. The heat balance test and the grid independent test of the code were conducted and shown in the previous publications extensively [6].

IV. THE TEMPERATURE PROFILE

In this analysis for acetone and water as working fluid, the input heat flux supplied is taken as 2.4 W/cm² and the coefficient of heat transfer in the condenser is taken as 650W/m²K, which are reasonable values in electronic devices generating heat [6]–[8]. From Fig. 2 it is clear that the temperature profiles are as anticipated based on the previous literature [6]–[8]. The influence of the evaporator is observed in the smooth behaviour of temperature distribution at the evaporator-adiabatic junction and that of the condenser is seen at the adiabatic-condenser junction. Since the state equation is used to approximate vapour pressure, both vapour temperature and vapour pressure exhibit a consistent longitudinal fluctuation. Micro heat pipe performance is analysed by determining the effective thermal conductivity using the vapour temperature distributions.

V. PERFORMANCE EVALUATION

To evaluate the relative performance of different micro heat pipe designs, researchers use effective thermal conductivity [6]–[8]. According to Fourier's rule of thermal conduction, it is defined as follows:

$$k_{eff} = \frac{Q}{A_c \frac{\Delta T}{L}} \quad (1)$$

Wire-bonded micro heat pipes using acetone as the working fluid are shown to have an effective thermal conductivity of 168.83 kW/mK, while water only has an effective thermal conductivity of 127.27 kW/mK. Acetone is showing better effective thermal conductivity in the selected heat flux input and heat transfer coefficient of a condenser.

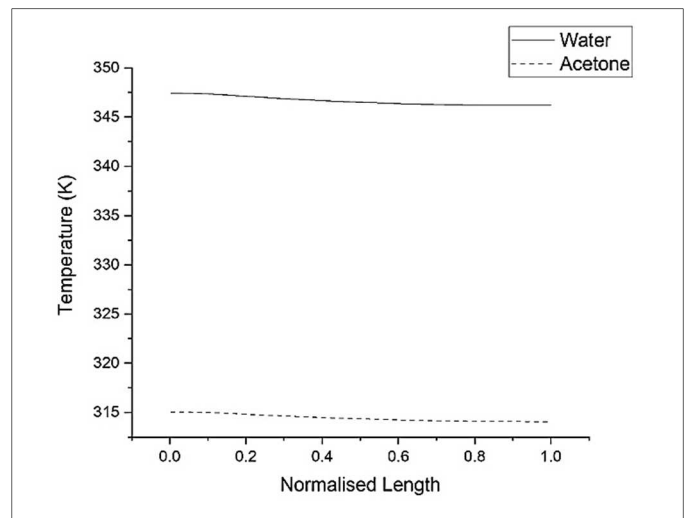


Fig. 2. Temperature profile for 2.4 W/cm² input heat flux and 650 W/m²K condenser heat transfer coefficient

VI. CONCLUSIONS

In order to compare the efficiency of wire-bonded micro heat pipes using acetone and water as working fluid and copper as material, a computational analysis is carried out.

Using a fully implicit finite difference approach, the mathematical model is solved to obtain the temperature profiles for both working fluids. With an effective thermal conductivity of 168.83 kW/mK, acetone proves to be a great medium for a heat pipe, outperforming even water.

REFERENCES

- [1] T. P. Cotter, "Principles and prospects for micro heat pipes," in *Proceedings of the 5th International Heat Pipe Conference*, Tsukuba, Japan, Jan. 1984, vol. 1984, pp. 328–335. Accessed: Apr. 27, 2022. [Online]. Available: <https://www.osti.gov/biblio/5246927>
- [2] G. P. Peterson, *An introduction to heat pipes: modeling, testing, and applications*. New York: Wiley, 1994.
- [3] C. Sobhan, R. Rag, and G. Peterson, "A review and comparative study of the investigations on micro heat pipes," *Int. J. Energy Res.*, vol. 31, pp. 664–688, May 2007, doi: 10.1002/er.1285.
- [4] Y. Wang and G. Peterson, "Analysis of Wire-Bonded Micro Heat Pipe Arrays," *J. Thermophys. Heat Transf. - J THERMOPHYS HEAT Transf.*, vol. 16, pp. 346–355, Jul. 2002, doi: 10.2514/2.6711.
- [5] J. P. Longtin, B. Badran, and F. M. Gerner, "A One-Dimensional Model of a Micro Heat Pipe During Steady-State Operation," *J. Heat Transf.*, vol. 116, no. 3, pp. 709–715, Aug. 1994, doi: 10.1115/1.2910926.
- [6] R. L. Rag and C. B. Sobhan, "Computational Analysis of Fluid Flow and Heat Transfer in Wire-Sandwiched Microheat Pipes," *J. Thermophys. Heat Transf.*, vol. 23, no. 4, pp. 741–751, 2009, doi: 10.2514/1.44101.
- [7] R. L. Rag and C. B. Sobhan, "Computational Analysis and Optimization of Wire-Sandwiched Micro Heat Pipes," *Int. J. Micro-Nano Scale Transp.*, vol. 1, no. 1, pp. 57–78, 2010.
- [8] R. L. Rag, C. Sobhan, and G. Peterson, "Computational Analysis of Wire-Bonded Micro Heat Pipe: Influence of Thermophysical Parameters," *J. Thermophys. Heat Transf.*, vol. 32, pp. 1–8, Apr. 2018, doi: 10.2514/1.T5359.
- [9] C. Sobhan and G. Peterson, "Modeling of the Flow and Heat Transfer in Micro Heat Pipes," Rochester, NY, Jan. 2004, pp. 883–890. doi: 10.1115/ICMM2004-2426.

CALL FOR BOOK CHAPTERS



CRC Press
Taylor & Francis Group

Advances of Machine Learning for Knowledge Mining in Electronic Health Records

ISBN: 9781032526102

TOPICS OF INTEREST (BUT NOT LIMITED TO)

1. Introduction to EHR
2. Structured Data in EHR
3. Unstructured Data in EHR
4. Supervised Learning for EHR
5. Unsupervised Learning for EHR
6. Deep Learning in EHR
7. Temporal Mining in EHR
8. Cohort Identification in EHR
9. Risk Prediction in EHR
10. Applications of EHR



No Publication Fee

BOOK EDITORS

Dr. P. Mohamed Fathimal, Government Polytechnic College, R.K Nagar, Chennai, India.

Dr. T. Ganesh Kumar, SCSE, Galgotias University, Greater Noida, Delhi NCR, India.

Dr. J.B. Shajilin Loret, Francis Xavier Engineering College, Tirunelveli, Tamilnadu, India.

Dr. Venkataraman Lakshmi, University of Virginia, Virginia State, USA.

Dr. Manish T.I., SCMS School of Engineering and Technology, Kerala, India.

Important Dates

Last Date for Abstract Submission - 20 January 2023.

Notification of Abstract Acceptance - 25 January 2023.

Last Date for Full Chapter Submission - 31 April 2023.

Please Submit your abstract to

amlehr2023@gmail.com

The accepted chapters will be published in Taylor and Francis Book and Highly indexed in Scopus.

Filtering of Spurious Sonar Signals

Srutheshna U¹, Sharik Ashraf² and Litty Koshy³

¹Student, Department of Master, of Computer Application. SCMS School of Engineering & Technology, VidyaNagar, Karukutty, Ernakulam

Email: srutheshnaunni@gmail.com

²Scientist-E, Naval Physical and Oceanographic Laboratory, P.B.NO.6, NGO Quarters, Thrikkara, Vazhakkala, Kochi

Email: Shark.npol@gov.in

³Assistant Professor, Department of computer science & Engineering, SCMS School of Engineering & Technology, VidyaNagar, Karukutty, Ernakulam

Email: littykoshy@scmsgroup.org

Abstract—Navy uses a harmonic filter to extract the propel sounds in ships. Usually, Sonar processing uses the harmonic filter to remove unwanted harmonics. The proposed system is used for filtering unwanted noise from lower frequency noise using the machine learning technique. Some sonar may have higher frequency sounds, which can be difficult to hear. Using this sound frequency humans can identify their target by experience. Automate these sounds and using a trained neural network, Classify the sounds. Retrieve non-frequency voice and avoid harmonics using a neural network.

Index Terms— MFCC, MLP, High pass filter, Discrete cosine transform.

I. INTRODUCTION

Currently, there is no specialized machine learning technique for the classification of the frequency of sonar: higher frequency and lower frequency. The word "sonar"[1] (short for "sound navigation ranging") refers to a technique for using sound waves to locate and measure the size and location of submerged objects. Sonar equipment detects sound waves emitted by or reflected from the item and analyses them to determine what information is contained.

The main objective of this topic is to classify the frequency of sound, and then remove the noise in high-frequency sonar. This problem was very difficult to deal with because the research on sonar classification and filtering of sonar is processed by normal techniques, in this work using deep learning method is used to process the classification and filtering of sonar sound. The extraction of the needed signal from background noise is one of the most serious issues in many application fields. Background noise is random, as is the appearance and behavior of signals. Basically in navy use a harmonic filter to remove unwanted noises. It is a time-consuming process. In this work, the Classification of sonar sound is done by a Multilayer perceptron algorithm and a high pass filter is used to remove the unwanted noises from high-frequency sonar sound.

Classification of the frequency of sonar and removing noises from sonar sound is helpful to detect the target. Sonar is a method that employs sound propagation to navigate, measure distances, communicate with, or detect objects on or below the water's surface, such as other boats. classification of sonar sound in normal ways returns a time-consuming process, using trained neural network got a better accuracy result of classification. Normally harmonic filter is used for filtering unwanted noise from high-frequency sonar sound, which is also a time-

consuming process, high pass filter is better to use for a filtering process.

II. METHODOLOGY

The classification of frequency of sonar sound using multi-layer perceptron and filtering of high sonar sound is time reducing process. In normal audio, there is a signal and so many noises. first, take input as a wav file with noises and get output as filtered audio only without any spurious signal. Humans can identify their target by experience utilizing sonar that has a higher frequency that can be challenging to hear.

A. MFCC

Mel-frequency cepstrum (MFC)[2], which are employed in sound processing, are representations of a sound's short-term power spectrum that are based on a linear cosine transform of a log power spectrum on a nonlinear Mel scale of frequency. Several coefficients collectively referred to as Mel-frequency cepstral coefficients make up an MFC (MFCCs).

MFCCs are frequently employed as features in speech recognition systems, including those[3] that can automatically identify telephone number pronunciations. Applications for music information retrieval such as genre categorization, auditory similarity measurements, etc. are also increasingly using MFCCs.

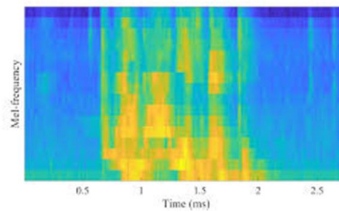


Fig 1:Mel-frequency Cepstrum

B. MLP

The term "Multilayer Perceptron"[4] refers to a fully connected multi-layer neural network (MLP). It contains three levels, one of which is buried. It is referred to as a deep ANN if it has more than one hidden layer. A common illustration of a feedforward artificial neural network is an MLP. MLP is used for [5]a number of applications, including stock analysis, image identification, spam detection, and election voting 11 predictions. Basically, add more parameters to the model by adding more hidden layers and neurons per layer. Then permit the model to fit intricate functions.

C. High pass filter

A high pass filter is a[6] straightforward, efficient EQ curve that removes unwanted low frequencies from any audio source. When used properly to fix sloppy signals and tighten up arrangements, they are great. Low pass filter: The image is smoothed using this particular style of frequency-domain filter. The low-frequency[7] components are preserved while the high-frequency components are attenuated. High pass filter: A high pass frequency-domain filter is used to enhance the sharpness of the image.

III. IMPLEMENTATION

Filtering of spurious sonar signals consists of the following steps:

- Padding of given wav file dataset.
- Feature extraction of audios.
- Classification of frequency of sonar sounds.
- Removal of unwanted harmonics from an audio file.

Sonar sound can be classified by the neural network, in this work, MLP is used for classification purposes.

First, take all datasets; the dataset contains two folders high-frequency sound and low-frequency sound. The dataset contains 250 audios within each folder. categorize and label this dataset into two.

Padding each audio with respect to a fixed sample rate, so get the dataset containing each audio with the same length. In this work, each audio has a size of 5. The dataset is a wav file and Audio padding is necessary for classification. Librosa library[8] is used for padding. This is also a pre-processing step of the dataset. For feature extraction, the MFCC algorithm is used. In this work, the extracted feature is frequencies by the MFCC algorithm. Find the MFCC value of each audio file after padding. The main steps in the MFCC[9] feature

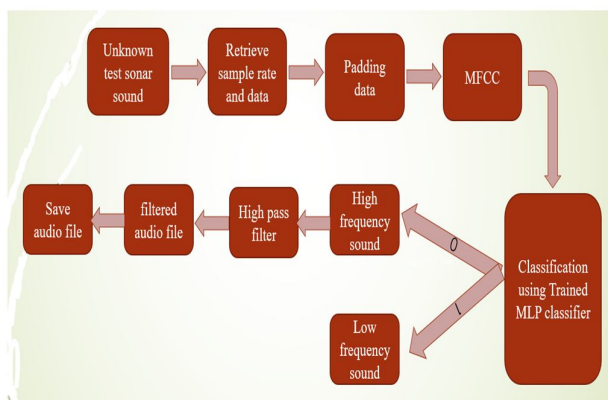


Fig 2: High-Level_Architecture

TABLE I: LIST OF SOUND FREQUENCY

Labels	categories
0	High-frequency sound
1	Low-frequency sound

extraction method are windowing the signal, running the DFT, getting the log of the magnitude, warping the frequencies on a Mel scale, and finally running the inverse DCT.

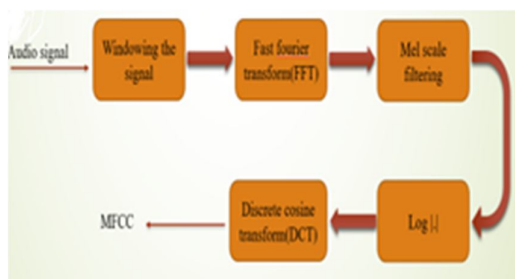


Fig 3: Diagram of MFCC

Building a proper network architecture is required to acquire a trained model immediately after receiving a clean database. Build a model using a multi-layer perceptron algorithm and having 2 hidden layers with 4 neurons. To train the built model, the training dataset was split into patches, and the training loop sent each batch through an optimizer to train our model, with training accuracy being evaluated for each batch. Then the model is now ready to be tested with new audio after completing the training stage. After classification, if it is a high-frequency sound remove the noises using a High pass filter. An easy-to-use, efficient EQ curve that removes undesired low frequencies from any audio source is a high pass filter. When properly applied, they are wonderful for cleaning up errant signals and tightening up arrangements.

IV. RESULT AND DISCUSSION

The project was able to build filtering of spurious sonar signals using machine learning techniques, which will classify the sonar sounds as high-frequency sounds and low-frequency sounds using multilayer perceptron and remove unwanted harmonics using a high pass filter. MLP algorithm used was able to classify the sonar sounds. The experimental findings are acquired by training with a number of audios. The sonar sound dataset is used for training purposes, which consists of 2 folders high-frequency sound and low-frequency sound and contains 300 audios within each folder. The classification accuracy is 84%, which is also a good result, it also works properly and very well.

The accuracy is more feasible when optimum iterations are performed. Test an audio file with a trained model, which gives output as 0 as High-frequency sound or 1 as Low-frequency sound. Passing a high pass filter to remove the unwanted noises from High-frequency sound, which save an audio signal without noises.

V. CONCLUSION AND FUTURE SCOPE

Filtering of spurious sonar signals using machine learning techniques shows a wide range of applications in NAVY. The main objective of this project is the classification of the frequency of sonar sounds and the filtering of noises from high-frequency sonar sounds. Deep learning is the most powerful science in working with pictures by completing feature extractions to categorize what this image includes, according to studies. Related work surveys are conducted by reading several papers written by earlier scientists and developers that attempted to address the classification of sonars and target detection of sonar, some of which used the Fast Fourier transform algorithm and Artificial neural network. Python is utilized to implement this project since it is the most popular language for Artificial Intelligence and Deep Learning. The project has some limitations; because the availability of frequency of sonar sounds and removal of unwanted harmonics from a lower frequency audio file take more time, which is called LOFAR processing. Hence this process is done on high-frequency sonar sounds only. Here the best classification algorithm convolutional neural network (CNN) failed to perform the expected task because of the limited access to the dataset. Later it was executed well using MLP and it was successful.

REFERENCES

- [1] Hartvich, Filip, et al. "Landslide-dammed lake sediment volume calculation using waterborne ERT and SONAR profiling." *Earth Surface Processes and Landforms* 45.14 (2020): 3463-3474.
- [2] Martin, Betty, and Vimala Juliet. "Extraction of feature from the acoustic activity of RPW using MFCC." *Recent Advances in Space Technology Services and Climate Change 2010 (RSTS & CC-2010)*. IEEE, 2010.
- [3] Gupta, Shikha, et al. "Feature extraction using MFCC." *Signal & Image Processing: An International Journal* 4.4 (2013): 101-108.
- [4] He, Yunan, et al. "Surface emg pattern recognition using long short-term memory combined with multilayer perceptron." *2018 40th Annual International Conference of the IEEE Engineering in Medicine and Biology Society (EMBC)*. IEEE, 2018.
- [5] Fazeen, Mohamed, Ram Dantu, and Parthasarathy Guturu. "Identification of leaders, lurkers, associates and spammers in a social network: context-dependent and context-independent approaches." *Social Network Analysis and Mining* 1.3 (2011): 241-254.
- [6] Zhang, Kai, et al. "Direct repetitive control of SPWM inverter for UPS purpose." *IEEE Transactions on Power Electronics* 18.3 (2003): 784-792.
- [7] Magid, Salma Abdel, et al. "Dynamic high-pass filtering and multi-spectral attention for image super-resolution." *Proceedings of the IEEE/CVF International Conference on Computer Vision*. 2021.
- [8] Mushtaq, Zohaib, and Shun-Feng Su. "Environmental sound classification using a regularized deep convolutional neural network with data augmentation." *Applied Acoustics* 167 (2020): 107389.
- [9] Phadke, Sujay, et al. "On design and implementation of an embedded automatic speech recognition system." *17th International Conference on VLSI Design. Proceedings.. IEEE*, 2004.



Browse

My Settings

Help

Institutional Sign In

Institutional Sign In

All



ADVANCED SEARCH

Conferences > 2023 Advanced Computing and C... ?

Deep learning architectures for Brain Tumor detection: A Survey

Publisher: IEEE

Cite This

PDF

Divya K S ; Manish T I All Authors



180 Full Text Views

Alerts

Manage Content Alerts Add to Citation Alerts

Abstract



Download PDF

Document Sections

- I. Introduction
- II. Deep Learning Techniques for Braintumor Detection
- III. Conclusion

Abstract:Deep learning methods are used in various fields of medical imaging like medical image localization/Detection segmentation, classification, and registration. Various medi... **View more**

► Metadata

Abstract:

Deep learning methods are used in various fields of medical imaging like medical image localization/Detection segmentation, classification, and registration. Various medical conditions can be detected, monitored, and treated with deep learning techniques. One such condition is brain tumors. The main cause of brain tumors is the fast and uncontrolled development of brain cells. Over time, numerous techniques for detecting brain tumors have been developed. Manual analysis of brain tumor images will be time-consuming and it requires expert radiologists. Deep learning techniques can solve this issue since it is a fully automated process. Various deep learning architectures are used nowadays for different pattern recognition tasks in medical imaging. This survey aims to deliver different recent deep learning models developed to detect brain tumors and to present the drawbacks of existing techniques.

Published in: 2023 Advanced Computing and Communication Technologies for High Performance Applications (ACCTHPA)

Date of Conference: 20-21 January 2023

DOI: 10.1109/ACCTHPA57160.2023.10083385

Date Added to IEEE Xplore: 03 April 2023

Publisher: IEEE

► ISBN Information:

Conference Location: Ernakulam, India

Authors

References

Keywords

Metrics

More Like This

Divya K S

Department of CSE, Adi Shankara Institute of Engineering and Technology, Kalady, Kerala

Manish T I

Department of CSE, SCMS School of Engineering and Technology, Kerala



I. Introduction

In medical systems, the analysis of medical image services is significant in many fields like Magnetic Resonance Imaging (MRI), Radiography, endoscopy, Computed Tomography, Mammography Images, Ultrasound images, Positron Emission Tomography (PET), etc. Due to the lack of radiologists, manually analyzing medical images requires a significant amount of effort. Thus emerges different deep learning models for analyzing medical images. The most significant models are Convolutional neural networks which belong to the category of supervised deep learning algorithms. Unsupervised algorithms mainly include Generative Adversarial Networks (GAN) and Autoencoders.

Sign in to Continue Reading

Authors ^

Divya K S
Department of CSE, Adi Shankara Institute of Engineering and Technology, Kalady, Kerala

Manish T I
Department of CSE, SCMS School of Engineering and Technology, Kerala

References v

Keywords v

Metrics v

More Like This

FCN Based Deep Learning Architecture for Medical Image Segmentation
2023 2nd International Conference on Edge Computing and Applications (ICECAA)
Published: 2023

Annotation Cost Minimization for Ultrasound Image Segmentation Using Cross-Domain Transfer Learning
IEEE Journal of Biomedical and Health Informatics
Published: 2023

Show More

IEEE Personal Account

CHANGE
USERNAME/PASSWORD

Purchase Details

PAYMENT OPTIONS
VIEW PURCHASED
DOCUMENTS

Profile Information

COMMUNICATIONS
PREFERENCES
PROFESSION AND
EDUCATION
TECHNICAL INTERESTS

Need Help?

US & CANADA: +1 800
678 4333
WORLDWIDE: +1 732
981 0060
CONTACT & SUPPORT

Follow



[About IEEE Xplore](#) | [Contact Us](#) | [Help](#) | [Accessibility](#) | [Terms of Use](#) | [Nondiscrimination Policy](#) | [IEEE Ethics Reporting](#)  | [Sitemap](#) | [IEEE Privacy Policy](#)

A not-for-profit organization, IEEE is the world's largest technical professional organization dedicated to advancing technology for the benefit of humanity.

© Copyright 2024 IEEE - All rights reserved.

IEEE Account

- » [Change Username/Password](#)
- » [Update Address](#)

Purchase Details

- » [Payment Options](#)
- » [Order History](#)
- » [View Purchased Documents](#)

Profile Information

- » [Communications Preferences](#)
- » [Profession and Education](#)
- » [Technical Interests](#)

Need Help?

- » **US & Canada:** +1 800 678 4333
- » **Worldwide:** +1 732 981 0060

[» Contact & Support](#)

[About IEEE Xplore](#) | [Contact Us](#) | [Help](#) | [Accessibility](#) | [Terms of Use](#) | [Nondiscrimination Policy](#) | [Sitemap](#) | [Privacy & Opting Out of Cookies](#)

A not-for-profit organization, IEEE is the world's largest technical professional organization dedicated to advancing technology for the benefit of humanity.
© Copyright 2024 IEEE - All rights reserved. Use of this web site signifies your agreement to the terms and conditions.



Institutional Sign In

All



[ADVANCED SEARCH](#)

Conferences > 2023 International Conference...

Impact Analysis of Distributed DoS Attack by Multiple HTs in TCMP Architectures

Publisher: **IEEE**

[Cite This](#)

PDF

Josna Philomina ; Rekha K James ; Shirshendu Das ; Daleesha M Vishwanathan [All Authors](#) ...



34
Full
Text Views

Alerts

[Manage Content Alerts](#)
[Add to Citation Alerts](#)

Abstract



Downl
PDF

Document Sections

- I. Introduction
- II. TCMP BASELINE ARCHITECTURE
- III. Related Works
- IV. Proposed Work
- V. Experiments and Results

[Show Full Outline](#) ▾

Authors

Figures

References

Keywords

Metrics

More Like This

Abstract: Tiled Chip Multicore Processors (TCMP) with packet switching Network-on-Chip (NoC) have become a common method for on-chip connectivity. The performance of the entire sys... [View more](#)

► Metadata

Abstract:

Tiled Chip Multicore Processors (TCMP) with packet switching Network-on-Chip (NoC) have become a common method for on-chip connectivity. The performance of the entire system may suffer if a malicious Hardware Trojan (HT) is present in the NoC routers as it might negatively disrupt communication between tiles. Detecting Trojans in complicated multi-processor System on Chips (SoCs) using traditional pre and post silicon validation approaches is a huge difficulty. In this paper the presence of multiple HTs in the routing unit is modelled and its impact analysis is done for both synthetic traffic and real benchmarks using gem5 simulator. It can be observed that the presence of multiple trojans decrease the overall performance of the system.

Published in: 2023 International Conference on Control, Communication and Computing (ICCC)

Date of Conference: 19-21 May 2023

DOI: 10.1109/ICCC57789.2023.10165276

Date Added to IEEE Xplore: 04 July 2023

Publisher: IEEE

► ISBN Information:

Conference Location: Thiruvananthapuram, India

Josna Philomina
School of Engineering, CUSAT, Kerala, India

Rekha K James
School of Engineering, CUSAT, Kerala, India

Shirshendu Das
Indian Institute of Technology, Ropar, Punjab, India



Contents

I. Introduction

System-on-Chips (SoCs) began containing third party Intellectual Property (IP) blocks to lower the overall cost of microprocessors used in embedded systems and the Internet of Things. Several chip manufacturing firms outsource the automated integrated circuit design, production, and testing due to the high design costs [1]. The logical and operational security of such devices are at danger because suspicious third parties were involved at different stages of chip manufacture. During the SoC's verification and testing process, malicious circuits known as Hardware Trojans (HT) concealed inside a trustworthy blueprint design may go undetected [2]. HTs may modify the system's behaviour in order to launch attacks including data breaches, unauthorised access, functional defects, and service delays [3]. Because these intermittent HTs are only active for a brief period of time, HT identification is difficult [4].

Authors

Josna Philomina
School of Engineering, CUSAT, Kerala, India

Rekha K James
School of Engineering, CUSAT, Kerala, India

Shirshendu Das
Indian Institute of Technology, Ropar, Punjab, India

Daleesha M Vishwanathan
School of Engineering, CUSAT, Kerala, India

Figures

References

Keywords

Metrics

More Like This

Load balanced adaptive routing with reduced overhead for Network on Chip (NoC) Systems
2013 International Conference on Information Communication and Embedded Systems (ICICES)
Published: 2013

TCAR: Thermal and Congestion-Aware Routing Algorithm in a Partially Connected 3D Network on Chip

IEEE Personal Account

CHANGE
USERNAME/PASSWORD

Purchase Details

PAYMENT OPTIONS
VIEW PURCHASED
DOCUMENTS

Profile Information


COMMUNICATIONS
PREFERENCES
PROFESSION AND
EDUCATION
TECHNICAL INTERESTS

Need Help?

US & CANADA: +1 800
678 4333
WORLDWIDE: +1 732
981 0060
CONTACT & SUPPORT

Follow



[About IEEE Xplore](#) | [Contact Us](#) | [Help](#) | [Accessibility](#) | [Terms of Use](#) | [Nondiscrimination Policy](#) | [IEEE Ethics Reporting](#)  | [Sitemap](#) | [IEEE Privacy Policy](#)

A not-for-profit organization, IEEE is the world's largest technical professional organization dedicated to advancing technology for the benefit of humanity.

© Copyright 2024 IEEE - All rights reserved.

IEEE Account

- » [Change Username/Password](#)
- » [Update Address](#)

Purchase Details

- » [Payment Options](#)
- » [Order History](#)
- » [View Purchased Documents](#)

Profile Information

- » [Communications Preferences](#)
- » [Profession and Education](#)

» [Technical Interests](#)

Need Help?

» **US & Canada:** +1 800 678 4333

» **Worldwide:** +1 732 981 0060

» [Contact & Support](#)

[About IEEE Xplore](#) | [Contact Us](#) | [Help](#) | [Accessibility](#) | [Terms of Use](#) | [Nondiscrimination Policy](#) | [Sitemap](#) | [Privacy & Opting Out of Cookies](#)

A not-for-profit organization, IEEE is the world's largest technical professional organization dedicated to advancing technology for the benefit of humanity.

© Copyright 2024 IEEE - All rights reserved. Use of this web site signifies your agreement to the terms and conditions.



International Conference on Smart Trends for Information Technology and Computer Communications

SmartCom 2023: **Smart Trends in Computing and Communications** pp 671–679

[Home](#) > [Smart Trends in Computing and Communications](#) > [Conference paper](#)

Image Forgery Detection Using Deep Learning

[Litty Koshy](#)  & [K. Chithu](#)

Conference paper | [First Online: 15 June 2023](#)

153 Accesses

Part of the [Lecture Notes in Networks and Systems](#) book series (LNNS, volume 650)

Abstract

Since cameras are so widely available, taking pictures has become more and more common. In order to gain more information, it is frequently necessary to enhance photographs, which are crucial in our daily lives as memories or sources of wealth of information. There are many tools accessible to enhance the quality of photos; however, some of them are also widely used to alter images, leading to the dissemination of false

information. This makes picture forgeries more severe and frequent, which is now a major cause of concern. To identify fake images, many conventional methods have been developed over time.

Convolutional neural networks (CNNs) have drawn a lot of interest recently, and they have had an impact on the area of picture fraud detection as well. However, the majority of CNN-based picture forgery detection methods currently used in the literature are restricted to identifying a certain kind of fraud (either image splicing or copymove). As a result, a method that can quickly and precisely identify any hidden forgeries in a picture is needed. We present a powerful deep learning-based approach for detecting picture forgeries in this study. The RGB format images converted to error level analysis (ELA) are used to train our model. The suggested model is compact, and its effectiveness shows that it outperforms cutting-edge methods in terms of speed. The experiment's findings are promising, with a 91.37% total validation accuracy.

Keywords

Error level analysis

Convolutional neural network Image splicing

Copy move

This is a preview of subscription content, [log in via an institution](#).

▼ Chapter	EUR 29.95
	Price includes VAT (India)
<ul style="list-style-type: none">• Available as PDF• Read on any device• Instant download• Own it forever	
<input type="button" value="Buy Chapter"/>	
> eBook	EUR 234.33
> Softcover Book	EUR 279.99

Tax calculation will be finalised at checkout

Purchases are for personal use only

[Learn about institutional subscriptions](#)

References

1. Bayram S et al (2006) Image manipulation detection. *J Electron Imaging* 15(4):041102

2. Al-Qershi OM, Khoo BE (2013) Passive detection of copy-move forgery in digital images: state-of-the-art. *Forensic Sci Int* 231(1–3):284–295

3. Qazi T et al (2013) Survey on blind image forgery detection. *IET Image Process* 7(7):660–670

4. Dong J, Wang W, Tan T (2013) Casia image tampering detection evaluation database. In:

2013 IEEE China summit and international conference on signal and information processing. IEEE

5. Yadav S, Singh S (2015) A review on image compression techniques. *Int J Adv Res Comput Eng & Technol (IJARCET)* 4(9):3513–3521

6. Gregor K et al (2015) Draw: a recurrent neural network for image generation. In: *International conference on machine learning*. PMLR

7. Ryu J, Yang M-H, Lim J (2018) DFT-based transformation invariant pooling layer for visual classification. In: *Proceedings of the European conference on computer vision (ECCV)*

8. Ma W, Lu J (2017) An equivalence of fully connected layer and convolutional layer. [arXiv:1712.01252](https://arxiv.org/abs/1712.01252)

9. Kattenborn T et al (2021) Review on convolutional neural networks (CNN) in vegetation remote sensing. *ISPRS J Photogramm Remote Sens* 173:24–49

10. Schmidt-Hieber J (2020) Nonparametric regression using deep neural networks with

ReLU activation function. Ann Stat 48(4):1875–1897

11. Dunne RA, Campbell NA (1997) On the pairing of the softmax activation and cross-entropy penalty functions and the derivation of the softmax activation function. In: Proceedings of 8th Australian conference on the neural networks, Melbourne, vol 181. Citeseer

12. Galbally J, Marcel S (2014) Face anti-spoofing based on general image quality assessment. In: 2014 22nd international conference on pattern recognition. IEEE

Author information

Authors and Affiliations

**Department of Computer Science and
Engineering, SCMS School of Engineering &
Technology, Ernakulam, India**

Litty Koshy

**Master of Computer Applications, SCMS School
of Engineering & Technology, Ernakulam, India**

K. Chithu

Corresponding author

Correspondence to [Litty Koshy](#).

Editor information

Editors and Affiliations

University of the Ryukyus, Nishihara, Japan

Tomonobu Senjyu

Khon Kaen University, Khon Kaen, Thailand

Chakchai So-In

Global Knowledge Research Foundation,

Ahmedabad, India

Amit Joshi

Rights and permissions

[Reprints and permissions](#)

Copyright information

© 2023 The Author(s), under exclusive license to Springer Nature Singapore Pte Ltd.

About this paper

Cite this paper

Koshy, L., Chithu, K. (2023). Image Forgery Detection Using Deep Learning. In: Senjyu, T., So-In, C., Joshi, A. (eds) Smart Trends in Computing and Communications. SmartCom 2023. Lecture Notes in Networks and Systems, vol 650. Springer, Singapore. https://doi.org/10.1007/978-981-99-0838-7_57

[.RIS](#) [.ENW](#) [.BIB](#)

DOI	Published	Publisher Name
https://doi.org/10.1007/978-981-99-0838-7_57	15 June 2023	Springer, Singapore

Print ISBN	Online ISBN	eBook Packages
------------	-------------	----------------

978-981-99-0837-0	978-981-99-0838-7	Intelligent Technologies and Robotics
		Intelligent Technologies and Robotics (R0)

Publish with us

[Policies and ethics](#)

The IRMA Community

Calls for Papers

Online Symposium

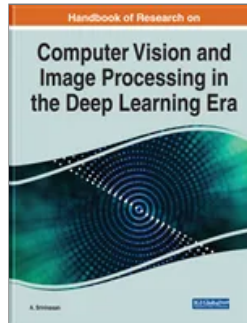
Newsletters

Research IRM

Click a keyword to search titles using our InfoSci-OnDemand powered search:

- Business Management
- Environmental IS
- Healthcare
- Electronic Commerce
- Library Science
- Computer Science
- Social Science
- Multimedia IS
- Information Systems
- Public Administration

Predictive Analytics on Female Infertility Using Ensemble Methods



[View Sample PDF](#)

Author(s): Simi M. S. (Adi Shankara Institute of Engineering and Technology, India) and Manish T. I. (SCMS School of Engineering and Technology, India)

Copyright: 2023

Pages: 12

Source title: Handbook of Research on Computer Vision and Image Processing in the Deep Learning Era

Source Author(s)/Editor(s): A. Srinivasan (SASTRA University (Deemed), India)

DOI: 10.4018/978-1-7998-8892-5.ch024

Keywords: Artificial Intelligence / Computer Science & IT / Computer Vision & Image Processing / Information Science Reference

Purchase

View Predictive Analytics on Female Infertility Using Ensemble Methods on the publisher's website for pricing and purchasing information.

Abstract

With the accessibility of healthcare data for a significant proportion of patients in hospitals, using predictive analytics to detect diseases earlier has become more feasible. Identifying and recording key variables that contribute to a specific medical condition is one of the most difficult challenges for early detection and timely treatment of diseases. Conditions such as infertility that are difficult to detect or diagnose can now be diagnosed with greater accuracy with the help of predictive modeling. Infertility detection, particularly in females, has recently gained attention. In this work, the researchers proposed an intelligent prediction for female infertility (PreFI). The researchers use 26 variables for the early diagnosis and determine a subset of these 26 variables as biomarkers. These biomarkers contribute significantly to a better prediction of the problem. The researchers designed PreFI using ensemble methods with biomarkers and improved the performance of the predictive system.

Related Content

Acceleration of Image Processing and Computer Vision Algorithms

Aswathy Ravikumar, Harini Sriraman. © 2023. 18 pages.

Acceleration of Computer Vision and Deep Learning: Surveillance Systems

Ezhilarasie R., Aishwarya N., Subramani V., Umamakeswari A.. © 2023. 10 pages.

Deep Learning Architecture for a Real-Time Driver Safety Drowsiness Detection System

Sangeetha J.. © 2023. 13 pages.

Deep Learning-Based Computer Vision for Robotics

Manivannan Doraipandian, Sriram J., Yathishan D., Palanivel S.. © 2023. 14 pages.

Deep Learning for Emotion Recognition

T. Kavitha, Malini S., Senbagavalli G.. © 2023. 36 pages.

Smart Surveillance System Using Deep Learning Approaches

Uma K. V., Aakash V., Deisy C.. © 2023. 23 pages.

Role of Deep Learning in Image and Video Processing

Alageswaran Ramaiah, Arun K. S., Yathishan D., Sriram J., Palanivel S.. © 2023. 17 pages.

IRMA Offers Over 2,500 Full Text

Open Access Research Papers for Free Download

[Click to Start Searching Free IRM Research!](#)

IRMA Sponsors



Disseminating Innovative Research Worldwide Since 1988

We recommend eContent Pro International for all of your editorial needs!

IRMA Members Receive 25% Discount for Copy Editing

eContent Pro International's Additional Services:

Expert Translation Professional Proofreading

[Click Here to Save 25%](#)

Now Available

Encyclopedia of Information Science and Technology, Fourth Edition



[Click to Recommend to Your Librarian](#)

IGI Global Disseminator of Knowledge



[About Us](#) | [Contact](#) | [Sitemap](#) | [Legal](#) | [Policies](#)

Copyright ©2024, Information Resources Management Association. 701 East Chocolate Avenue, Hershey, PA 17033.

Malware Detection using Dynamic Analysis

Anandhi V¹, Vinod P², Varun G Menon³, Abhijith Krishna E R⁴, Akshay Shilesh⁵, Akshay Viswam⁶, and Amin Shafiq⁷

^{1,3-7}Department of Computer Science and Engineering, SCMS School of Engineering and Technology, Ernakulam.

^{1,3-7}Affiliated to APJ Abdul Kalam Technological University, Thiruvananthapuram, Kerala, India.

²Department of Computer Applications, Cochin University of Science and Technology, Kerala, India.

Email: ¹anandhi@scmsgroup.org, ²vinod.p@cusat.ac.in, ³varunmenon@scmsgroup.org, ⁴abhijith.krishna@scmsgroup.org

Abstract—Malware detection is an indispensable factor in the security of internet-oriented machines. The number of threats have been increased day by day. Malware analysis is a process of performing analysis and a study of the components and behavior of malware. The use of dynamic analysis will help the system to classify malware more accurately and to detect any malware samples. Dynamic analysis is a method in which the malware runs in a Sandbox environment, and artifacts are collected. The system uses Cuckoo Sandbox for executing the malware samples in a controlled environment. The system compares bidirectional long short-term memory and convolutional neural network models for machine learning algorithms to detect and classify the malware samples. Unlike a typical signature-based detection, where patterns are checked in the source file, a type of static detection, here, dynamic analysis is used to extract necessary reports, which are then preprocessed to get features like dynamic link library (dlls), kernel module names, services used, etc. to try creating a list of text, which can explain the behaviour of the executable file. These are tokenized and embedded to obtain numerical data, which is passed to the models. The accuracy of trained models is compared, which describes the performance of the models on the dataset. Thus providing grounds for testing future models and later building a better detection system based on it.

Index Terms—malware analysis, cuckoo sandbox, bidirectional long short-term memory, dynamic analysis

I. INTRODUCTION

Malware is malicious software distributed over a network that infects, steals, examines, or performs any function an attacker desires. Nowadays, malware detection is important as it serves as an essential alert system for the computer's security against cyber threats. It is the process of identifying malware on a host system and determining whether the particular software is harmful or not. It prevents hackers from gaining access to the computer, and avoids risking sensitive data, altering system settings or contents, or propagating through the network. The best measures against malware are antivirus monitoring and firewall software. The number of malware has expanded at an unprecedented rate due to the extensive use of computer systems and networks. With the expanding usage of susceptible online systems and various operating systems, a growing variety of dangers is emerging. As a result, the issue is to locate and identify risks that can be generalized to avoid future attacks on computer systems.

According to the Symantec threat report [1], 4818 unique websites were victims of form jacking code. Every month,

stolen credit card data is sold for up to \$2.2 million to cyber criminals. Similarly, McAfee Labs reported that the DarkSide ransomware has resulted in a policy issue between the US and Russia [2]. In 2022, the Trellix company reported that the cyber attackers used the Log4shell flaw, a software vulnerability, and attacked Ukrainian Infrastructure. There were several campaigns conducted for the cyber threats in the region of Eurasia against Ukraine and identified HermeticWiper. This malware steals digital certificates and gains write access to various low-level data structures on the organizations [3].

In the research carried out, the main contributions of this paper are as follows:

- We develop a malware detection system using Convolutional Neural Network over two benchmark malware datasets namely Malware Bazaar and VirusShare.
- We conduct experiments on images using BiLSTMs to classify malware. and show significant improvement in the performance of deep learning models.
- We compare our proposed system with the state-of-the-art approaches and found that a combination of CNN and BiLSTM achieved better classification results.

The paper is organized as follows. Section II discusses related work on static and dynamic analysis. Section III covers the motivation, methodology used including the BiLSTM architecture. In Section IV, we present our dataset used with the experimental results obtained. Finally, Section V concludes the paper, and we mention future work.

II. RELATED WORK

In today's world, the vulnerabilities of computer systems are well exploited by cybercriminals. There are several types of malware detection methods [4–7]. They are (a) static detection (b) dynamic detection (c) hybrid (d) ML-based detection (e) DL-based detection and (f) visualization.

In the static malware detection method, a malware file is examined without running the program. The main advantage of the static feature extraction method is that it reduces the feature size by considering the entire binary content, thereby detecting the invariants before runtime [8]. Dynamic analysis involves running the malware executable file and analyzing its behavior to eliminate the infection or prevent it from spreading to other systems [9].

Zhang [10] proposes a deep learning architecture that includes both a CNN layer and an LSTM layer where API call sequences are used to train the model. The CNN model consists of filters, LSTM layer, a dropout layer, and lastly fully connected layer for classification. The proposed model achieved an accuracy of nearly 100%.

Mishra et al. [11] proposed a BiLSTM based model to classify malware in a cloud-based system. CNN layer is the basic block and the model is trained on system call sequences. An accuracy of 90% was achieved. They also made a comparison by substituting the BiLSTM for a normal LSTM layer which resulted in a worse case of detection.

Mcdole et al. [12] records and analyzes the behavior of malware executables using dynamic analysis. The information collected during execution is the memory access, API calls, and network communications.

Usman et al. [13] proposed a novel cyber security techniques on hybrid approach based on dynamic malware analysis that can identify malicious Internet Protocol addresses before communication. Huang et al. [14] propose a malware detection method based on malware visualization and deep learning. The static visualization images are generated by Cuckoo Sandbox. It is used to generate dynamic visualization images. Then form hybrid images that merge the static and dynamic images. Finally, the model train the hybrid images yielding a test accuracy of 92.50% for the hybrid approach.

A novel method for detecting malware by deep learning-based analysis was proposed by Liu et al. [15] on API calls. They used cuckoo sandbox and Filtering techniques were employed to extract the API calls sequence of malicious programs. A comparison on the experimental results with standard models were done. The proposed LSTM has the best performance for malware detection, reaching the accuracy of 97.85%.

Wu et al. [16] proposed an architecture with CNN integrated with attention block used to extract effective features of the load impact factors. Then prediction is forecasted by the LSTM combined with BiLSTM layers and found that the proposed method has better forecasting performance than the state-of-art approaches. Peng et al. [17] proposed a deep learning model based on Bi-directional long short-term memory, sine cosine algorithm, and complete ensemble empirical mode decomposition with adaptive noise for forecasting and found that the model obtained higher prediction accuracy than the existing models.

III. PROPOSED METHOD

The overall method consists of five different modules namely, input data preprocessing, feature representation, feature encoding, feature extraction, and classification.

A. Motivation

The motivation of this paper is that the traditional classification methods have to be improved as there is various limitation in static and dynamic methods. Dynamic malware analysis of new samples is highly time-consuming and requires proper tuning to achieve good performance with an acceptable result.

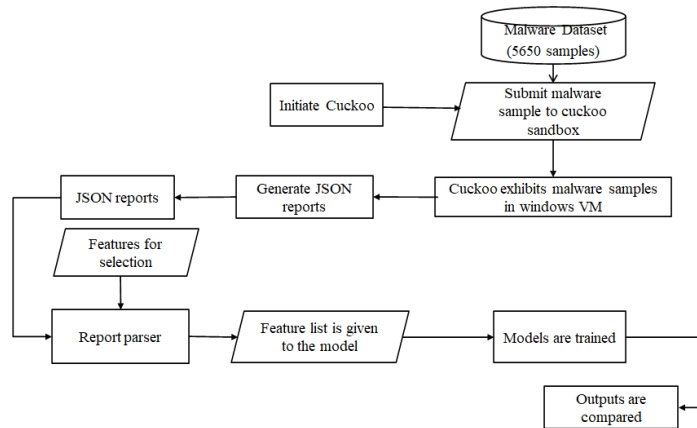


Fig. 1. Flow diagram of proposed system

B. Methodology

Digital security is an important aspect of our daily life. This paper aims to contribute in the direction of classifying malware as accurately as possible. The proposed system is a malware classification system that uses BiLSTM and CNN model to analyse the behavior of malware samples in a controlled sandbox environment and have the model learn to properly identify a malware sample from a benign one. This system being dynamic, can actively classify malware that have not been classified before unlike current antivirus software. The samples are first fed into the sandbox and after receiving a log file containing the executed operations, it is fed into the models, and the results obtained are compared between the models. The proposed block diagram and its interconnection along with the various stages involved are depicted in Fig 1.

The significance of feature selection increases the accuracy and reduces the redundant features, thereby increasing the prediction time.

C. Algorithm

The purpose is to parse the report.json files and extract wanted features into specific files. The input is the location to the output of dumps. The output is files written to the output directory which are text files that contain the features. The detailed step-by-step process is given in Algorithm 1.

D. Cuckoo Sandbox

Basically, a cuckoo sandbox is a Linux Ubuntu host that in turn contains a nested Windows 7 machine in it [18]. The open-source tool called Cuckoo Sandbox is used to analyze malware automatically. This tool works in a controlled and secure environment. This tool makes an intention to the malware that it has affected a true host machine, which then records the malware activity. Finally generates a malware report on the activities done by the malware on the virtual machine (VM).

Linux commands or GUI can be used for accessing the cuckoo sandbox. The malware is submitted to the VM to the

Algorithm 1 Parser Algorithm

Require: Iterate through each folder (classes) for batch folders

Ensure: For each file report file in each batch, perform the following steps to extract the features from JSON files

- 1: Extract dll from pe_imports
- 2: Extract name from pe_sections
- 3: Extract kernel_mod_name from modscan data
- 4: Extract service from svscan data
- 5: Extract proc_name from malfind data
- 6: Extract process from pslist data
- 7: Extract mut_name from mutscan data
- 8: Combine these values separated by newline

Require: Write output txt file with features for each malware sample in a fixed output directory

Windows guest. The malware once submitted runs on the VM. The malware behavior is recorded and this activity is fed to the Ubuntu host and a report is generated based on the activity.

E. Bidirectional long short-term memory

Although LSTM is popular and has more advantages, it could not completely solve the vanishing gradient problem. This model uses more resources and takes more time to get trained. They use high memory and bandwidth because of the layers connected in serial fashion. Thus, LSTMs do not use the hardware efficiently.

LSTM requires more computation as more parameters are required. So Bidirectional long short-term memory or BiLSTM, is used. A Bidirectional Long Short-term Memory [19], is a model that processes information with two LSTMs in a forward and backward direction as shown in Fig. 2. The efficiency of the model is increased by understanding the context, which allows the model to learn the preceding and following words. Bidirectional recurrent neural networks are simply adding up two RNNs where one works forward and the other in a reverse direction.

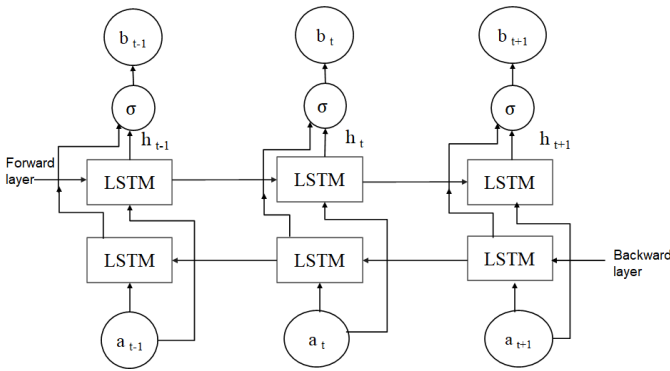


Fig. 2. BiLSTM structure

F. Word Embedding

Word embedding is a technique where words of similar meaning are given the same pattern representation as real-valued vectors. There are fewer dimensions in this type of representation. This method is used to train on any natural language processing task as it is easy to understand.

G. Text Vectorization

The process of converting text into numerical representation is Text Vectorization.

TF-IDF (Term Frequency–Inverse Document Frequency) captures the number of occurrences the word is available in the whole document. The words occurring frequently are given less weight. This inverse weighting for frequently occurring words is known as Inverse Document Frequency. This term gives the relative importance of words in a collection of texts or sets of documents. TF-IDF calculation is used in Natural Language Processing problems where the more frequently occurring words have less weight and words which are not repeated will have more weight. Let w denote TF-IDF weight of any feature x , $tf(x)$ denote frequency of feature x , N be the number of ransomware samples in the document, and IDF denotes the instances that contain the feature x . The following steps are used for calculating TF-IDF as shown in Equation 1.

- Define the term frequency values
- Calculate inverse document frequency values (IDF)
- Multiply the above two values. This indicates how often the words occur in the document

$$w(x) = tf(x) * \log \frac{N}{IDF(x) + 1} \quad (1)$$

H. Convolutional Neural Network

Convolutional neural networks have always become the predominant machine learning algorithm [20] since CNN is a simple feed-forward network that uses automatic feature extraction and uses adjacent pixel information to downsample the image effectively. CNN is a typical neural network in which at least one layer is a convolutional layer. In CNNs, with more hidden layers, the gradient vanishes which stops the learning phase.

IV. EXPERIMENTAL RESULTS

The experiments are conducted using Precision, Recall, F1 measure, and Accuracy as evaluation metrics for the classification.

Categorical accuracy: Categorical accuracy measures the average accuracy rate across all predictions. This is calculated by comparing the one-hot vectors of truths and predictions and then taking an average over the vector. In the proposed system, accuracy is calculated using the metric given below for both training and validation.

$$Accuracy(A) = \frac{TP + TN}{TP + TN + FP + FN}. \quad (2)$$

where True Positive (TP - indicates the number of malware samples correctly identified as malware), True Negative (TN

- indicates the number of benign samples accurately identified as legitimate.), False Positive (FP - is the number of benign samples misclassified as malware), and False Negative (FN - indicates the number of wrongly classified malware images).

Implementation and Setup: The Linux OS system with Ubuntu 20.04 is installed on the Virtual Machine. The Cuckoo Sandbox and Python with windows are installed on a Virtual Machine. Now both OS can be used without using a separate boot system.

Dataset: The experiments are performed on two malware datasets, Malware Bazaar [21] and VirusShare [22]. In this paper, we used around 5650 executables belonging to 6 classes including 1471 benign samples. 70% of the dataset is used for training and the remaining 30% is reserved for testing. 3955 files for training and 1695 files for validation. A Windows operating system (OS) is installed in the cuckoo sandbox virtual machine and is used to extract the system calls from the malware executable samples.

By using the appropriate measures, the performance of the models is calculated. We conduct the three experiments on the dataset:

- **Experiment-1:** Performance of CNN model in detecting malware executables.
- **Experiment-2:** Performance of BiLSTM model in detecting malware executables.
- **Experiment-3:** Performance of CNN-BiLSTM model in detecting malware executables.

A. Performance of CNN model in detecting malware executables

CNN model consisting of text_vectorization layer, word embedding, three CONV layers, each followed by a Pooling layer, Flattening, and finally the fully connected layer.

A convolutional neural network consists of the following layers:

- Convolutional layers - First layer is the convolution layer which is presented with training and testing malware images. A filter is convolved across the width and height of the input image to extract patterns specific to malware and benign files. Here the kernel size chosen is a 3×3 filter. The kernel is slid over the input and the product is computed at all positions. The convolution layer gives maximum information by reducing the noise in the input features. Parameters include stride, step filter size, and filter count, which is the number of filters used.
- Pooling layers - Next is the max pooling layer which reduces the data processing by taking the maximum value obtained in the first slide of the kernel. A 2×2 is the window size or the filter size used for the max pooling operation. Max pooling takes the maximum value from each group of neurons from the previous layer. This is also called the sub-sampling layer as the computation is performed by downsampling the features, thereby reducing the processing involved.
- Dense layers - Finally, the fully connected dense layer is incorporated where every neuron in one layer is con-

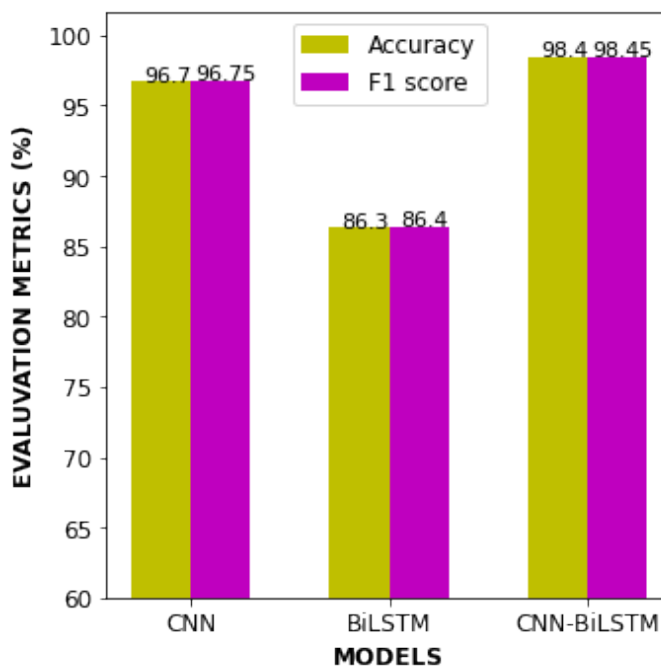


Fig. 3. Accuracy and F1 score for three models

nected to every other neuron in the other layer. The basic principle of CNN is the same as the multilayer perceptron. The flattened matrix after max pooling passes through the fully connected layer to classify the images. The network is trained by the back-propagation method where the weights and bias are updated and the loss is calculated. When the loss function is close to zero, the learning phase terminates.

The model produced an average accuracy of 96.7% as shown in Fig 3. Since the dataset is a balanced set, we get approximately the same scores.

B. Performance of BiLSTM model in detecting malware executables

BiLSTM model consists of text_vectorization layer, input, embedding layer, two BiLSTM layers with dropout layers, and finally the dense layer. In the proposed model, the input to the BiLSTM is an array. By knowing the input, past, and future states of its local neighbors, BiLSTM can predict the present input. We have used a Dropout of 0.25 on the BiLSTM layer. Sigmoid is used as an activation function. Finally, the image vector representation passes through the dense layer. The activation function used by all feed-forward layers is Tanh and the final prediction is achieved using the softmax function. The model produced an average accuracy of 86.3% as shown in Fig 3.

C. Performance of CNN-BiLSTM model in detecting malware executables

The proposed CNN-BiLSTM consists of text vectorization layer, an input layer, word embedding layer, two convolution layers, pooling layers (maxpool), BiLSTM layer, dropout layer, and finally the dense fully connected layer for classification. Figure 3 shows that the model produced an average accuracy of 98.4%.

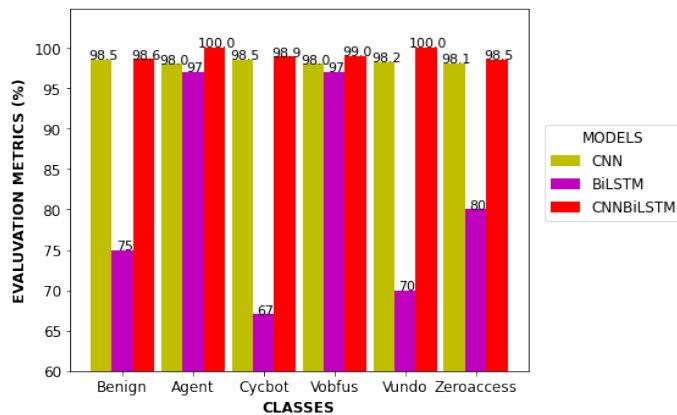


Fig. 4. Classification accuracy for three models

We considered 597 malware executables from agent, 936 from cycbot, 926 from vobfus, 600 from vundo, 1120 from zeroaccess malware families for the dynamic analysis, and 1471 benign files with a total of 5650 files belonging to 6 classes, where 3955 files were used for training and 1695 files for validation phase. Figure 4 shows the evaluation metrics for the six classes considered for all three models. It is observed that the average accuracy of 98.5% is obtained for a combination of CNN with BiLSTM for all families considered. The proposed model has shown efficient performance for the classification, which extracts useful features and better feature representation, resulting in achieving better accuracy.

V. CONCLUSION AND FUTURE SCOPE

In recent times, the amount of malware affecting systems has become enormous and diverse in nature. Automating the detection and classification of new malware helps the forefront of defenders to rest a bit ease. The effectiveness of machine learning has encouraged peers to find methods to tackle this problem. The study here uses Dynamic analysis techniques to extract malware artifacts and process them using BiLSTM and CNN models and experiments with them to classify across five malware classes and a benign class. A combination of CNN-BiLSTM model produced an average accuracy of 98.4%. The CNN-BiLSTM model performs better than the BiLSTM model in classification and detection of malwares. There is a gradual increase in accuracy when compared with the other state of art methods.

In future work, we intend to include more models and more malware classes, specifically towards self-attention models to

improve the overall accuracy further. We also intend to provide a web and android app interface, where one can submit a file, and get a report summary on the file, detecting any malicious instructions within the file. This would help the layman have free, and bleeding-edge access to a malware-detection system, which does not rely on signatures and similar concepts.

REFERENCES

- [1] <https://docs.broadcom.com/docs/istr-04-march-en>
- [2] <https://www.mcafee.com/enterprise/en-us/assets/reports/rp-ryuk-ransomware-targeting-webservers.pdf>
- [3] <https://www.trellix.com/en-us/threat-center/threat-reports/apr-2022.html>
- [4] Roundy, Kevin A., and Barton P. Miller. "Hybrid analysis and control of malware", In International Workshop on Recent Advances in Intrusion Detection, pp. 317-338. Springer, Berlin, Heidelberg, 2010.
- [5] Wang, Huanran, Weizhe Zhang, and Hui He, "You are what the permissions told me! Android malware detection based on hybrid tactics", Journal of Information Security and Applications 66, 2022.
- [6] Ijaz, Muhammad, Muhammad Hanif Durad, and Maliha Ismail, "Static and dynamic malware analysis using machine learning", In 2019 16th International bhurban conference on applied sciences and technology (IBCAST), pp. 687-691, 2019.
- [7] Nataraj, Lakshmanan, Sreejith Karthikeyan, Gregoire Jacob, and S. Manjunath, "Malware images: visualization and automatic classification", In Proceedings of the 8th international symposium on visualization for cyber security, pp. 1-7, 2011.
- [8] Adel Abusitta, Miles Q. Li, Benjamin C.M. Fung, "Malware classification and composition analysis: A survey of recent developments", Journal of Information Security and Applications, vol. 59, 2021.
- [9] Singh, Jagsir, and Jaswinder Singh. "A survey on machine learning-based malware detection in executable files." Journal of Systems Architecture 112, 2021.
- [10] J. Zhang, "DeepMal: A CNN-LSTM Model for Malware Detection Based on Dynamic Semantic Behaviours," 2020 International Conference on Computer Information and Big Data Applications (CIBDA), pp. 313-316, 2020.
- [11] Mishra, P., Khurana, K., Gupta, S., & Sharma, M. K., "VMAnalyzer: Malware Semantic Analysis using Integrated CNN and Bi-Directional LSTM for Detecting VM-level Attacks in Cloud", Twelfth International Conference on Contemporary Computing (IC3), 2019.
- [12] Mcdole, Andrew & Gupta, Maanak & Abdelsalam, Mahmoud & Mittal, Sudip & Alazab, Mamoun, "Deep Learning techniques for Behavioral Malware Analysis in Cloud IaaS", 2020.
- [13] Usman, Nighat, Saeeda Usman, Fazlullah Khan, Mian Ahmad Jan, Ahthasham Sajid, Mamoun Alazab, and Paul Watters, "Intelligent dynamic malware detection using machine learning in IP reputation for forensics data

- analytics”, *Future Generation Computer Systems* 118, pp. 124-141, 2021.
- [14] Huang, Xiang, Li Ma, Wenyin Yang, and Yong Zhong, ”A method for Windows malware detection based on deep learning”, *Journal of Signal Processing Systems* 93, no. 2, pp. 265-273, 2021.
- [15] Liu, Yingying, and Yiwei Wang, ”A robust malware detection system using deep learning on API calls”, In *2019 IEEE 3rd Information Technology, Networking, Electronic and Automation Control Conference (ITNEC)*, pp. 1456-1460, 2019.
- [16] Wu, K., Wu, J., Feng, L., Yang, B., Liang, R., Yang, S., & Zhao, R., ”An attention-based CNN-LSTM-BiLSTM model for short-term electric load forecasting in integrated energy system”, *International Transactions on Electrical Energy Systems*, 31(1), 2020.
- [17] Peng, T., Zhang, C., Zhou, J., & Nazir, M. S., ”An integrated framework of Bi-directional long-short term memory (BiLSTM) based on sine cosine algorithm for hourly solar radiation forecasting”, *Energy*, 221, 2021.
- [18] Nunes, Matthew, Pete Burnap, Omer Rana, Philipp Reinecke, and Kaelon Lloyd, ”Getting to the root of the problem: A detailed comparison of the kernel and user-level data for dynamic malware analysis”, *Journal of Information Security and Applications* 48, 2019.
- [19] Zhiyong Cui, Ruimin Ke, Ziyuan Pu, Yinhai Wang, ”Deep Bidirectional and Unidirectional LSTM Recurrent Neural Network for Network-wide Traffic Speed Prediction”, *Computer and information sciences*, 2018.
- [20] Daniel Gibert, Carles Mateu, Jordi Planes, and Ramon Vicens, ”Classification of Malware by Using Structural Entropy on Convolutional Neural Networks”, *The Thirtieth AAAI Conference on Innovative Applications of Artificial Intelligence*, 2018.
- [21] <https://bazaar.abuse.ch/browse/>
- [22] <https://virusshare.com>

Wearable Fabric Tactile Sensors for Robotic Elderly Assistance

Mary Catherine V G
Division of Electronics
 Cochin University of Science
 and Technology
 Cochin, India
 marycatherinevg@cusat.ac.in

Binu Paul
Division of Electronics
 Cochin University of
 Science and Technology
 Cochin, India
 binupaul@cusat.ac.in

Vinoj P G
Department of ECE
 SCMS School of Engineering
 and Technology
 Karukutty, India
 vinojpg@scmsgroup.org

Abstract—The demand for Robots in Elderly assistance is increasing due to the lack of human caregivers. In the context of Robot coexisting with the human beings in a home environment, for the safe and friendly interaction it is essential to endow the sense of touch through Tactile sensor systems. This paper proposes a novel scalable approach for tactile sensors based on low cost wearable conductive fabric. Fabric tactile sensor (FABTAC) is conformable with the robot body and can be used as a tactile sensing skin that perceives touch and force applied at the contact location. FABTAC sensors are developed as an array of touch sensors sewed on the cloth substrate with the stainless-steel conductive thread. The thermistor sensors are also sewed to fabric to perceive the temperature information. The FABTAC sensors are integrated on to the custom-made 3D printed Robotic hand and the tactile data is processed with a novel wearable electronic FLORA microcontroller platform. The acquired data can be used to provide a real time tactile feedback for performing assistive tasks like grasping objects of diverse profiles, avoiding slippage. The FABTAC sensors has the advantage of utilizing flexible, light weight sensors with good spatial and temporal resolution. Thus, the system can potentially aid the automation of daily life activities of the Elderly thereby enhancing the quality of their life.

Keywords—Tactile sensing, Human Robot Interaction, Wearable sensors, Fabric sensors, Tactile feedback

I. INTRODUCTION

The number of caregivers is not growing in tandem with the growth of the Elderly population. The high expense of elderly support is due to the relative scarcity of caregivers for the elderly. The enormous expense of providing care for the elderly could be significantly reduced by using robots in this scenario. Robots with a tactile sensing skin is required for interactions to be both secure and safe. Our human brain senses the touch with the somatosensory system containing a large network of nerve endings and touch receptors on skin, which transmit the tactile information to the brain which in turn tells the body how to react to different senses. The tactile sensors being the electronic counterpart of biological skin, enables the robot to perceive their environment and create a reactive behavior in response to human expectations.

Bioinspired, tactile sensing is important for robots which works in close interaction with the human beings as in elderly care applications. Tactile sensors can estimate the contact parameters like mechanical touch, pressure and temperature at the contact area [1].

Unlike the visual and auditory senses, human skin is not a localized sensory organ which makes the tactile sensing more challenging in terms of transduction technology [2]. And the sensors should be distributed throughout the body. As touch can take many forms-shapes, texture, force, pain, temperature it is not one physical property to be sensed which makes the sensor design more complex and thereby making it difficult to mimic the tactile sensing [3].

A. Criteria for Selection of Tactile Sensors

The Criteria for selection of tactile sensors are reported below[3]

- a) Spatial resolution
- b) Contact Parameters to be measured
- c) Response profile
- d) Time resolution

B. Transduction Techniques

Earlier, the research in the field of tactile sensing focused towards the transduction technology/sensor design.

Various tactile sensor systems have been proposed to cover the robot body for the grasping and manipulation of fine and fragile objects with dexterity. Capacitive tactile sensors are based on changes in the distance between the parallel plates on mechanical touch thereby changing capacitance. This effect can be utilized to detect static touch. They have high sensitivity and has a large dynamic range[4]-[7]. Piezoelectric tactile sensors works on piezoelectric effect where the materials generate an electrical voltage on application of external force . This effect can be utilized for dynamic touch sensing [9][10]. Optical tactile sensors utilizes changes in light intensity to detect external force applied at the point of touch as reported in [11][12].

II. RELATED WORK

The human Interactive Robot RI-MAN [13] embedded with tactile sensors has been developed for assistive care applications to determine the contact load while carrying a dummy human. 320 tactile pressure-sensing elements are integrated on the body with each sensor sheet having 8 x 8 elements placed at the chest and forearms.

A tactile sensor suit, flexible and soft, that has 192 sensing regions has been proposed [14]. The designed robotic suit used electrically conductive cloth and string to build the sensor outfit. Each sensing region functions as a binary switch. The tactile sensing is based on a layered architecture.

A low-cost simple method has been reported [15] to transform a knitted glove to a scalable tactile glove with a sensor array of 548 sensors. The glove has a piezoresistive film connected to conductive thread electrodes. The glove can be utilised to recognise distinguish object and to estimate their weight while grasping.

A fabric-based stretchable tactile sensing skin to measure force and temperature parameters has been reported in [16]. The sensors were integrated on MEKA M1 Mobile Manipulator to make contact on the arms of human being which demonstrated the feasibility of the system for Human Robot Interactive environment.

III. PROPOSED ARCHITECTURE

The Literature reports shows that the large area coverage of sensors at high spatial resolution comes at the expense of high cost technology requirements. This paper presents a novel low-cost approach to tactile sensors for robots based on conductive fabric which can sense human touch utilizing the capacitance transduction effects.

The experimental study was conducted towards creating a tactile sensing skin to perceive touch, force and temperature parameters at the contact area of touch. The work proposed here is the multimodal wearable approach to tactile sensing so as to utilize this tactile information for dynamic feedback control of robotic hand assistance to Elderly people.

The Hardware Configuration of Wearable FABTAC sensors integrated to robotic hand which can be used in grasping assistance for Elderly persons is shown in the Fig. 1.

The robotic hand can be operated in Grasp mode. For the grasp mode operation, dynamic control of hand is achieved based on the real time feedback from the FABTAC sensors to prevent slippage of objects grasped. This paper highlights on the work on the development and integration of FABTAC sensors on the custom made 3D printed InMoov Robotic Hand.

The wearable FABTAC sensors are developed as an array of tactile elements (taxels) with the Conductive Fabric touch sensors and Force Sensitive Resistor (FSR) placed on the fabric substrate in a two layer architecture. The current version of the array consists of 12 taxels each of dimension 20mm x 20mm with a spatial resolution of 2 mm. The capacitive touch sensors detect the static touch in response to the human finger based on the predetermined threshold level. The FSR placed under the first layer of sensors separated with the spacer estimates the force applied at the

taxels corresponding to the resistance variation. The temperature sensors are sewed to the fabric to perceive the temperature of the human finger at the contact area.

The Fabric tactile sensor array consists of strips of woven conductive fabric, fabricated of Copper and Nickel-plated polyester has been sourced from Adafruit Industries. The tactile sensors are sewed to wearable microcontroller electronic platform -FLORA controller using stainless steel conductive thread which has a fairly low resistivity of 10 ohms per foot. The array structure can be scaled up for the full coverage of the dorsal and palmar side of hand and the fingers of robotic hand.

FSRs placed below the fabric layer allows to detect physical pressure applied on its sensing region [Adafruit Industries]. FSRs changes its resistive value depending on the external pressure applied on it. The resistance change gives the calculation for the amount of force applied when touched.

NTC Thermistors are also sewed to the fabric substrate to estimate the temperature of the human finger when touched.

The tactile data acquired by FABTAC sensors are given to the wearable FLORA microcontroller for further processing and Control action.

IV. METHODOLOGY

The acquired touch sensor data are processed using a FLORA microcontroller which is a fabric friendly wearable electronic platform with ATMEGA 32u4 microcontroller having 14 sewing pads for electrical connections. The FLORA microcontroller is configured in slave mode and reduces the load of high level processing at the Arduino UNO Master controller. This configuration helps for better scalability when large area coverage of sensors on the robotic body is required.

The slave FLORA microcontroller transmits the touch data wirelessly using the module nRF24L01 connected through SPI interface with a data rate of 100 Mbps. The nRF24L01 module is suitable for low power applications. At the receiver side, the tactile data is received using the nRF receiver module and fed to an Arduino Uno controller. For the Experimental study the touch response has been demonstrated using an LED display at the destination side. The Robotic hand with the integrated FABTAC sensors can be activated by elderly touch and dynamic control of the hand can be achieved based on reactive control feedback from the sensors in future work.

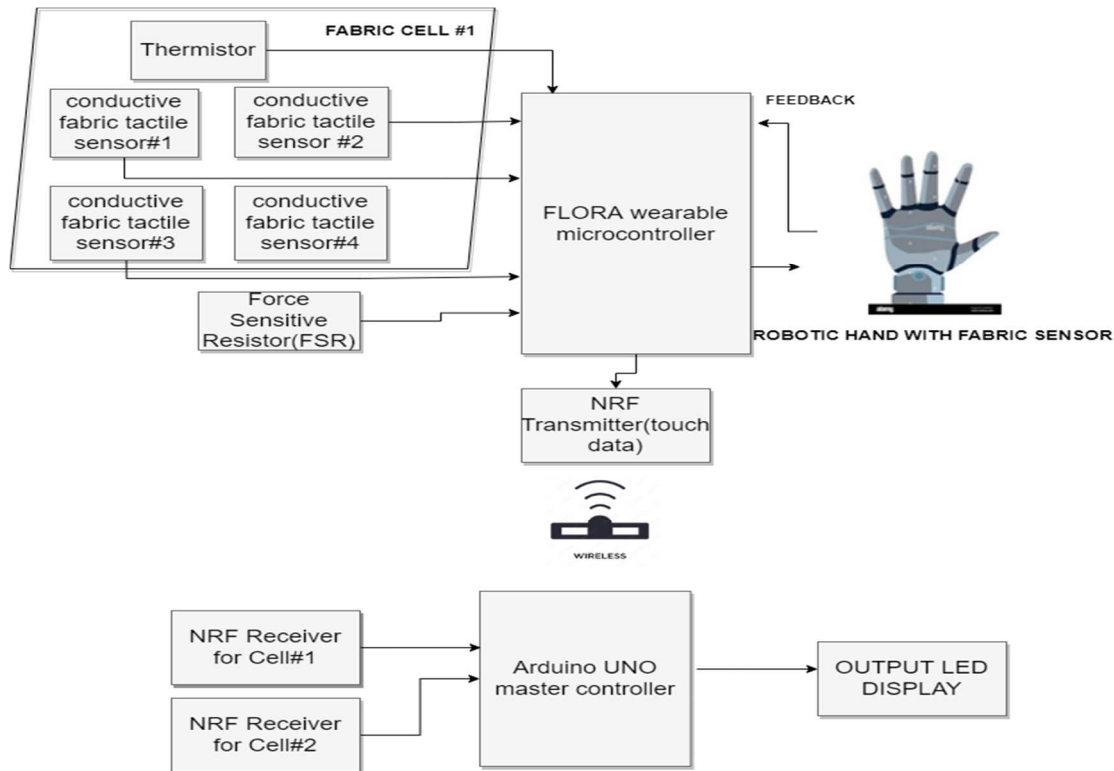


Fig. 1 Hardware Configuration set up of wearable FABTAC sensors for Robotic Hand control

V. RESULTS AND DISCUSSION

The feasibility study of various flexible, light weight, fabric tactile sensors that can be incorporated to Robotic hand Elderly Assistance System has been conducted in this paper.

a) Woven Conductive Fabric Touch Sensor

The experimental results show the response of Woven Conductive Fabric sensor to single finger static touch and a plastic pen. The touch detected with the human finger as shown in Fig 2 (a) has high sensitivity. The dielectric constant increases as a result of the finger's interaction with the capacitor's electric field, thereby increasing capacitance. It has also been inferred that the touch response can be obtained with two fingers simultaneously. The touch response of the plastic material with a low dielectric value could not detect the touch as depicted in Fig 2(b).

The Fig. 2(c) demonstrates the capacitive fabric sensors sewed on the cloth substrate using the conductive thread. The tactile data is fed to the digital pins of the sewing pad of FLORA. A simple hand running stitch is used for sewing the sensors and the microcontroller so as to allow the current flow through the conductive thread. The Fig 2(d) shows the response of touch using the neo pixel RGB LED's which are fabric friendly.



Fig. 2(a)



Fig. 2(b)



Fig. 2(c)



Fig. 2(d)

Fig. 2(a) Single finger touch on Conductive Fabric sensor (b) Touch using plastic pen on Fabric sensor (c) Fabric sensors sewed to FLORA controller using stainless steel conductive thread (d) Touch response of sensor using neo pixel RGB LED

b) Velostat/ Pressure Sensitive sheet Sensor

The study of Velostat sensor was conducted to demonstrate a dynamic touch like vibration on the surface as shown in Fig. 3(a). Velostat is carbon impregnated polyethylene film which can be vibrated and a change in resistance corresponding to vibration was observed.

c) Thermistor

The experimental study of interfacing NTC 10K thermistor with FLORA was conducted. The thermistor was sewed to the cloth substrate and the observations are obtained as in Table 1. Observations are made at Room temperature, soldering iron and a prolonged contact with single finger. It has been observed that the resistance decreases with the increase in temperature and a prolonged contact of finger on the thermistor recorded values as shown in the table. The equivalent temperature T is calculated using Stein Hart Equation as in (1)

$$\frac{1}{T} = \frac{1}{T_0} + \frac{1}{B} \ln\left(\frac{R}{R_0}\right) \quad (1)$$

T_0 is the Room temperature, B is Coefficient of thermistor, R_0 is Resistance at Room temperature and R is unknown resistance calculated.

d) Force Sensitive Resistor(FSR) Sensor

The Fig. 3 (b) shows experimental set up of FSR with a 38 mm square sensing region and the change in resistance when force applied at the touch point can be calculated. The resistance variation is converted to analog voltage with a base resistance of 10K. The figure 5 (a) shows the variation of Voltage and Resistance and it can be observed that the resistance decreases with the increase in voltage which corresponds to increase in force applied on the sensing region. The Fig 5(b) shows the Force vs Voltage variation and Fig 5 (c) demonstrates the change in Force vs Resistance. The various types of touch based on Force in Newtons has been indicated. The types of touch observed are Light touch with less than 1 N is recorded, Light Squeeze on the sensing square region showed up the Force between 2 N and 4 N, Medium Touch (5 -9 N) and Big Touch(10- 66 N).

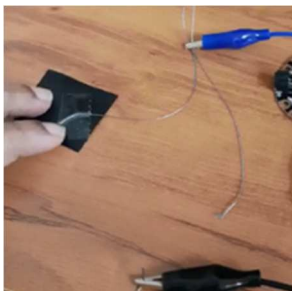


Fig. 3 (a) Dynamic Touch on Velostat sensor (b) Experimental set up of FSR Interfacing with controller

e) Integration of FABTAC sensors on Robotic Hand

The hardware consists of custom - made 3D printed robotic arm InMoov with 2 DOF controlled using MG996R servos. The developed wearable FABTAC sensors are integrated on to the robotic hand and the response of robotic hand when activated by human touch was demonstrated. The Fig 5(a) shows the 3D printed Robotic hand (without tactile sensors) and Fig 5(b) Hand with Wearable FABTAC sensors

TABLE I: TEMPERATURE vs RESISTANCE VARIATION

Temperature (°C)	Resistance (KΩ)	
27.44	8.979	Room temperature
27.53	8.94	
28.09	8.72	Soldering iron used
28.81	8.45	
29.82	8.09	
31.79	7.44	Prolonged Contact with single finger
32.02	7.34	
32.55	7.21	
31.79	7.445	
32.41	7.251	
32.64	7.181	
32.60	7.193	
32.51	7.222	
32.41	7.251	



Fig 4 (a) 3D Printed InMoov Robotic Hand (b) Robotic Hand with wearable FABTAC Sensors

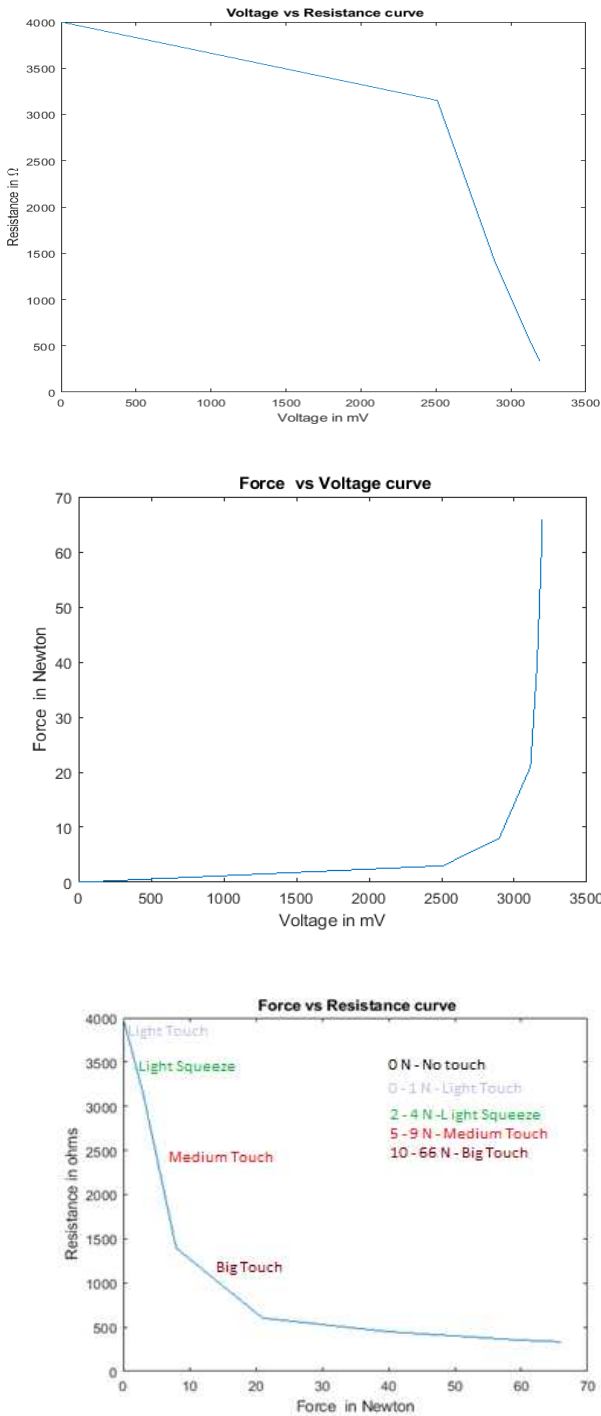


Fig 5(a) Voltage and Resistance Curve (b) Force vs Voltage Curve (c) Force vs Resistance and classification of touch based on Force applied at the contact area.

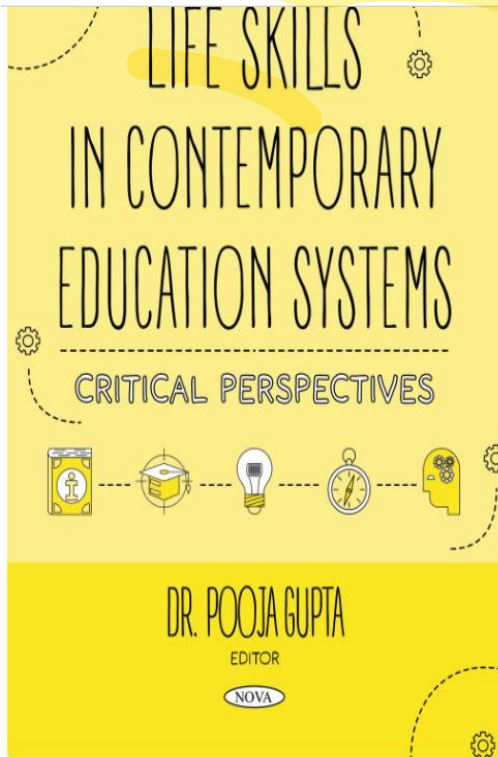
VI. CONCLUSION

The work presented in this paper demonstrates the feasibility study of fabric tactile sensors that can be worn by the robots in an environment where human beings and robots co-exist. The growing demand of robotic platforms in the field of nursing and assistive care emphasize the importance of tactile sensors which are cost effective, scalable and conformable. The tactile sensors and the wearable controller chosen for this work are light weight and flexible thereby providing an advantage of smaller size tactile sensing skin suitable for robotic platforms. The work can be extended in

future to provide tactile feedback based on FABTAC sensors for dynamic control of the robotic hand in Elderly assistance.

REFERENCES

- [1] Dahiya, R. S., Metta, G., Valle, M., & Sandini, G. (2010). Tactile Sensing. Pdf. IEEE Transactions on Robotics, 26(1), 1–20.
- [2] Silvera-Tawil, D., Rye, D., & Velonaki, M. (2015). Artificial skin and tactile sensing for socially interactive robots: A review. *Robotics and Autonomous Systems*, 63(P3), 230–243. <https://doi.org/10.1016/j.robot.2014.09.008>
- [3] M. H. Lee and H. R. Nicholls, "Review Article Tactile Sensing for Mechatronics—A State of the Art Survey," *Mechatronics*, Vol. 9, No. 1, 1999, pp. 1-31. doi:10.1016/S0957 4158(98)00045-2
- [4] P. A. Schmidt, E. Mael, and R. P. Wurtz, "A sensor for dynamic tactile information with applications in human-robot interaction & object exploration," *Robot. Auto. Syst.*, vol. 54, no. 12, pp. 1005–1014, Dec. 2006
- [5] Dahiya, R. S., Mittendorfer, P., Valle, M., Cheng, G., & Lumelsky, V. J. (2013). Directions toward effective utilization of tactile skin: A review. *IEEE Sensors Journal*, 13(11), 4121–4138. <https://doi.org/10.1109/JSEN.2013.2279056>
- [6] H.-K. Lee, S.-I. Change, and E. Yoon, "A flexible polymer tactile sensor: Fabrication and modular expandability for large area deployment," *J. Microelectromech. Sys.*, vol. 15, no. 6, pp. 1681–1686, Dec. 2006.
- [7] M. Maggiali, G. Cannata, P. Maiolino, G. Metta, M. Randazzao, and G. Sandini, "Embedded tactile sensor modules," in *Proc. 11th Mechatron. Forum Biennial Int. Conf.*, 2008, pp. 1–5.
- [8] P. A. Schmidt, E. Mael, and R. P. Wurtz, "A sensor for dynamic tactile information with applications in human-robot interaction & object exploration," *Robot. Auto. Syst.*, vol. 54, no. 12, pp. 1005–1014, Dec. 2006
- [9] Dai, Y., & Gao, S. (2021). A Flexible Multi-Functional Smart Skin for Force, Touch Position, Proximity, and Humidity Sensing for Humanoid Robots. *IEEE Sensors Journal*, 21(23), 26355–26363. <https://doi.org/10.1109/JSEN.2021.3055035>
- [10] C. Domenici and D. De Rossi, "A stress-component-selective tactile sensor array," *Sens. Actuators A, Phys.*, vol. 13, nos. 1–3, pp. 97–100, Mar. 1992.
- [11] M. Ohka, H. Kobayashi, J. Takata, and Y. Mitsuya, "Sensing precision of an optical three-axis tactile sensor for a robotic finger," in *Proc. 15th Int. Symp. Robot Human Interact. Commun.*, Sep. 2006, pp. 214–219.
- [12] B. Ward-Cherrier, N. Pestell, L. Cramphorn, B. Winstone, M. E. Giannaccini, J. Rossiter, and N. F. Lepora, "The TacTip Family: Soft Optical Tactile Sensors with 3D-Printed Biomimetic Morphologies," *Soft Robotics*, 2018
- [13] Mukai, T., Onishi, M., Odashima, T., Hirano, S., & Luo, Z. (2008). Development of the tactile sensor system of a human-interactive robot "RI-MAN." *IEEE Transactions on Robotics*, 24(2), 505–512. <https://doi.org/10.1109/TRO.2008.917006>
- [14] Inaba, M., Hoshino, Y., Nagasaka, K., Ninomiya, T., Kagami, S., & Inoue, H. (1996). Full-body tactile sensor suit using electrically conductive fabric and strings. *IEEE International Conference on Intelligent Robots and Systems*, 2, 450–457. <https://doi.org/10.1109/iro.1996.570816>
- [15] Sundaram, S., Kellnhofer, P., Li, Y., Zhu, J. Y., Torralba, A., & Matusik, W. (2019). Learning the signatures of the human grasp using a scalable tactile glove. *Nature*, 569(7758), 698–702. <https://doi.org/10.1038/s41586-019-1234-z>
- [16] Wade, J., Bhattacharjee, T., Williams, R. D., & Kemp, C. C. (2017). A force and thermal sensing skin for robots in human environments. *Robotics and Autonomous Systems*, 96, 1–14. <https://doi.org/10.1016/j.robot.2017.06.008>



\$82.00

Pooja Gupta, PhD – Assistant Professor, School of Liberal Studies, UPES, India

Series: Education in a Competitive and Globalizing World

BISAC: EDU000000; EDU015000; EDU048000

DOI: <https://doi.org/10.52305/FUNM6586>

Life skills education has gained considerable momentum in recent times while grabbing the attention of education policymakers, researchers, and industry 4.0 for leading a more fulfilling life at personal as well as professional levels. This book is comprised of nine chapters written by experienced and passionate academicians and professionals from varied disciplines, which gives this book a multi-disciplinary outlook. The chapters include research pertaining to work-life balance, self-awakening techniques for overall development, and discussions on life skills essential for professional as well as personal growth. One of the focal points of the chapters is how to manage daily stress, develop stress reduction techniques, and understand the benefits of work-life balance confirming the research on the persuading elements of work-related stress and developing techniques to maintain work-life balance.

Binding

eBook

Publication Date: April 20, 2023

Activate Windows

Go to Settings to activate Windows.

¹Wisdom Public School, Veerapandianpattnam, TN, India

²Sri Meenakshi Govt. Arts College for Women, Madurai, TN, India

Chapter 5. Behavioural Economics and Emotional Quotient

Pragati Bakshi

Assistant Professor in Economics, Yogoda Satsanga Mahavidyalaya, Ranchi, Jharkhand, India

Chapter 6. Life-Skills Courses in an Indian Legal Education Framework

Dr. Sujata Bali¹, Dr. Purnima Bali² and Bharti Nair Khan¹

¹School of Law, University of Petroleum and Energy Studies, Dehradun, India

²Department of English, Shoolini University, Solan, India

Chapter 7. A 'Novel' Approach to Inculcating Life Skills

Deepna Rao

Department of English, Jai Hind College (Autonomous), Affiliated with the University of Mumbai, Mumbai, India

Chapter 8. Enhancing Life Skills in Learners of the New Age Economy

Suruchi Sharma¹, PhD and Seema Verma², PhD

¹School of Management, Graphic Era Hill University, Dehradun, Uttarakhand, India

²School of Aviation, Banasthali Vidyapith, Tonk, Rajasthan, India

Chapter 9. Self-Awakening: An Important Life Skill

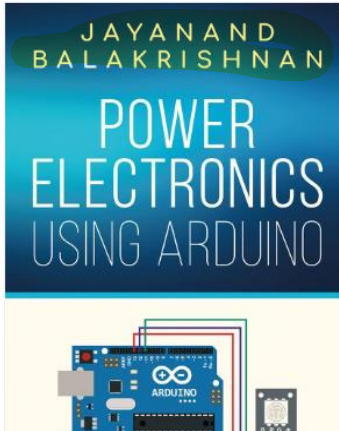
Beena Puthillath

Department of EEE, SCMS School of Engineering and Technology, Ernakulam, Kerala, India



Activate Windows

Go to Settings to activate Windows.



Power Electronics using Arduino

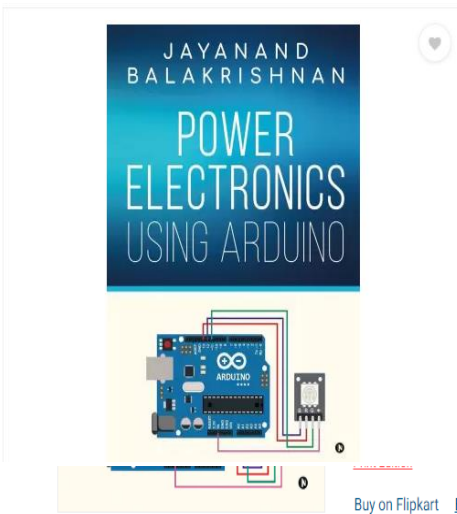
Author Name: [Jayanand Balakrishnan](#) | Format: [Paperback](#) | Genre: [Technology & Engineering](#) | [Other Details](#)

Having difficulties in practical implementation of power electronic projects? If so, this book is for you. This book provides several recipes for making implementation of power electronic circuits and systems simple by using arduino programs. Most power electronic textbooks deal with only the power circuits. This book provides everything needed for practically implementing power electronic circuits, containing theory, control electronics and arduino prog

[Read More...](#)

Paperback: ₹ 249

Also Available On



Author: **Jayanand Balakrishnan**

Highlights:

- Language: English
- Binding: Paperback
- Publisher: Notion Press
- Genre: Technology & Engineering
- ISBN: 9798890267573

Services: [Cash on Delivery available](#) ?

Seller: **BOOKNETZ** 3.4★

- 7 Days Replacement Policy ?

[See other sellers](#)

SuperCoin For every ₹100 Spent, you earn 2 SuperCoins
Max 50 coins per order

[Buy on Flipkart](#) [Buy on Amazon.in](#) [Buy on Amazon.com](#) [Buy on Amazon.co.uk](#)

Jayanand Balakrishnan



Prof. Jayanand B obtained his M Tech and Ph D degrees from IIT, Madras, India. He has 33 years of teaching at UG and PG levels in varioud Government Engineering Colleges in Kerala, India. He got retired from government sevice in the year 2021 from Govt Engineering College, Thrissur, the institution from which he got his bachelor degree. At present, he is working as a Professor at SCMS School of Engineering and Technology, Ernakulam, India. He had guided several Ph D scholars. He was a member of Board of Studies at the University of Calicut and at Kerala Technological University and got involved in the design of curriculum and syllabus in these universities. He was a recipient of Career Award for Young Teachers of All India Council for Technical Education in the year 2000. He is an industrial consultant and had completed several industrial consultancy projects. He holds a couple of patents for his works.

[Read Less...](#)

International Conference on Materials for the Millennium

MatCon-2023

January 12-14, 2023

Conference Proceedings

Organized by



Department of Applied Chemistry

Cochin University of Science and Technology

Kochi-682022, India

Sponsored by

DST-SERB, DRDO, DBT, CUSAT

MatCon 2023

Book of Proceedings

Publication Team

Prof. (Dr.) K. N. Madhusoodanan, Vice Chancellor, CUSAT (Patron)
Prof. (Dr.) P. M. Sabura Begum, Head of the Department,
Department of Applied Chemistry (Chairman), CUSAT

Editorial Board

Prof. (Dr.) Manoj N. (Chief Editor)
Dr. Leena R. (Chief Editor)
Dr. Suja Haridas (Chief Editor)
Ms. Shamna S. (Associate Editor)
Ms. Athira M. P (Associate Editor)

Members

Prof. K. Girish Kumar	Dr. Kala R.
Pof. K. Sreekumar	Ms. Amoolya Chandran
Prof. P.V. Mohanan	Dr. Manoj E.
Smt. Bindu S.	Ms. Saranya P. K.
Prof. Yoosaf Karuvath	Dr. Sindhu Mathai
Ms. Sumi P. M.	Ms. Athira K. S.
Prof. Jayasree E. G.	Prof. S. Prathapan
Prof. Jayasree E. G.	Dr. Sanu K. Anand
Dr. Sebastian Nybin Remello	Dr. Shandev P. P.
Ms. Devika S. R.	Ms. Ansa Santu

Published by

Directorate of Public Relations and Publications For
Dept. of Applied Chemistry
CUSAT, Kochi-682022

ISBN: 978-81-954804-8-7

- MXene: Preparation, properties, and applications,” *Front. Phys.*, vol. 10, no. 3, pp. 276–286, 2015, doi: 10.1007/s11467-015-0493-x.
5. L. Li *et al.*, “Carbon Dot-Regulated 2D MXene Films with High Volumetric Capacitance,” *Ind. Eng. Chem. Res.*, vol. 59, no. 31, pp. 13969–13978, 2020, doi: 10.1021/acs.iecr.0c01440.
 6. E. E. Elemike, J. Adeyemi, D. C. Onwudiwe, L. Wei, and A. O. Oyedeji, “The future of energy materials: A case of MXenes-carbon dots nanocomposites,” *Journal of Energy Storage*, vol. 50: 2022, doi: 10.1016/j.est.2022.104711.

PP 36

Copper(II) Based Potential Pharmaceutical Drugs Against Cancer

Nithya Mohan*^{a,b}, Sreejith S.S^a, M.R.P. Kurup^a,
P.V.Mohanan^{a*}

^aDepartment of Applied Chemistry, Cochin University of Science and Technology, Kochi 682 022, Kerala, India, ^bSCMS School of Engineering & Technology (SSET), Vidya Nagar, Palissery, Karukutty - 683 576, Kerala, India.

*nithyanedumpilly@gmail.com.

The report of the World Health Organization on cancer reveals some fearful results and the report says that in 2020, 10 million people have succumbed to death worldwide owing to this deadly disease and it is the second most common cause of death after cardiovascular diseases. The recent report of Freddie Bray *et al.*¹

reveals that by 2040 the rate of this disease is expected to be increased to 28.4 million. So, there is a pressing need to develop a drug which could effectively interact and destroy the affected cell. Herein, we are reporting our work on the development of a potential metallodrug based on tetradentate Schiff base.

We have systematically designed and synthesized four Cu(II) salen compounds (**1** to **4**) (Figure 1) and characterized using various spectroscopic and analytical techniques. The binding affinity of the complexes with CT-DNA was explored by UV-visible and fluorescence techniques. The compounds exhibit excellent DNA binding and cleavage activities. The binding mechanism were probed by molecular docking studies. These results display high binding constant values owing to the intercalative type of binding. In addition, binding affinity of the compounds with protein were also studied *via in silico* molecular docking method using Human Serum Albumin as receptors. Cleavage of DNA strands was investigated by gel electrophoresis. All the tested compounds show high binding constant value with both DNA and protein. Preliminary *in vitro* studies with L929 (a mouse fibroblast cell line) and HeLa cells (human cervical cancer cell line) indicated the cytotoxic effect of the complexes; however, detailed molecular studies may be required to confirm the mode of anti-cancer mechanism. Considering the results and comparing the existing reports²⁻³, we are proposing a promising candidate (compound **4**) for the development of efficient therapeutic drugs.

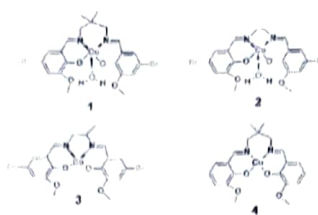


Figure 1. Synthesized pharmaceuticals drugs (1-4)

References

1. S.S.Massoud, A.F.Louka, N.E.Bordelon, R.Fischer, F.A. Mautner, J.Vanco, J.Hošek, Z.Dvorak and Z.Travnicek, *New Journal of Chemistry*, **2019**, *43*, 6186-6196.
2. A.Paul, P.Singh, M.L.Kuznetsov, A.Karmakar, da Silva, B.Koch, A.J.Pombeiro, *Dalton Transactions*, **2021**, *50* (10), 3701-3716.
3. S.Banerjee, P.Ghorai, P.Brandão, D.Ghosh, S.Bhuiya, D.Chattopadhyay, S.Das, A.Saha, *New Journal of Chemistry*, **2018**, *42* (1), 246-259.

PP 37

Design and Development of Cobalt-based Single-Atom Catalyst for Efficient CO₂ Utilization



ICETEST 2023

7th INTERNATIONAL CONFERENCE ON
EMERGING TRENDS IN ENGINEERING,
SCIENCE AND TECHNOLOGY
19-21 April 2023

CERTIFICATE

This is to certify that

Mr/Ms/Dr **AKHILA M**

SCMS School of Engineering and Technology, Ernakulam

has presented a paper titled

Effect of Fines on Static Liquefaction of Sand

in the

**International Conference on Civil Engineering and Architecture for
Sustainable Infrastructure Development and Environment**

CEASIDE 2023

under the aegis of the

**7th International Conference on Emerging Trends in
Engineering, Science and Technology**

ICETEST 2023

"Society, Energy & Environment - Showcasing the Roadmap for Tomorrow"

organised by **Govt. Engineering College Thrissur**

during 19 - 21 April 2023.

Dr. JAYAN A R
Organising Secretary

Dr. UMA SYAMKUMAR
Organising Secretary

Dr. SATISH K P
Organising Chairman

Funded by :

Technical Education
Quality Improvement
Programme
TEQIP

Organised by :

Govt. Engineering College
Thrissur - 680009, Kerala
www.gectcr.ac.in





Sri Sivasubramaniya Nadar College of Engineering

Rajiv Gandhi Salai (OMR), Kalavakkam, Chennai-603110, India

This Certificate is presented to

Ms. LAKSHMI PRIYA

**SEMS SCHOOL OF ENGINEERING AND
TECHNOLOGY, KARUKUTTY, KERALA**

For the paper entitled

**“Selection of most suitable remediation technology
for contaminated sites using remediability score”**

**in the 7th International Conference on “Recent
Advancements in Chemical, Environmental &
Energy Engineering” (RACEEE-2023)**

organized by the

**Department of Chemical Engineering,
Sri Sivasubramaniya Nadar College of Engineering,
Rajiv Gandhi Salai, Kalavakkam-603110,
Chennai, Tamil Nadu, India**

held on

16 and 17th February 2023



A handwritten signature in black ink, appearing to read 'Harsha Vardhan'.

Dr. Kilaru Harsha Vardhan
Convenor

A handwritten signature in black ink, appearing to read 'P. Senthil Kumar'.

Dr. P. Senthil Kumar
Convenor

A handwritten signature in black ink, appearing to read 'B. Chitra'.

Dr. B. Chitra
Convenor

A handwritten signature in black ink, appearing to read 'K. Sathish Kumar'.

Dr. K. Sathish Kumar
Prof. & Head

A handwritten signature in black ink, appearing to read 'V. E. Annamalai'.

Dr. V. E. Annamalai
Principal



Certificate of Appreciation

This is to certify that

Geethu R Babu

had presented the paper titled

Comparitive study on the effect of core shape on blast resistance of sandwich panel

in KSCSTE sponsored 3rd INTERNATIONAL CONFERENCE ON INNOVATIVE TRENDS IN ENGINEERING FOR SUSTAINABILITY (ICITES 2023), organized by Department of Civil Engineering, Toc H Institute of Science & Technology, Arakkunnam, Ernakulam, Kerala, in association with ASCE student chapter (under probation) held on 11th -13th April 2023.

Asst. Prof. Sahimol Eldhose
Conference Secretary

Assoc. Prof. (Dr.) Vasudev R
Convenor, HOD

Prof. (Dr.) Preethi Thekkath
Principal, TIST



CERTIFICATE

THIS IS TO CERTIFY THAT

V Anandhi

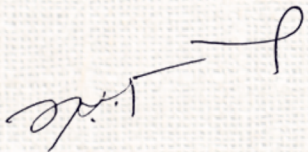
APJ Abdul Kalam Technological University, SCMS School Of Engineering and Technology

has presented a paper entitled

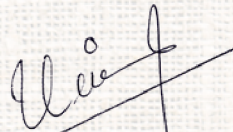
Malware Detection using Dynamic

Analysis

in the **IEEE International Conference on Advances in Intelligent Computing and Applications (AICAPS-2023)** organized by **Department of Computer Applications, Cochin University of Science and Technology, Kochi, Kerala, India,** during **February 1-3, 2023**



Dr. M. V. Judy
Conference Chair



Dr. Vinod P.
TPC Chair



Dr. Vishnukumar S.
Conference Coordinator



BANNARI AMMAN INSTITUTE OF TECHNOLOGY



An Autonomous Institution, Affiliated to Anna University, Approved by AICTE,
Accredited by NAAC with 'A+' Grade,

Department of ECE, EIE - Accredited by NBA New Delhi and Accredited by IET(UK) & Department of BME
Sathyamangalam- 638 401, Tamilnadu, India

CERTIFICATE

This is to certify that the author **Vinoj P G** has presented a paper entitled

Wearable Fabric Tactile Sensors for Robotic Elderly Assistance

at the Second International Conference on Smart Technologies, Communication, and Robotics

2022 (IEEE-STCR 2022) organised by the Department of ECE, EIE & BME during 10 – 11

December 2022.


Dr. C. Poongodi
HoD/ECE


Dr. C. Ganesh Babu
HoD/EIE


Dr. C. Palanisamy
Principal

